Glacial-to-deglacial ^{14}C reservoir ages of surface and deep waters from the mid- and low-latitude Atlantic

Dissertation

In fulfillment of the requirements of the degree “Dr. rer. nat.”

Of the Faculty of Mathematics and Natural Sciences

At Kiel University

Submitted by

Sven Balmer

Kiel, 2016

Referent: Prof. Dr. Wolfgang Kuhnt

Koreferent: Prof. Dr. Michael Sarnthein

Tag der Disputation: 15.07.2016

Zum Druck genehmigt:15.07.2016

Der Dekan:

Eidesstattliche Erklärung

Hiermit erkläre ich an Eides statt, dass die vorliegende Dissertation mit dem Titel “Glacial-to-deglacial ^{14}C reservoir ages of surface and deep waters from the mid- and low-latitude Atlantic“, abgesehen von der Beratung durch meine akademischen Lehrer, in Inhalt und Form meine eigene Arbeit darstellt.

Ich habe diese Arbeit, ganz oder zum Teil, an keiner anderen Stelle im Rahmen eines Prüfungsverfahrens vorgelegt. Teile dieser Arbeit wurden zur Veröffentlichung in Fachzeitschriften eingereicht oder sind in Vorbereitung um eingereicht zu werden.

Diese Arbeit ist unter Einhaltung der Regeln guter wissenschaftlicher Praxis der Deutschen Forschungsgemeinschaft (DFG) entstanden.

Kiel, den ----------

Sven Balmer

Acknowledgements

The research presented in this thesis would not have been possible without the help and support of many people. First and foremost, I thank my Ph.D supervisor Prof. Michael Sarnthein for giving me the opportunity to work on this interesting and challenging topic. Moreover, I thank him for his help and guidance in all these years. I appreciate his extensive help in improving my manuscripts.

I would like to thank Prof. Wolfgang Kuhnt for acting as the 1st referee on this thesis, for providing me with shelter in the MiPa corridor and for giving me the opportunity to participate in a research cruise on the RV Sonne in 2011. Furthermore I thank Dr. Ann Holbourn for helping me with the identification of the benthic formaminifera and for her internal review of the third manuscript that helped to improve the text. My thanks go also to Prof Pieter M. Grootes and Prof Brigit Schneider for the interesting discussions and their continuous help.

All appreciation goes to my friends at MiPa, in particular to Janne and Nick for the great times we had, to Jan, for the Whiskey tastings and for helping me assemble my furniture. I wish you all the best for your Ph.D thesis and your family. Thank you Elena for making Kiel a little bit more comfortable, and of course for the coffee breaks. Thanks to my former office mate Mohamed, for all the talks about the meaning of live, and to my new office mate Sebi, for the constant supply of chocolate, all the help and for driving me home in the last few months. Thanks to Karlos and his wife Deborah, you are awesome. What else is there to say? Thanks to Tante Janika, for the encouraging chats, the nice BBQs and for making me look like Hercules.

Of course there are many other people that made my time in Kiel memorable. Kevin, don't forget, ne Harfe ist so'n Gartenzaun wo man reingrabscht! Henrik, Svea, Larissa, Claudia and Johannes, Dörte Mischkl, and Marcus Regenberg and all the other people from Kiel that I forgot to mention.

Special thanks go to my friends Niko, Alex, Arno and Nils. Thank you guys for visiting me, and for bringing the Schwabenländle to Kiel.

I am especially indebted to my parents Irene and Rainer who supported me in every step of my education and in every other part of my life. And last but not least, I thank Verena for her constant support and her encouraging words over the last two years. Moreover, for sparing me the mensa food, for taking me on my first vacation in 11 years and for making the last two years the best I had in a long time.

Summary

The ^{14}C reservoir age of ocean surface waters shows small-scale spatial and temporal variations. Accordingly, correct estimates of reservoir ages are crucial for any reconstruction of a precise radiocarbon-based chronology of marine sediments. To meet this target in the mid- and low- latitude Atlantic we obtained both ^{14}C reservoir ages and an absolute age model for the glacial-to-deglacial sections of four marine sediment cores by means of the '^{14}C Plateau Tuning Technique'. This method is independent of any common conversion scheme of ^{14}C ages. The resulting empiric reservoir ages were compared with reservoir age estimates based on model simulations. In this way we tested the consistency of our data with those derived by General Circulation Models and the bearing of past changes in ocean circulation for the quality of the output of model simulations. In particular we focused on the following objectives: (1) Southwest of the Azores the new reservoir age records were paired with stable-isotope records to monitor meltwater incursions during Heinrich Stadial 1 (HS-1). (2) For three sediment cores (Azores, Namibian and Brazilian margin) the planktic reservoir ages were summed with paired benthic-planktic ^{14}C age differences and corrected for past changes in atmospheric ^{14}C concentration to obtain apparent deep-water ventilation ages that reveal glacial-to-deglacial changes in the geometry of Atlantic deep waters. In particular we study whether and to which extent the Arctic Mediterranean (AM) may have contributed to the old Southern Source Water (SSW) in the deep Atlantic during HS-1. (3) We addressed in five sediment cores the question, whether the suites of ^{14}C plateaus in planktic ^{14}C records either were merely a result of hypothetical short-lasting events of sediment deposition or rather controlled by a suite of changes in atmospheric ^{14}C. To test the two rationales for the interval 23–12 cal. ka we calculated hypothetical sedimentation rates for all ^{14}C plateaus identified in five Atlantic sediment cores assuming sediment pulses that either span 10, 100, 200, or 300

years each. These rates were compared to rates derived by ^{14}C plateau tuning that assumes an atmospheric origin of the plateaus.

With regard to surface waters our new reservoir age records differ by up to 500–2500 years from a previously assumed global average of ~400 years. This implies that many of the previously established age models need to be corrected by means of the new method. During HS-1, pronounced minima in planktic $\delta^{18}O$ of *G. bulloides* matched maximum planktic reservoir ages of ~1600 to 2170 yr southwest of the Azores here suggesting meltwater incursions that reached down to the subtropics. Strengthened trades off Benguela and summer winds off Brazil are reflected in local upwelling-induced surface water reservoir ages of up to 1000 yr during the Last Glacial Maximum (LGM). By contrast reservoir ages remained close to zero in the Cariaco Basin (South Caribbean) due to a lagoon-style isolation and as a result, a persisting dominance of air-sea CO_2 exchange. At 16 cal. ka reservoir ages of surface waters decreased throughout the South Atlantic to a minimum of 170–420 ^{14}C years, possibly a response to the coeval rapid rise in pCO_2 and Antarctic temperatures. Spatial and temporal changes in ^{14}C reservoir age that our empiric data estimate for peak glacial and deglacial surface waters in part deviate significantly from the simulated reservoir ages of Franke et al. [2008] but are consistent with those of the more advanced ocean circulation model of Butzin et al. [2012] that also incorporates empiric LGM sea surface temperature patterns.

Our records of apparent deep-water ventilation ages show peak glacial values of 340–740 yr near the Azores. The low ages suggest local formation of North Atlantic Deep Water (NADW) reaching down >3100 m, a depth that contrasts with a widely accepted shoaling of glacial deep-water formation. During HS-1, local benthic ventilation ages rose up to 2200–2550 yr, thus probably reflect an incursion of old southern-source deep waters, an instable regime that was interrupted by brief pulses of young-NADW formation near 16, 15.6 and 14.9/14.7 cal. ka. In the South Atlantic the two core sites show incoherent signals of deep-

water ventilation, since they represent ocean regimes at opposed continental margins and different water depths. During LGM and Bølling-Allerød (B/A) ventilation ages off Namibia amount to ~2000 yr. At the onset of HS-1 they dropped to ~500 yr. At 16 cal. ka they returned to ~3000 yr in waters showing geochemical properties of SSW. At the Brazilian Margin ventilation ages amount to ~2800 yr in early HS-1 and reach a maximum of 4600 yr in the middle of HS-1 (16.3–16.1 cal. ka). These old waters may either represent a (Coriolis forced) tongue of ^{14}C-depleted SSW that moved northward or the terminal advance of AM waters. During B/A a ventilation age of ~200 yr records a pulse of northern deep waters at 13.8–14.3 cal. ka, possibly also at 15.4 cal. ka. The sampling density in the two cores from the South Atlantic is insufficient to constrain more precisely millennial-to centennial-scale ventilation changes. Thus we cannot precisely constrain the timing and potential contribution of AM vs. that of SSW to the old HS-1 waters in the deep Atlantic.

The comparison between the sedimentation rates of hypothetical short-lasting sediment pulses and the sedimentation rates derived by means of plateau tuning show at least one or two cases of extreme values in the hypothetical rates of each plateau suite. These extreme values exceed rates reported for short-lasting pulses of sediment deposition in contourites by a factor of 50. Hence they are considered unrealistic. Moreover, they result in entire suites of plateau structures that ‘incidentally’ appear closely aligned to the pattern of atmospheric ^{14}C plateau suites rather than to any pulses of climate-controlled sediment discharge.

Zusammenfassung

Radiokarbon (^{14}C) Reservoiralter mariner Oberflächenwässer zeichnen sich durch starke örtliche wie zeitliche Unterschiede aus. Folglich sind korrekte Angaben über Reservoiralter wesentlich, um mittels der Radiokarbonmethode ein exaktes Altersmodel für marine Sedimente zu erstellen. Die vorliegende Arbeit dient dem Versuch, erstmals durchgehende Zeitserien der planktischen Reservoiralter für die mittleren und niedrigen Breiten des Atlantiks bereit zu stellen, die den Zeitraum des letzten Hoch- und Deglazials abdecken. Dafür wurde die Methode des ^{14}C-Plateau-Tunings an vier marinen Sedimentkernen eingesetzt, eine Technik, die nicht an die konventionellen Ansätze der Konversion von ^{14}C-Altern in „Kalender-Alter " gebunden ist. Durch sie erhält man einerseits ein absolutes Altersmodell, andererseits die den einzelnen Altern zugehörigen örtlichen ^{14}C Reservoiralter. Diese empirischen Reservoiralter der Oberflächenwässer und die durch sie belegten Änderungen der Ozeanzirkulation wurden mit publizierten Ergebnissen aus Ozeanzirkulations-Modellen (OZM) verglichen. So konnte die Qualität der Modelldaten im Vergleich mit empirischen Daten direkt überprüft werden.

Unser Hauptaugenmerk lag im speziellen auf folgenden Themen: (1) Südwestlich der Azoren wurden die neuen Reservoiralter der Oberflächenwässer und gepaarte Messungen stabiler O- und C-Isotope verwendet, um Schmelzwasser-Eintrag während Heinrich Stadial 1 (HS-1) nachzuweisen. (2) Die planktischen ^{14}C Reservoiralter dreier Sedimentkerne (vor den Azoren, vor Namibia und vor Brasilien) wurden mit der Differenz aus paarweisen benthischen und planktischen ^{14}C Altern aus jeweils gleichen Kerntiefen kombiniert, um das scheinbare benthische Ventilationsalter zu bestimmen. Dies gibt Aufschluss über Veränderungen in der räumlichen Verteilung atlantischer Tiefenwässer. Im speziellen wollten wir herausfinden ob und in welchen Ausmaß das Arktische Mittelmeer (AM) zu den alten Tiefenwässern aus dem

Südozean (SSW) beigetragen haben mag, die den tiefen Atlantik während HS-1 dominierten. (3) Die Daten von fünf Sedimentbohrkernen wurden verwendet um zu klären, ob ^{14}C Plateauabfolgen in planktischen ^{14}C-Kurven vielleicht nur das Resultat von hypothetischen kurzzeitigen Sedimentations-Pulsen gewesen sein mögen, oder ob sie eher von Veränderungen des atmosphärischen ^{14}C-Gehalts gesteuert würden. Um dies zu testen, wurden für alle ^{14}C Plateaus zwischen 23–12 cal. ka (ka = 1000 Jahre), die in den fünf Kernen identifiziert wurden, hypothetische Sedimentationsraten berechnet. Dafür wurde jeweils eine theoretische Dauer von 10, 100, 200 und 300 Jahren für die einzelnen Sedimentationsereignisse angenommen. Die Ergebnisse wurden anschließend mit den Sedimentationsraten der fünf Kerne verglichen, die auf ^{14}C-Plateau-Tuning beruhen, also auf einem atmosphärischen Ursprung der ^{14}C Plateaus.

Unsere neuen planktischen Reservoiralter weichen um bis zu 500–2500 (^{14}C-) Jahre von einem bisher allgemein angenommen globalen Durchschnitt von ~400 Jahren ab. Viele der bisherigen Altersmodelle wären somit durch die neue Technik zu korrigieren. Südwestlich der Azoren stimmen ausgeprägte $\delta^{18}O$-Minima, gemessen an der Planktonforaminifere *G. bulloides*, zeitlich mit Maxima der Reservoiralter von ~1600–2500 Jahren überein, ein deutlicher Hinweis, dass Schmelzwasser bis in die Subtropen transportiert wurde. Während des Letzten Glazialen Maximums (LGM) führten stärkere Passatwinde vor Benguela und verstärkte Sommerwinde vor Brasilien zu verstärktem Auftrieb vor den Küsten, was durch planktische Reservoiralter von bis zu 1000 Jahren widergespiegelt wird. Im Gegensatz dazu blieben die ^{14}C Reservoiralter im südkaribischen Cariaco Basin nahe bei null. Dies ist der lagunenartigen Abgrenzung zuzuschreiben, die eine anhaltende Dominanz des CO_2-Austauschs zwischen Oberflächenwasser und Atmosphäre zur Folge hatte. Vor rund 16 ka fielen sämtliche Reservoiralter im Südatlantik auf ein Minimum von 170–420 Jahren ab. Dies war möglicherweise eine Reaktion auf den schnellen Anstieg des atmosphärischen pCO_2

und der Temperaturen in der Antarktis, die zur selben Zeit stattfanden. Die zeitlichen und örtlichen Unterschiede unserer empirischen Reservoiralter weichen signifikant von Reservoiraltern der Oberflächenwässer ab, die Franke et al. [2007] simulierten, stimmen aber weitgehend mit den Ergebnissen von Butzin et al [2012] überein. Diese basieren auf einem OZM, das auch empirische Meeresoberflächentemperaturen des LGM miteinbezieht.

Unsere scheinbaren benthischen Ventilationsalter liegen am Mittelatlantischen Rücken nahe den Azoren während des Hochglazials bei 340–740 Jahren. Solch niedrige Alter deuten auf eine lokale Bildung von Nordatlantischem Tiefenwasser (NADW), das bis in Tiefen von >3100 m hinab reichte. Dies steht im Widerspruch zu einer bisher weithin angenommenen abgeflachten Tiefenwasserbildung. Während HS-1 stiegen die lokalen benthischen Ventilationsalter auf bis 2200–2550 Jahre an. Wahrscheinlich spiegeln sie damit eine alte Wassermasse aus dem Südozean. Dies war ein instabiler Zustand, der durch kurze Pulse jungen NADWs vor 16, 15,6 und 14,9/14,7 cal. ka unterbrochen wurde. Die Zeitserien benthischer Ventilationsalter aus den beiden Sedimentbohrkernen im Südatlantik zeigen keinerlei Zusammenhang, da sie das Ozeanregime an zwei gegenüberliegenden Kontinentalrändern und aus sehr unterschiedlichen Wassertiefen repräsentieren. Während des LGM und Bølling-Allerød (B/A) betrugen die Ventilationsalter vor Namibia ~2000 Jahre. Zu Beginn von HS-1 fielen sie auf ~500 Jahre, stiegen danach aber bis 16 cal. ka auf bis zu ~3000 Jahre. Diese alte Wassermasse zeigt deutlich die geochemischen Eigenschaften, d.h. das Pa/Th-Verhältnis des Südozeans.

Am brasilianischen Kontinentalhang betrugen die Ventilationsalter während des frühen HS-1 ~2800 Jahre, erreichten dann aber ein Maximum von 4600 Jahren im mittleren HS-1 (16,3–16,1 cal. ka). Diese alten Wassermassen waren entweder eine Zunge von SSW (durch die Corioliskraft in der Südhemisphäre nach Westen abgelenkt), die sich nach Norden hin

ausbreitete, oder sie waren evtl. das Ende von AM-beeinflusstem Tiefenwasser aus dem Norden. Während des B/A weisen Ventilationsalter von ~200 Jahren auf einen Puls von jungem NADW bei 13,8–14,3 cal. ka, möglicherweise sogar auch schon bei 15,4 cal. ka. Die Probendichte in den beiden Sedimentbohrkernen aus dem Südatlantik ist unzureichend, um tausend oder nur wenige hundert Jahre andauernde Veränderungen in der Tiefenwasserventilation anzuzeigen. Deshalb können wir den potentiellen Beitrag des AM zu den alten Tiefenwässern im tiefen Atlantik während HS-1 nicht hinreichend feststellen.

Der Vergleich zwischen den hypothetischen kurzen Pulsen im Sediment-Eintrag und den aus Plateau Tuning errechneten Sedimentationsraten zeigt, dass in jeder Plateauabfolge bei theoretischen Sedimentations-Pulsen mindestens ein bis zwei Extremwerte der Rate enthalten wären. Diese überstiegen bei weitem die bekannten Raten von kurzzeitigen Sedimentations-Ereignissen in hemipelagischen Ablagerungen (Konturite) um einen Faktor von 50. Damit können sie als unrealistisch betrachtet werden, während die atmosphärisch gesteuerten ^{14}C Plateaus durchaus realistische und einigermaßen konsistente Sedimentations-Raten liefern. Außerdem zeigen die aus hypothetischen Annahmen errechneten Sedimentationsraten Ähnlichkeit mit atmosphärischen ^{14}C Plateauabfolgen und nicht mit allgemein bekannten Klimasignalen, die für Veränderungen des Sedimenttransports in die Ozeane verantwortlich gemacht werden.

Table of Contents

List of Figures

Chapter 5

List of Tables

Chapter 2

Chapter 3

Chapter 4

Chapter 5

Chapter 1

Introduction

1.1 Objectives

Reservoir ages of surface waters resemble the ^{14}C age difference between the surface ocean and the contemporaneous atmosphere. A correct estimate of reservoir ages is crucial for accurate ^{14}C dating since they may bias ^{14}C ages of marine sediment records towards older values as compared to the contemporaneous atmosphere. Surface water reservoir ages were previously assumed to be constant over time and at any particular site near 400 yr [*Bard*, 1988]. In contrast, they show temporal and spatial variations as summarized in Stuiver and Braziunas [1993] for today and the last 10 kyr and by Sarnthein et al. [2015] for last glacial-to-deglacial times. The changes can be linked to variations in coastal upwelling strength that influence the amount of old ^{14}C depleted water advected from the subsurface, and thereby increase or decrease the reservoir age of local surface waters. Furthermore, meltwater discharge may lead to a meltwater lid that inhibits gas exchange between the surface ocean and the atmosphere and results in increased reservoir ages of (sub-) surface waters [Sarnthein et al., 2001; 2015]. In particular these factors apply to the last glacial-to-deglacial transition that was subject to tremendous climatic changes and major modifications of Atlantic Meridional Overturning Circulation (AMOC) as suggested by Atlantic stable isotope transects [*Sarnthein et al*., 1994; *Curry and Oppo*, 2005].

Precise age control forms a crucial prerequisite to obtain ^{14}C reservoir ages. On the one hand, glacial-to-deglacial changes in reservoir age are deduced by means of model simulations that take into account (though to a different degree) past changes in climate and ocean circulation [*Franke et al*., 2008; *Butzin et al*., 2012]. On the other hand, reservoir ages may rely on the chronology of ash layers in the North Atlantic [*Bard et al*., 1994; *Waelbroeck et al*., 2001]. In the high latitudes short-term oscillations in sea surface temperatures (SST) and foraminifera abundance may be tuned to the incremental time scale of Greenland and Antarctic ice core

records of atmospheric temperature to provide an independent age scale as basis for deriving estimates of reservoir age [*Skinner et al*., 2010; *Thornalley et al*., 2011].

It was the main goal of this thesis to establish records of glacial-to-deglacial changes in ^{14}C reservoir age from various regions in the tropical and subtropical Atlantic in order to monitor past changes in ocean circulation and the potential influence of meltwater incursions (**Chapter 2** and **3**). Furthermore, the new data will supplement the set of scarce Atlantic ^{14}C reservoir ages and serve for testing model-based estimates of reservoir age (**Chapter 3**). To reach this goal we employ the '^{14}C Plateau Tuning Technique' [*Sarnthein et al*., 2007; 2015]. This method tunes plateau structures in high-resolution planktic ^{14}C records of glacial-to-deglacial times to pertinent structures in the atmospheric ^{14}C record of Lake Suigetsu, the age model of which is based on varve counts [*Bronk Ramsey et al*., 2012]. In this way we obtain a new absolute age model independent of any common conversion scheme of ^{14}C ages (e.g., IntCal13). It may be discussed, whether plateau structures in planktic ^{14}C records are a result of atmospheric ^{14}C changes or merely one of sedimentary processes, a question addressed in **Chapter 4**. Moreover, the difference between paired planktic and benthic ^{14}C ages can be summed with planktic reservoir ages to obtain apparent benthic ventilation ages that record the time span passed since a water mass has lost its contact with the atmosphere. These ages increase with growing distance from the site of deep-water formation [*Matsumoto*, 2007]. Accordingly they may be used to unravel glacial-to-deglacial AMOC geometries that paralleled past climatic change (**Chapter 2** and **5**).

1.2 The deglacial setting

The last deglacial episode covers the transition from Marine Isotope Stage (MIS) 2 to MIS 1, lasting from 19 to 10 cal. ka [*Svensson et al*., 2008]. The deglacial is marked by the Earths' last fundamental climate change that cannot be related to anthropogenic influence.

Atmospheric pCO_2 rose in three major steps from 190 ppm to pre-industrial values of 280 ppm [*Monnin et al.*, 2001, *Marcott et al.*, 2014], when the ^{14}C concentration in the atmosphere dropped by 400‰ [*Bronk Ramsey et al.*, 2012]. Global atmospheric temperatures increased by 3-6° [*Schneider von Deimling et al.*, 2006] synchronous with a global sea level rise of 134 m [*Lambeck et al.*, 2014]. In the beginning the transition from the Last Glacial to the Holocene warm period was delayed in the Northern Hemisphere by Heinrich Stadial 1 (HS-1), later interrupted by the Younger Dryas Cold Event. Vice versa, the Antarctic Cold Reversal in the Southern Hemisphere matched the first intensive warming, the Bølling-Allerød (B/A) in the north, a result of significant changes in AMOC geometry summarized by the concept of inter-hemispheric seesaw [*Stocker*, 1998].

During LGM a general AMOC shoaling is widely assumed [*Ferrari et al.*, 2014], however, questioned by Kitoh et al. [2001] who postulate a slightly deepened NADW formation and by Hewitt et al. [2003] who postulate an unchanged vertical reach of AMOC. The deep Atlantic was flooded by waters from the Southern Ocean that mixed with northern source waters up to depths of 2500 m to the south of the Azores, as suggested by benthic $\delta^{13}C$ (Fig. 1.1) [*Sarnthein et al.*, 1994, *Curry and Oppo*, 2005] and Cd/Ca transects [*Marchitto and Broecker*, 2006]. During HS-1 ^{13}C- and ^{14}C-depleted waters filled the deep Atlantic up to the northeastern North Atlantic [*Sarnthein et al.*, 1994; *Thornalley et al.*, 2011]. In addition, old waters were probably advected from the Arctic Mediterranean [*Thornalley et al.*, 2015].

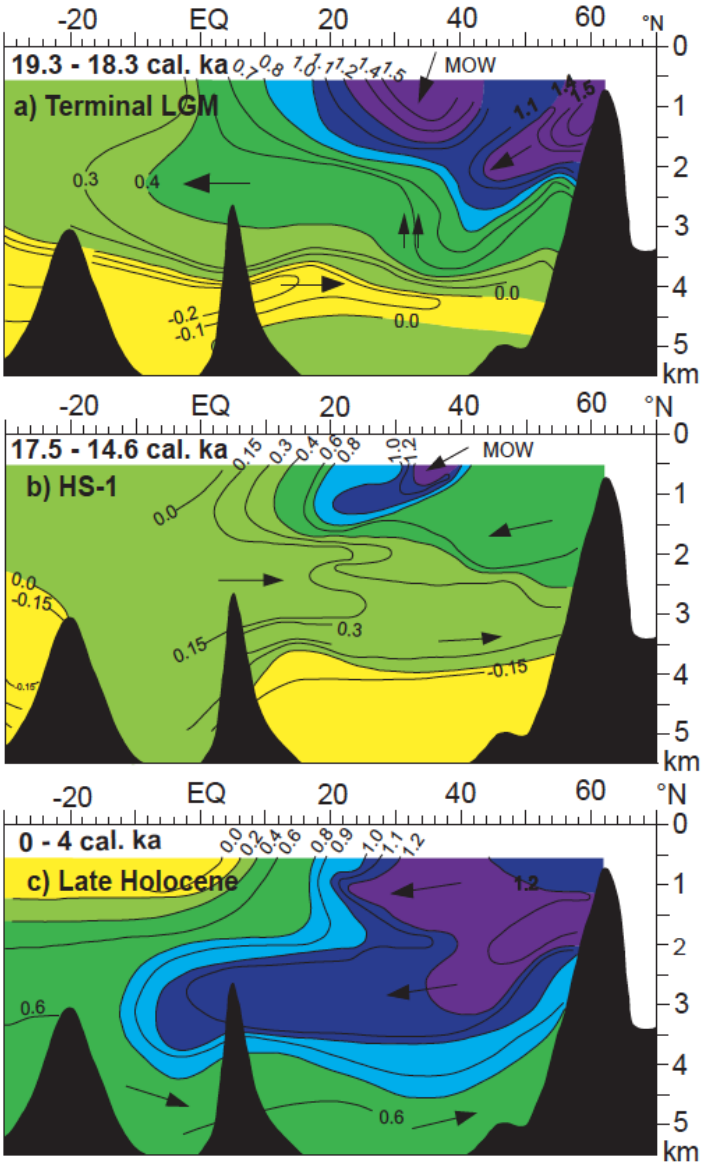

Figure 1.1: N–S transects of benthic $\delta^{13}C$ across the east Atlantic for glacial-to-deglacial times. a) Terminal Last Glacial Maximum (LGM), b) Heinrich Stadial 1 (HS-1), c) Late Holocene. MOW = Mediterranean Outflow Water. Black arrows indicate flow direction of different water masses [*Sarnthein et al.*, 1994; modified].

The onset of the B/A warm period is marked by a modern AMOC geometry. The North Atlantic Deep Water (NADW) reached down to 4500 m; below Antarctic Bottom Water (AABW) extended to 60°N [*Sarnthein et al.*, 1994]. The wide range of deglacial AMOC changes led to short-term changes in the reservoir age of local surface waters as summarized by Sarnthein et al. [2015] (Fig. 1.2) and discussed in **Chapters 2** and **3**.

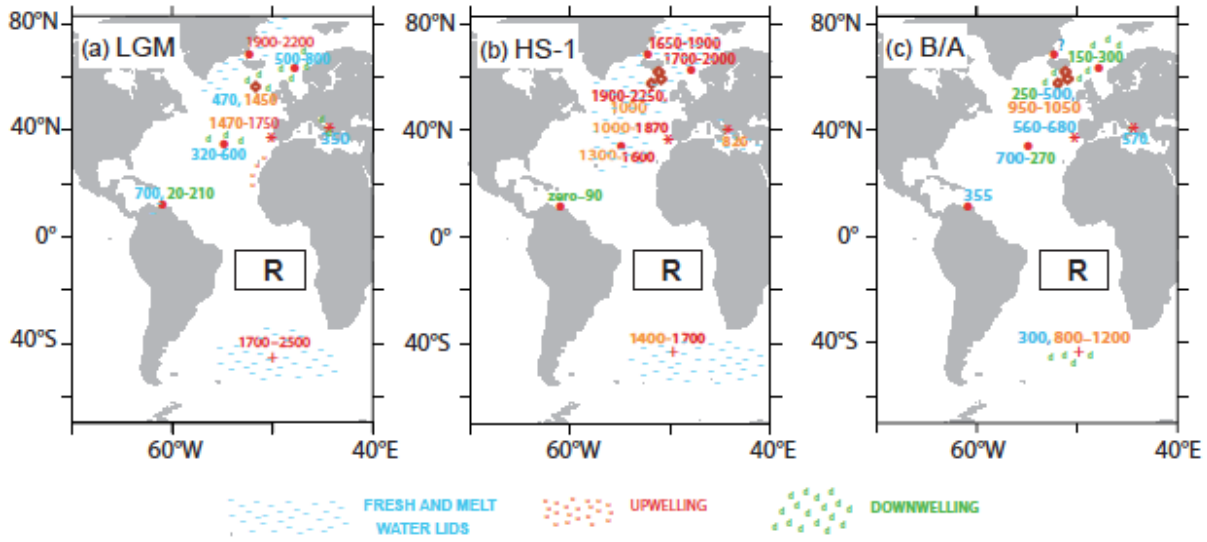

Figure 1.2: Glacial-to-deglacial ^{14}C reservoir ages of Atlantic surface waters. a) Last Glacial Maximum (LGM), b) Heinrich Stadial 1 (HS-1), c) Bølling-Allerød (B/A) [*Sarnthein et al.*, 2015; modified].

During the LGM extreme highs in local reservoir age were associated with upwelling regions, moreover, with high latitudes where ice cover and meltwater lids inhibited an air-sea gas exchange. Low reservoir ages generally marked the low latitudes. During HS-1 extremely high ages occurred all over the mid- and high-latitude North Atlantic as a result of meltwater incursions due to increased iceberg discharge. In contrast, the B/A widely showed low reservoir ages in the North Atlantic in line with modern AMOC geometries.

1.3 Methods

1.3.1 AMS ^{14}C dating

Samples of monospecific planktic and, preferably, epibenthic foraminifera were used for ^{14}C dating. Tests of miliolid species (e.g., *Pyrgo sp.*) were excluded, since they their low ^{14}C contents may significantly bias ^{14}C ages toward older values [*Magana et al.*, 2010] (details on species selection, size fraction and number of specimens see **Chapter 2**, **3** and **5**). Samples were dated at the Leibniz Laboratory, Kiel, and the KECK Carbon Cycle AMS facility, University of California, Irvine.

Sample processing in the Leibniz Laboratory included sample cleaning with 15% H_2O_2 in an ultrasonic bath to remove dust and detrital carbonate as well as organic surface coatings. CO_2 was released from the samples with 100% H_3PO_4 at 90°C and graphitized with H_2 using about 2 mg Fe powder as catalyst. The ^{14}C concentration was measured by comparison of simultaneously collected ^{14}C, ^{13}C, and ^{12}C beams of each sample with those of Oxalic Acid standard CO_2 and those of pre-Eemian planktic foraminifera [*Nadeau et al*., 1998]. Samples submitted to the KECK AMS Group were cleaned and leached prior to graphitization and hydrolyzed in H_3PO_4. Before ^{14}C analysis the released CO_2 was graphitized under H_2 on an iron catalyst [*Vogel et al*., 1984]. ^{14}C results were related to spare calcite as ^{14}C-dead blank. All ^{14}C values were converted into conventional ^{14}C ages following Stuiver and Pollach [1977]. Details on ^{14}C dating of marine sediments can be found in Hughen [2007].

1.3.2 ^{14}C plateau tuning and derivation of planktic reservoir age

Following Sarnthein et al. [2007; 2015] we correlated plateaus and jumps in our planktic ^{14}C record to pertinent features in the varve-counted atmospheric ^{14}C record of Lake Suigetsu [*Bronk Ramsey et al*., 2012]. Thus the ages of atmospheric plateau boundaries provide absolute age control. The Lake Suigetsu ^{14}C record is the only decadal-to-centennial scale resolution atmospheric ^{14}C and $\Delta^{14}C$ record extending beyond 13.9 cal. ka (IntCal13; [*Reimer et al*., 2013]). We regard its varve counted time scale as superior to the modeled time scale for peak glacial and deglacial times (IntCal13), because the modeled time scale is partially based on the U/Th-based time scale of corals and carbonates of the Hulu 2 speleothem. These carbonate-based ^{14}C dates may suffer from possibly variable ‘dead-carbon’ fractions (broadly discussed in Sarnthein et al. [2015]), moreover, likewise from variable surface water reservoir ages in the ocean.

Sarnthein et al. [2007; 2015] defined several boundary conditions for the process of ^{14}C plateau tuning and the calculation of planktic ^{14}C reservoir ages (see **Chapter 2**):

(1) To display ^{14}C plateaus as short as 300 yr, marked by two or three ^{14}C dates each, sedimentation rates should exceed 10 cm/kyr. Moreover, the sampling resolution should be better than 100–150 yr.

(2) To identify more objectively the ^{14}C plateaus and jumps in the ^{14}C record we also employ a mathematical method that uses the first derivative of all down-core changes in the ^{14}C age–core depth (or –calendar age) relationship [*Sarnthein et al.*, 2015].

(3) To identify the individual ^{14}C plateaus, the complete suite of plateaus and their internal structures need to be considered. In case of several tuning choices, the lowest possible planktic reservoir age estimates are accepted, if no different stringent evidence is suggesting any higher value. For example, paired benthic ^{14}C ages that are lower than the coeval planktic ^{14}C age may necessarily imply increased planktic ^{14}C reservoir ages to provide an apparent benthic ^{14}C ventilation age larger than ~400 yr [Matsumoto, 2007], since smaller values are rare and negative benthic ventilation ages physically impossible.

As listed under **Chapter 2** and **3**, Sarnthein et al. [2015] introduced an objective mathematical approach to identify ^{14}C jumps and plateau boundaries in a curve of y = ^{14}C years over x = core depth (or calendar years), otherwise identified by visual inspection only. The approach is based on the first derivative or slope of the curve over time, $y'(x) = dy(x)/dx$. By definition plateaus have low slope values, ideally one of zero, while ^{14}C jumps result in peaks of the 1st derivative (see **Chapter 3**). A test run for the atmospheric ^{14}C record of Lake Suigetsu yielded (varve counted) calendar ages of plateau boundaries with a deviation that does not exceed the range of decades to 100 yr. The resulting ‘calendar’ ages hardly differ from those established by visual inspection and corroborate the accuracy of the definition of planktic ^{14}C

plateau boundaries. Thus, we stick to the use of planktic plateau boundaries as age control points, that are correlated by visual inspection to atmospheric ^{14}C plateau boundaries in the Lake Suigetsu record.

Average planktic reservoir ages were calculated by subtracting one-by-one the average atmospheric ^{14}C age of a plateau in the Suigetsu record from the average ^{14}C age of the pertinent planktic ^{14}C plateau. Our approach is always based on considering the full suite of ^{14}C plateaus. Accordingly, the robustness of the plateau tuning technique does not suffer from the loss of any single plateau, which in turn may provide important insights into changes of the sedimentation regime such as the detection of hiatuses (e.g., see **Chapter 3**).

1.3.3 Derivation of apparent benthic ventilation ages

'Raw' apparent benthic ventilation ages present the sum of (1) the ^{14}C age difference between paired benthic and planktic foraminifera ages and (2) the planktic reservoir age of the ^{14}C plateau that covers the pair of benthic and planktic dates. Thus 'raw' ventilation ages (in ^{14}C yr) present the difference between an atmospheric and benthic ^{14}C level at the site and time of foraminifera deposition. As first shown by Adkins and Boyle [1997] and recently summarized by Cook and Keigwin [2015], 'raw' ventilation ages need to be converted to 'actual' benthic ventilation ages by means of the 'projection' technique. Accordingly, 'raw' ages need to be corrected for changes in atmospheric ^{14}C over brief glacial-to-deglacial time spans that preceded sediment deposition. These intervals each start with the formation of deep waters that incorporated an initial ^{14}C signal from the sea surface (arbitrarily assumed equal to the planktic reservoir age at the site and time of foraminifera deposition) and end with the growth of benthic foraminifera that finally incorporated the ^{14}C signal in deep-sea sediments, though somewhat modified by radioactive decay. Our approach disregards any mixing of water

masses that originate from different source regions and contribute differential ^{14}C ventilation ages, thus justify the modifier 'apparent' (see **Chapter 2** and **5**).

1.3.4 Further methods employed

X-ray fluorescence (XRF) spectrometry was employed on Core GeoB 3910-1 (see **Chapter 3**). This method allows a qualitative determination of the geochemical composition of the sediment at mm-scale resolution [*Jansen et al*., 1992]. Measurements were conducted at MARUM, Bremen University, Germany, using an XRF Core Scanner II (AVAATECH Serial No. 2). XRF data were collected every 4 mm using generator settings of 10 kV, a current of 0.5 mA, and a sampling time of 20 seconds. The surface of the sediment core was covered with a 4-micron thin SPEXCerti Prep Ultralenel foil to avoid contamination of the XRF measurement unit and desiccation of the sediment. The reported data were acquired by a Canberra X-PIPS Silicon Drift Detector (SDD; Model SXD 15C-150-500) with 150 eV X-ray resolution, the Canberra Digital Spectrum Analyzer DAS 1000, and an Oxford Instruments 50W XTF5011 X-Ray tube with Rhodium (Rh) target material. Raw data spectra were processed by the analysis of X-ray spectra by iterative square software (WIN AXIL) package from Canberra Eurisys.

Paired planktic $\delta^{13}C$ and $\delta^{18}O$ data are used to unravel the origin of short-lasting $\delta^{18}O$ minima in a glacial-to-deglacial sediment section of Core MD08 3180 from southwest of the Azores (see **Chapter 2**). The approach is based on the findings of Bemis et al. [2000]. Accordingly, negative $\delta^{13}C$ excursions in tests of *Globigerina bulloides* directly correlate with a warming of ambient seawater temperatures (Fig. 1.3). Thus, any short-lasting $\delta^{18}O$ minimum that does not match any minimum in $\delta^{13}C$ can be ascribed to a salinity reduction identified as meltwater incursion.

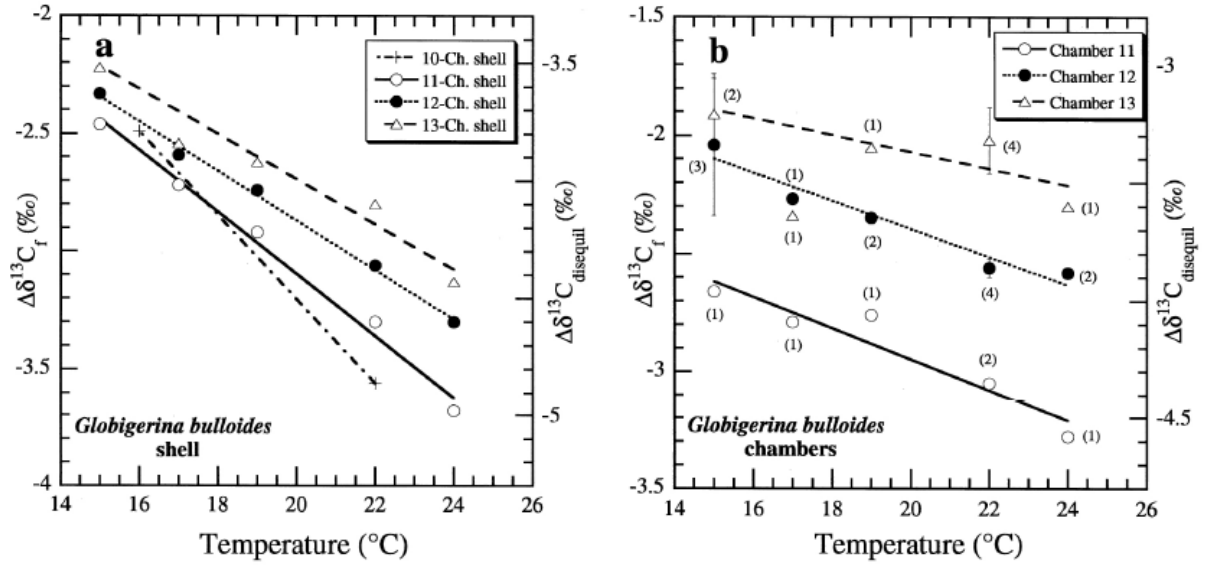

Figure 1.3: Mean $\delta^{13}C$ (±1σ) temperature relationship in *G. bulloides* [*Bemis et al*., 2000; modified]. $\Delta\delta^{13}C_f = \delta^{13}C_{foram} - \delta^{13}CSCO_2$ ($\delta^{13}CSCO_2 = \delta^{13}C$ of total dissolved inorganic carbon in the ocean); $\Delta\delta^{13}C_{disequil} = \Delta\delta^{13}C_f - \Delta\delta^{13}C_{EQ}$ ($\Delta\delta^{13}C_{EQ} = \delta^{13}C_{calcite} - \delta^{13}CSCO_2$). a) Reconstructed whole shells consisting of 11, 12 and 13 chambers. Each point represents a single calculated value based on mass balance. b) Chambers 11, 12, and 13. Numbers within parenthesis indicate the number of individual shell analyses represented by each point.

Stable isotopes ($\delta^{18}O$ and $\delta^{13}C$) were measured at the Leibniz Laboratory of Kiel University using a MAT 253 mass spectrometer. The system is equipped with a Carbo-Kiel Device (Type IV) for automated CO_2 preparation from carbonate samples for isotope analysis. Samples were reacted by individual acid addition (99% H_3PO_4 at 75°C). Precision was regularly checked using an internal Solnhofen limestone standard that was converted to the Vienna Pee Dee Belemnite (VPDB) standard using the National Bureau of Standards NBS-19 carbonate standard. External standard errors are better than ±0.08 ‰ for $\delta^{18}O$ and ±0.05 for $\delta^{13}C$. Details on the application of oxygen and carbon isotopes of foraminifera in paleoceanography can be found in Ravelo and Hillaire-Marcel [2007].

1.4 Structure of the Thesis

Chapter 2 uses planktic and benthic ^{14}C reservoir ages and paired planktic stable isotope records obtained from southwest of the Azores to monitor a meltwater incursion during HS-1. Moreover the study uses glacial-to-deglacial changes in apparent benthic ventilation ages to monitor regional variations of peak glacial and deglacial deep-water masses. The study is entitled 'Glacial-to-deglacial changes in North Atlantic meltwater advection and deep-water formation – Centennial-to-millennial scale ^{14}C records from the Azores Plateau' (manuscript subm. to *Quaternary Science Reviews*).

Chapter 3 compares glacial and deglacial Atlantic ^{14}C reservoir ages in the tropical and subtropical Atlantic, that on the one hand were derived by plateau tuning, on the other hand by model studies. The study is entitled 'Refined modeling and ^{14}C plateau tuning reveal consistent patterns of glacial and deglacial ^{14}C reservoir age of surface waters in low latitiudes Atlantic' (manuscript subm. to *Paleoceanography*).

Chapter 4 is a methodological study entitled 'Planktic ^{14}C plateaus, a result of short-term sedimentation pulses?' (manuscript subm. to *RADIOCARBON*). The study compares plateau-tuning derived sedimentation rates of five Atlantic core sites with hypothetical short-lasting sediment pulses that might have formed the sole origin of plateau structures in the planktic ^{14}C records.

Chapter 5 is a study entitled 'Intermediate- and deep-water ventilation ages as a record of glacial-to-deglacial AMOC flow patterns'. Apparent intermediate- and deep-water ventilation ages supplement the scarce Atlantic ventilation age data sets and monitor glacial-to-deglacial changes in Atlantic deep-water circulation.

Chapter 6 summarizes the results of the thesis and provides an outlook.

Chapter 2

Glacial-to-deglacial changes in North Atlantic meltwater advection and deep-water formation – Centennial-to-millennial-scale ^{14}C records from the Azores Plateau

Sven Balmer and Michael Sarnthein

Submitted to *Quaternary Science Reviews*

2.1 Abstract

The last deglacial was marked by tremendous changes in ocean temperature and circulation as well as atmospheric CO_2 and ^{14}C. We employed the "^{14}C plateau-tuning technique" to a centennial-scale planktic ^{14}C record of core MD08-3180 retrieved S.W. of the Azores Islands at ~3060 m water depth to establish both absolute age control and a record of past ^{14}C reservoir ages of ocean surface waters. Both $\delta^{18}O$ minima of *G. bulloides* and high planktic reservoir ages of ~1600 to 2170 yr suggest two major melt water incursions that reached down to the subtropics over Heinrich Stadial 1 (HS-1). In parallel, we established a robust record of benthic ventilation ages that sum planktic ^{14}C reservoir ages and the age difference between paired benthic and planktic foraminifera ^{14}C ages at the site and time of deposition, a sum finally adjusted to past changes in atmospheric ^{14}C preceding since the time of deep-water formation. Near the Azores apparent deep-water ages of the Last Glacial Maximum (LGM) were as low as 340–740 yr, which suggests local formation of North Atlantic Deep Water (NADW) in contrast to a widely assumed shoaling of glacial deep-water formation. During HS-1, local benthic ventilation ages rose up to 2200–2550 yr, thus reflect an incursion of old southern-source deep waters, an instable regime that was interrupted by brief pulses of NADW formation near 16, 15.6 cal. ka, and most impressive near 14.9/14.7.

2.2. Introduction

Peak glacial Atlantic Meridional Overturning Circulation (AMOC) and climate are widely considered as a state fairly stable over several thousand years, with a current geometry that may have been similar to that of today (Fig. 2.1b; benthic $\delta^{13}C$ records of Duplessy et al., [1988], Sarnthein et al., [1994], and Curry and Oppo [2005]). In this scheme glacial North Atlantic Deep Waters (NADW) initially penetrated down to almost 3600 m depth near the Azores [*Sarnthein et al.*, 1994]. Farther south, however, they were strongly diluted by southern-source waters admixed from below. In a second scheme, glacial AMOC as a whole may have shoaled up to less than 2000 m depth [*Ferrari et al.*, 2014; *Gebbie*, 2014]. Any decision on these hypotheses will take unequivocal evidence based on new paleoceanographic records.

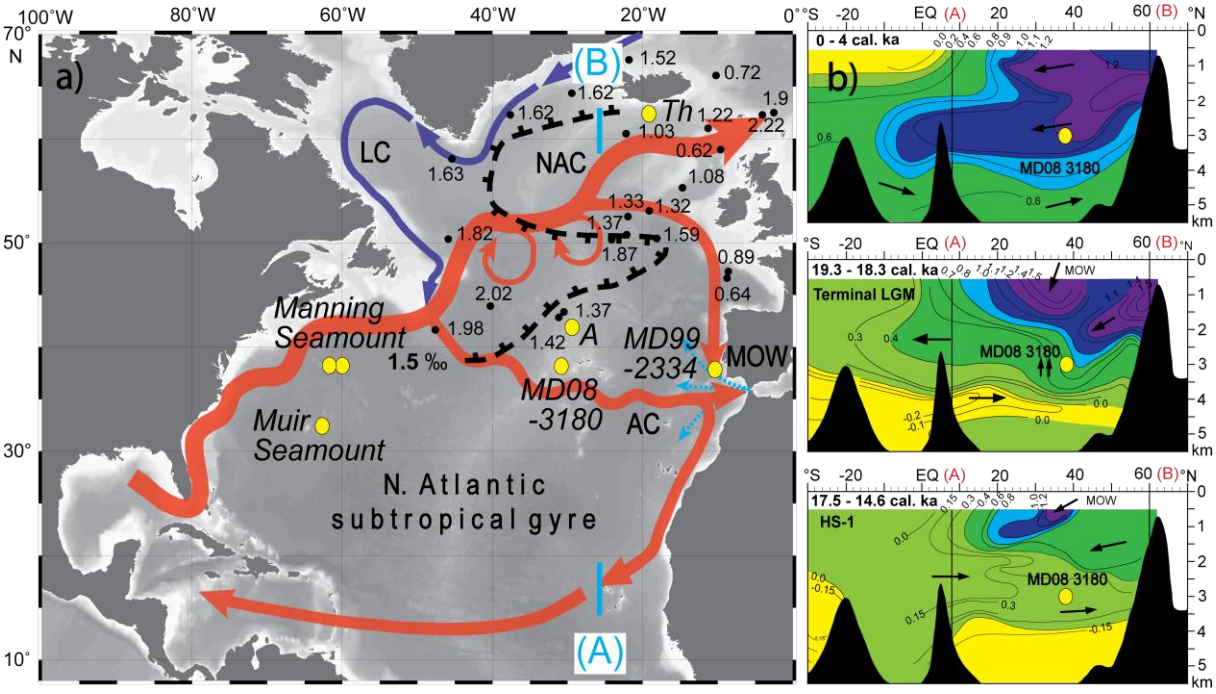

Figure 2.1: a) North Atlantic surface currents (Schott et al. [2004] and Schwab et al. [2012], modified) and Mediterranean Outflow Water (MOW; light blue arrows). AC: Azores Current, LC: Labrador Current, NAC: North Atlantic Current. Yellow dots are core locations. 'A' stands for samples from Azores Seamount [*Adkins et al.*, 1998], Th for RAPiD cores 15-4 and 17-5 [*Thornalley et al.*, 2011]. Small black numbers and broken 1.5‰ isoline show negative planktic $\delta^{18}O$ anomalies of HS-1 vs. LGM. High anomalies locate melt waters in northwest Atlantic [*Cortijo et al.*, 2005]. b) East Atlantic $\delta^{13}C$ transects for the last 4000 yr, terminal LGM, and HS-1 [*Sarnthein et al.*, 1994, modified). (A) and (B) give range of latitudinal transects shown in Fig. 1B.

In contrast, AMOC is regarded as highly instable during the last deglaciation (18–8 ka), marked by millennial-scale climatic events in the North Atlantic that include a major cooling during Heinrich Stadial 1 (HS-1), 17.5–14.7 ka, and an abrupt warming in subpolar sea-surface temperatures near and air temperatures over Greenland at the onset of the Bølling-Allerød (B/A) interstadial (14.7–13 ka) [*Grootes and Stuiver*, 1997; *Waelbroeck et al.*, 1998; *Bard et al.*, 2000; *Steffensen et al.*, 2008]. Similar to other stadials, HS-1 is marked by short-term minima in planktic $\delta^{18}O$ (Fig. 2.1a; [*Cortijo et al*. 2005]). They suggest a scenario of massive iceberg and melt water outbreaks originating from various source regions around the northern North Atlantic, in particular, from the Labrador Sea. Icebergs from the latter region were documented by source-specific ice rafted debris (IRD) all over the North Atlantic up to Morocco [*Kudrass and Seibold*, 1973; *Bond et al.*, 1992; *Grousset et al.*, 1993; *Bond and Lotti*, 1995; *Dowdeswell et al.*, 1995; *Vidal et al.*, 1997; *Hemming et al.*, 1998; *van Kreveld et al.*, 2000; *Bard et al.*, 2000].

In turn, the melt waters led to fundamental changes in AMOC [*Sarnthein et al.*, 1994; *Sarnthein et al.*, 2001; *McManus et al.*, 2004; *Liu et al.*, 2009], a pattern largely confirmed by recent coral data from the northwest Atlantic [*Thiagarajan et al*., 2014]. In contrast to modern and LGM AMOC geometries, HS-1 was marked by low benthic $\delta^{13}C$ values (Fig. 2.1b). These nutrient-enriched abyssal waters replaced NADW and dominated vast portions of the North Atlantic basin up to <1800 m water depth [*Sarnthein et al.*, 1994]. They probably had an origin in the Southern Ocean, a model to be constrained by further evidence.

Surface waters in the modern subtropical North Atlantic are dominated by eddies of the Azores Current (AC) that form the northern margin of the subtropical gyre [*Gould*, 1985; *Schiebel et al.*, 2002]. As a southern branch of the Gulf Stream the AC originates southeast of the Grand Banks, extends down to >1000 m water depth, and meanders across the Mid-

Atlantic Ridge near to the Azores Islands between 32° and 36°N up to Gibraltar [*Rogerson et al.*, 2004; *Volkov and Fu*, 2011]. The south dipping Azores Front (AF), defined by the 15°C isotherm, separates the AC from the subtropical gyre [*Gould*, 1985]. Recent model simulations suggest that meltwaters from icebergs originating from the Labrador Sea may cross the AF up to marginal regions of the subtropical gyre through mixing with Gulf Stream waters [*Hill and Condron*, 2014]. Consequentially the search for HS-1 meltwater incursions near the Azores forms a central target of this study, in particular, by employing negative planktic $\delta^{18}O$ excursions and extreme rises in planktic ^{14}C reservoir-age as proxies.

Modern ^{14}C reservoir ages of surface waters differ significantly over the global ocean, ranging from 270 yr in the Mediterranean and northern South China Sea up to 1300 yr off Antarctica [*Stuiver and Braziunas*, 1993; *Hua et al.*, 2005]. Likewise, they were highly variable in the northern North Atlantic over the last 20 kyr as derived from ^{14}C plateau tuning [*Sarnthein et al.*, 2007; 2015] and from age-calibrated deglacial climate events in sediment cores. Either these events are tied to pertinent tipping points in age-calibrated climate records of ice cores [*Thornalley et al.*, 2011; *Skinner et al.*, 2014] and/or to age control points fixed to volcanic ash layers [*Waelbroeck et al.*, 2001]. Occasionally planktic ^{14}C reservoir ages reached ~2170 yr during HS-1 and early B/A. Apparently aberrant reservoir ages for surface waters may actually belong to ^{14}C-depleted old subsurface waters that flew below HS-1 sea ice and meltwaters, with the highest ages linked to the center of melt water lids such as in the East Greenland Current today [*Sarnthein et al.*, 2001; 2007].

Today, centennial-scale changes in apparent deep-water ^{14}C ventilation ages help us to trace modern flow directions in the abyssal ocean at >1500 m w.d., since these ages rise with growing distance from the site of deep-water formation finally reaching a maximum of 2400 yr in upper deep waters of the North Pacific [*Matsumoto*, 2007]. By analogy, apparent deep-

water ventilation-ages may provide new insights into glacial-to-deglacial changes in the pattern of deep-water circulation. For example, Thornalley et al., [2011] and Sarnthein et al., [2013] suggest that the intensity of AMOC has strongly varied over the Last Glacial Maximum (LGM) and HS-1, showing millennial-scale reversals in deep-water flow as a result of short-lasting melt water incursions in the northern North Atlantic.

During HS-1 short-term breakdowns in NADW formation led to deep-water reservoir ages of 3300 yr along the Iberian Margin [*Skinner et al.*, 2014] and >5000 yr in the northeasternmost North Atlantic [*Thornalley et al.*, 2011], then a 'dead-end' of Atlantic deep-ocean circulation [*Sarnthein et al.*, 2013]. In the present study we focus on the regional distribution of past deep-water ventilation ages all over the North Atlantic to assign more closely the actual source of strangely old deep waters to northern or southern regions of deep and intermediate water formation.

Coral-based ^{14}C reservoir ages [*Robinson et al.*, 2005] and model results [*Liu et al.*, 2009] likewise suggest that the end of HS-1 was marked by an abrupt end of northern-source meltwater discharge and a sudden recovery and overshoot of AMOC in the northern North Atlantic directly at the onset of B/A [*Liu et al.*, 2009], an event now also to be constrained by our benthic $\Delta^{14}C$ records.

Sediments in the central mid-latitude Atlantic, the region of Site MD08-3180, offer an ideal high-resolution archive to resolve the objectives listed above. Here we discuss a paired record of benthic and planktic ^{14}C reservoir ages to trace past changes in AMOC and the composition and origin of deep waters in the Azores region at ~3060 m w.d. over glacial-to-deglacial times. In particular, we monitor past changes in the ^{14}C reservoir age of surface waters at ~20.5–13 cal. ka on the basis of ^{14}C plateau tuning. These ages are compared to

planktic $\delta^{18}O$ meltwater signals as tracer of past melt water incursions from the Labrador Sea, that possibly formed a trigger of short-term changes in deep-water formation.

2.3 Materials and methods

Square Core MD08-3180 Cq was retrieved from a sediment pocket at the Mid- Atlantic Ridge S.W. of the Azores Islands (38°N, 31°W, 3064 m w.d.) [*Kissel et al.*, 2008] (Fig. 2.1), where narrow, steep-flanked basins form traps for suspended sediments [*Richter*, 1998]. Discontinuities in trapping may lead to widespread, 2–4 cm thick sediment laminations at sedimentation rates reaching up to 60–160 cm / kyr (Fig. 2.2) details of sample processing in Suppl. Text 2.1).

Paired $\delta^{18}O$ and $\delta^{13}C$ records of the planktic foraminifer *Globigerina bulloides* [*Schwab et al.*, 2012], a species that inhabits shallow surface waters, in particular during winter and spring (M. Kucera, pers. comm.), were enlarged by 154 data from 1.6–11 mbsf to establish a stratigraphic framework of marine isotope stages (MIS) 1–3 as a base for optimizing sample locations of AMS ^{14}C dating (Fig. 2.2; details of sample treatment in Suppl. Text 2). The $\delta^{18}O$ record of *G. bulloides* is compared to sea surface temperature (SST) signals of a paired $\delta^{13}C$ record (Fig. 2.3d; following Bemis et al. [2000]), paired stable-isotope records of *Globigerinoides ruber* and *Globorotalia truncatulinoides* (Fig. S2.1), and a U_k^{37}–based SST record at 280 – 390 cm core depth (Fig. 2.3c) [*Schwab et al.*, 2012] to unravel the actual meaning of short-term $\delta^{18}O$ oscillations.

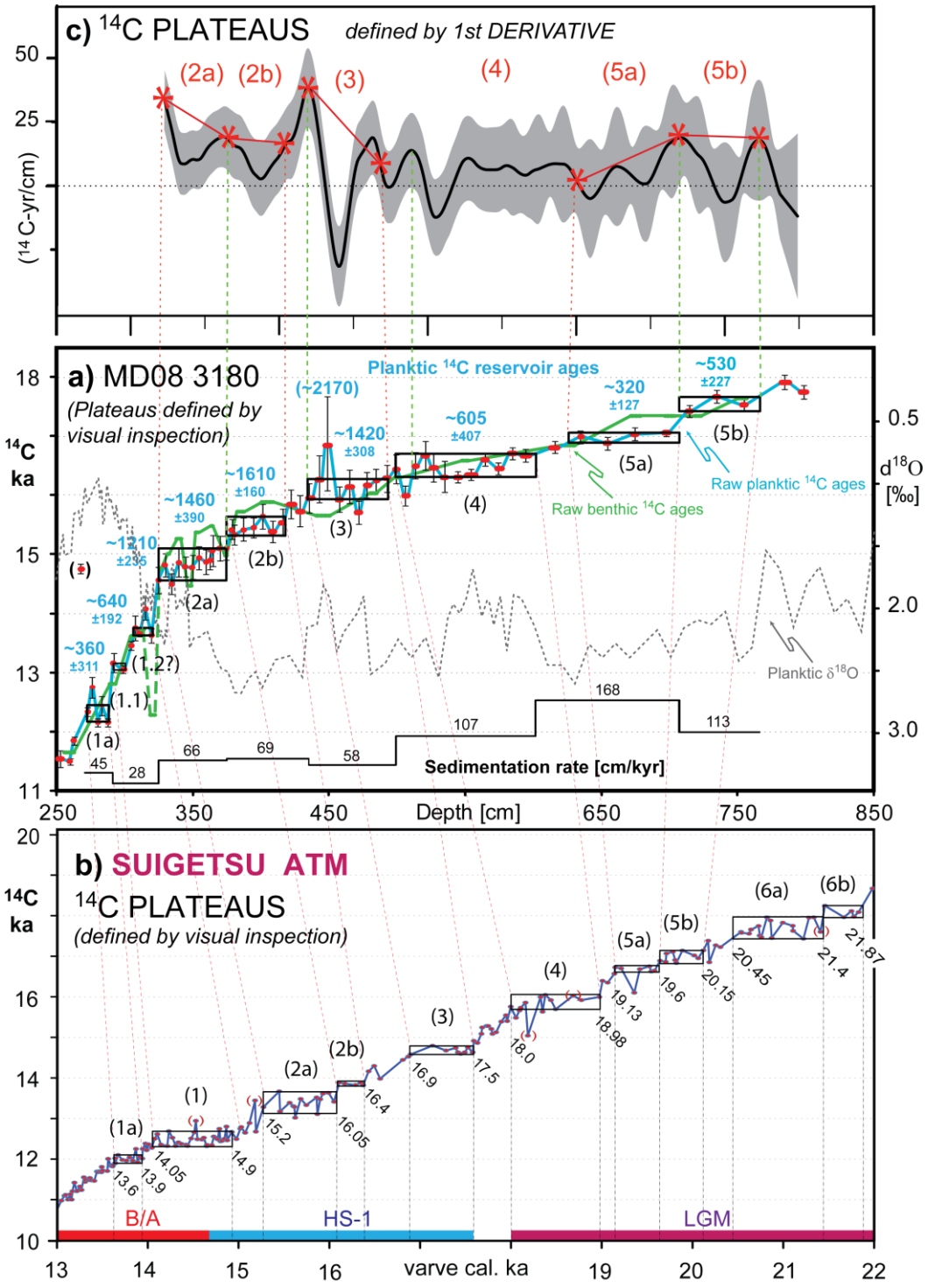

Figure 2.2: a) Planktic (red dots and blue line) and benthic (bold green line) ^{14}C records and planktic $\delta^{18}O$ record (black dotted line) of MD08-3180 plotted vs. core depth (*Sarnthein et al.*, [2015], modified). Upper and lower boundaries of planktic ^{14}C plateaus (horizontal boxes) are tuned (red broken lines) to (b) atmospheric (atm) ^{14}C plateau boundaries in ^{14}C record of Lake Suigetsu vs. varve age [*Bronk Ramsey et al.*, 2012]. Local planktic reservoir ages (blue numbers in (a)) represent the difference between average ^{14}C age of planktic ^{14}C plateaus measured in MD08-3180 and that of equivalent atmospheric ^{14}C plateaus numbered 1 – 6 (bold numbers in brackets). Sedimentation rates are interpolated between plateau boundary ages (see Suppl. Text 6). Top panel (c) shows units of the 1st derivative of the ^{14}C record in panel (a) in units of the change in ^{14}C yr per cm core depth, using a bandwith of 20 cm of the kernel function [*Sarnthein et al.*, 2015], with its 1-σ uncertainty ranges (ignoring a potential outlier age at 441–443 cm depth). Near-zero values of 1st derivative reflect ^{14}C plateaus (red numbers), short-term maxima ^{14}C jumps; negative values indicate age inversions. Red asterisks mark plateau boundaries either defined by ^{14}C jumps (tied to plateau boundaries in panel (a) by green broken lines) or by the half-height of derivative slopes (tied by red broken lines). Plateau 4 is poorly defined in record of 1st derivative. B/A = Bølling-Allerød, HS-1 = Heinrich Stadial 1, LGM = Last Glacial Maximum.

Except for rare specimens near the very top of HS-1, sediments in Core MD08-3180 are almost barren of epibenthic foraminifera tests. Thus it was impossible to prolong the (fairly noisy) epibenthic $\delta^{13}C$ record of lower B/A [*Repschläger et* al., 2015] further downcore back to the LGM, except for a single specimen analyzed near its top.

The backbone of our study forms a high-resolution planktic ^{14}C record from a sediment section at 250–800 cm core depth (Fig. 2.2a, Table S2.1). On average, ^{14}C samples are 8 cm wide spaced, somewhat closer near ^{14}C plateau boundaries. The record was measured on *G. bulloides*, a shallow-dwelling species that was abundant in the study area over glacial-to-deglacial times [*Schiebel et al.*, 2002].

23 paired ^{14}C ages were measured on mixed benthic species with a sampling density that provided 2–3 benthic age estimates for each planktic ^{14}C plateau (Table 2.1; analytical details in Suppl. Text 2.2 and 2.3). Ideally epibenthic species (e.g., *Cibicidoides wuellerstorfi*) were preferred for ^{14}C dating to avoid a bias of ventilation ages by infaunal species. However, insufficient epibenthic specimens (Table 2.1) led us to a dominant use of infaunal species such as *Bulimina sp*. In contrast, porcellaneous benthic species were excluded from analysis since Magana et al. [2010] showed that deep infaunal habitats of *Pyrgo sp*. and other taxa lead to calcification in old pore waters depleted in ^{13}C and ^{14}C and thus, to an aberrant increase of ^{14}C age. Since a major portion of benthic ^{14}C ages in MD08-3180 is equal to paired planktic ^{14}C ages or even younger (Figs. 2.2, 2.3e) infaunal habitats obviously were little relevant to local benthic ^{14}C ages.

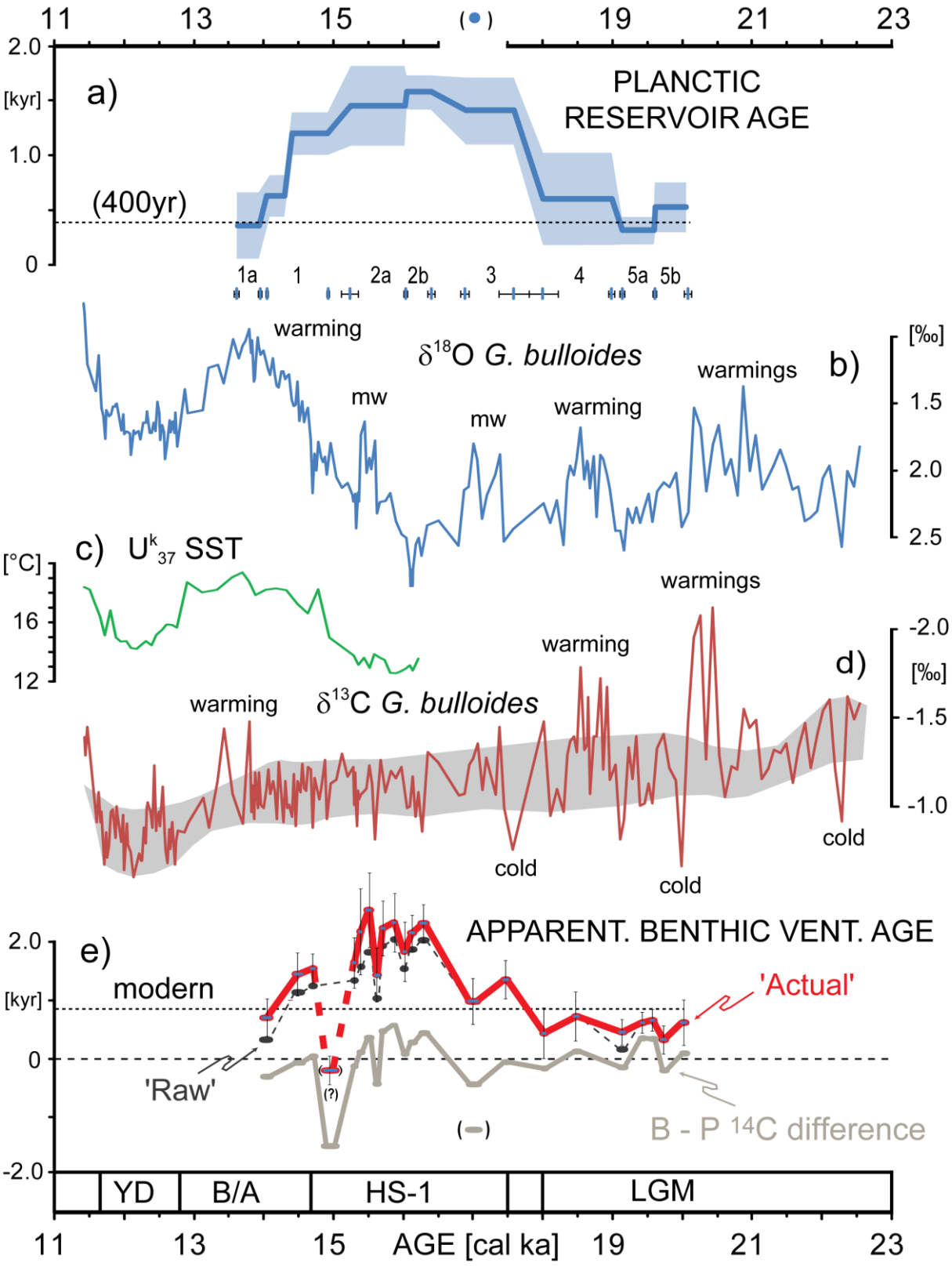

Figure 2.3: a) Early deglacial maximum in planktic reservoir ages at Site MD08-3180 and uncertainty in age assignment of ^{14}C plateau boundaries (indicated by numbers) plotted vs. cal. age. b) Planktic $\delta^{18}O$ record of short-term meltwater (mw) incursions (linked to high planktic reservoir ages) and warmings as indicated by (c) a rise in Uk^{37}-based SST (*Schwab et al.*, 2012) and (d) negative $\delta^{13}C$ excursions of *G. bulloides* beyond general noise level (–0.5 ‰ corresponds to ~5°C, based on empiric data of Bemis et al. [2000]. e) Difference between benthic and planktic ^{14}C ages (gray line), which serves as basis for estimates of 'raw' and 'actual' benthic ^{14}C ventilation ages calculated for the atmospheric ^{14}C inventory contemporary with sediment deposition (black broken line) and that coeval with antecedent deep-water formation (red line). Note the short-lasting extreme in planktic reservoir age near 17 cal. ka matches a negative excursion in benthic-planktic age difference and a marked planktic $\delta^{18}O$ minimum.

Table 2.1: Percentage of epibenthic species in benthic ^{14}C ages and derivation of apparent deep-water ventilation ages for MD08-3180. Actual ventilation ages are corrected for shifts in atmospheric ^{14}C inventory subsequent to deep-water formation. *No age correction for negative ventilation age

Depth [cm]	Calendar age [yr]	Raw Benthic ^{14}C age [yr]	1σ error [yr]	Pla. res. age [yr]	B-P age difference [yr]	Raw Benthic vent. age [yr]	Raw Benthic $\Delta\Delta^{14}C$ [‰]	'Actual' Benthic vent. age [yr]	'Actual' Benthic $\Delta\Delta^{14}C$ [‰]	Epi-benthic Species [%]
289.5–292.5	13995 - 14095	12810	±60	640	-300	340	50	700	100	36.05
304.5–307.5	14455 - 14545	13620	±60	1210	-60	1150	167	1460	217	2.86
312.5 –313.5	14695 - 14725	13730	±30	1210	50	1260	189	1560	239	8.6
***318.5–321.5**	14875 - 15038	12290	±60	1210	-1390*	-181*	-23	-181*	-	18
325.5–326.5	15287 - 15302	14770	±35	1460	-120	1340	200	1650	250	3.8
331.5–332.5	15377 - 15392	15010	+80/ -70	1460	120	1580	233	2180	333	2.9
338.5–341.5	15483 - 15528	15260	±80	1460	370	1830	265	2540	365	14.13
346.5–348.5	15604 - 15634	14470	±70	1460	-420	1040	165	1440	165	6.07
352.5–353.5	15694 - 15710	15370	±160	1460	480	1940	290	2240	340	4.3
363.5–364.5	15861 - 15876	15480	±160	1460	590	2050	305	2350	355	5.07
373.5–374.5	16012 - 16027	14980	±160	1460	90	1550	237	1850	287	3.22
382.5–387.5	16105 - 16148	15730	±90	1610	290	1880	282	2170	332	16.04
400.5–408.5	16259 - 16372	15890	+180/ -170	1610	450	2060	303	2330	353	0.53
440.5–450.5	16937 - 17063	15660	±200	1420	-430	990	162	990	162	3.6
480.5–484.5	17441 - 17491	16040	±60	1420	-50	1370	219	1370	219	0.27
498.5–502.5	18000 - 18028	16300	±100	605	-160	450	76	450	76	0.24
547.5–552.5	18454 - 18501	16590	±100	605	130	740	123	740	123	0.062
620.5–630.5	19066 - 19161	16850	±60	320	-140	180	32	460	81	1.35
671.5–678.5	19389 - 19438	17350	±110	320	360	680	109	630	109	0.07
697.5–703.5	19548 - 19582	17340	±130	320	350	670	116	670	116	0.36
718.5–723.5	19705 - 19749	17350	±60	535	-190	345	60	340	60	0.2
750.5–756.5	19987 - 20040	17640	±90	535	100	630	110	630	110	0.16

We derive both absolute calendar ages and planktic ^{14}C reservoir ages by means of the '^{14}C Plateau Tuning Method' [*Sarnthein et al.*, 2007; 2015]. That is, we correlate plateaus and jumps in our planktic ^{14}C record to pertinent features in the varve-counted atmospheric ^{14}C record of Lake Suigetsu [*Bronk Ramsey et al.*, 2012] between ~20.5 and 13 cal. ka (details in Suppl. Text 2.4). The Lake Suigetsu ^{14}C record is the only decadal-to-centennial scale resolution atmospheric ^{14}C and $\Delta^{14}C$ record extending beyond 13.9 cal ka [IntCal13; *Reimer et al.*, 2013]. We regard its varve counted time scale as superior to the modeled time scale for peak glacial and deglacial times (IntCal13), because the modeled time scale is partially based on carbonates and tuned to the U/Th-based time scale of the Hulu 2 speleothem. The carbonate-based oceanic and (Hulu Cave) speleothem ^{14}C dates may suffer from possibly

variable surface water reservoir ages and 'dead-carbon' fractions (broadly discussed in Sarnthein et al. [2015]).

Following Sarnthein et al. [2007; 2015] we defined several boundary conditions for the process of ^{14}C plateau tuning and the calculation of planktic ^{14}C reservoir ages:

(1) To display ^{14}C plateaus as short as 300 yr marked by two or three ^{14}C dates each sedimentation rates should exceed 10 cm/kyr, moreover, the sampling resolution should be better than 100–150 yr.

(2) To identify more objectively the ^{14}C plateaus and jumps in the ^{14}C record we also employ a mathematical method (Fig. 2.2c) that uses the first derivative of all down-core changes in the ^{14}C age–core depth (or –calendar age) relationship [*Sarnthein et al.*, 2015].

(3) To identify the individual ^{14}C plateaus, the complete suite of plateaus and their internal structures need to be considered. In case of several tuning choices, the lowest possible planktic reservoir age estimates are accepted, if no different stringent evidence is suggesting any higher value. For example, paired benthic ^{14}C ages that are lower than the coeval planktic ^{14}C age (examples in Fig. 2.2a) may necessarily imply increased planktic ^{14}C reservoir ages to provide an apparent benthic ^{14}C ventilation age larger than ~400 yr [*Matsumoto*, 2007], since smaller and negative benthic ventilation ages are physically impossible.

Planktic average reservoir ages were calculated by subtracting one-by-one the average atmospheric ^{14}C age of pertinent plateaus in the Suigetsu record from the average ^{14}C age of each planktic ^{14}C plateau. Our approach is based on tuning a full suite of ^{14}C plateaus. Accordingly, the robustness of the plateau tuning technique does not suffer from the loss of any single plateau, which in turn may provide important insights into changes of the sedimentation regime.

In turn, 'raw' apparent benthic ventilation-ages resulted from the sum of planktic ^{14}C reservoir ages and the difference between paired benthic and planktic ^{14}C ages (Fig. 2.4b and Suppl. Text 2.5). Finally, the raw benthic ventilation ages were corrected for changes in atmospheric ^{14}C concentration between the last contact of deep waters with the atmosphere and the time of sediment deposition (scheme in Fig. 2.4a). Thus the results employ a kind of backward 'projection method' [*Adkins and Boyle*, 1997], equivalent to $\Delta^{14}C_{0,adj}$ and $\Delta^{14}C_{0\text{-}atm}$ values defined by Cook and Keigwin [2015]. Note we implicitly assume that the planktic reservoir age at the time and site of sediment deposition was equal to that at the time and site of deep-water formation.

The stratigraphic boundaries of the LGM are slightly modified from those defined by Mix et al., [2001]. We use a time window of the 'Last Isotopic Maximum' defined by GLAMAP [Sarnthein et al., 2003a], that lasted slightly longer than the classical LGM, from 23–18 cal. ka, since the isotopic composition of North Atlantic Deep Water has persisted over ~1000 yr beyond the initial rise of deglacial sea-level. For HS-1 (17.5–14.7 cal. ka) we follow Denton et al., [2006] and Sarnthein et al., [2011], for the B/A (14.7–12.9 cal. ka) we follow the GICC05 time scale [*Svensson et al.*, 2008].

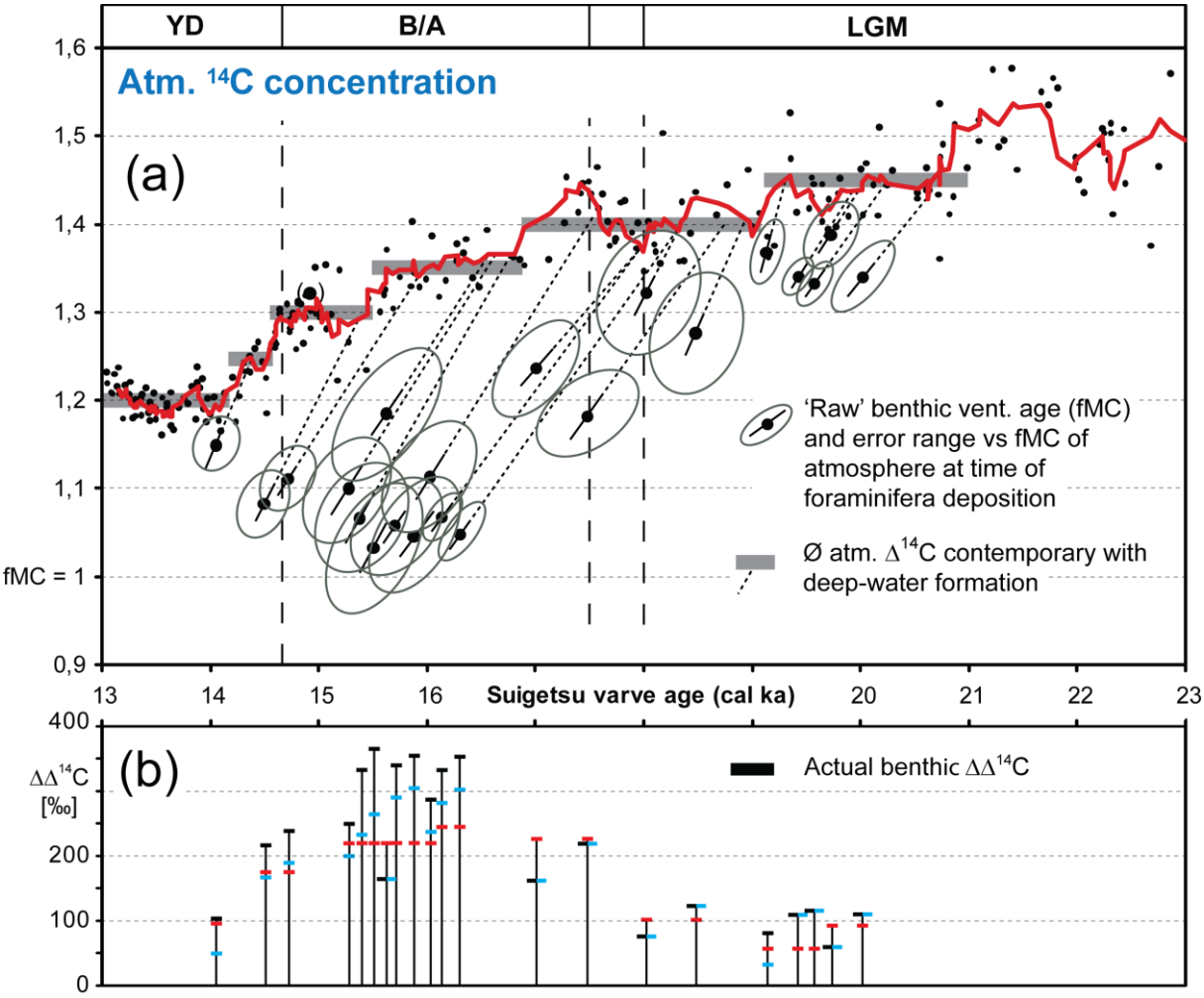

Figure 2.4: a) Glacial-to-deglacial changes in atmospheric ^{14}C concentration, presented as Fraction of Modern Carbon (fMC) (grey bars show long-term average) [*Bronk Ramsey et al.*, 2012], and 'raw' benthic $\Delta\Delta^{14}C$ values (equivalent to 'raw' benthic ventilation ages) shown as deviation (in per mil) from the average atmospheric ^{14}C concentration at the time and site of sediment deposition, with uncertainty ranges. 'Actual' apparent deep-water ages (excluding any mixing of deep waters from different ocean sources) are derived in two steps, (1) from the backward projection of the raw atmospheric-benthic $\Delta\Delta^{14}C$ anomalies over the time span of raw benthic ^{14}C ventilation ages to time of deep-water formation (per analogy to the horizontal leg of a right-angle triangle) and (2) from measuring the per mil fMC difference from the average atmospheric fMC at the time of deep-water formation (per analogy to the vertical leg of a right-angle triangle) shown by the intercept of (dotted) projection lines (that each present the hypotenuse of a right-angle triangle). In this way most raw $\Delta\Delta^{14}C$ values increase, in rare cases they decrease. This approach is consistent with requirements of Cook and Keigwin [2015] for $\Delta^{14}C_{0,adj}$ and $\Delta^{14}C_{0\text{-}atm}$ values, except for our use of straight projection lines instead of radioactive decay curves, a simplification legitimate in view of other much larger uncertainties such as the definition of intercepts with past atmospheric $\Delta^{14}C$ values (details in Suppl. Text S5). b) Summary of the derivation of 'actual' benthic $\Delta\Delta^{14}C$ values (equivalent to ^{14}C ventilation ages; black stroke; plotted vs. cal. age of sediment deposition) from the sum of planktic $\Delta\Delta^{14}C$ at the time and site of deposition (red stroke) plus the benthic–planktic $\Delta\Delta^{14}C$ difference (equivalent to benthic-planktic ^{14}C age difference at time of deposition; reaching up to the blue stroke) plus the shift in average atmospheric fMC between the time of deep-water formation and that of sediment deposition. Note we implicitly assume that the planktic reservoir age at the time and site of deposition was equal to that at the time and site of deep-water formation, actually unknown.

2.4 Results

2.4.1 Initial stratigraphic framework based on a $\delta^{18}O$ record

The planktic $\delta^{18}O$ record gave an initial overview of deglacial paleoceanography and a stratigraphic framework, to locate optimum sample depths in core MD08-3180 for AMS ^{14}C dating (Figs. 2.2a and 2.3b). Accordingly, $\delta^{18}O$ values average near 2.3 ‰ for the LGM (ignoring some meltwater-induced negative outliers at 630–310 cm core depth) and near 0.8–1.25 ‰ for the B/A. Four distinct tri- or bipartite $\delta^{18}O$ minima reaching 1.5, 1.7, 1.8, and 1.6 ‰ each occur at 820–770 (20.5–20.1 cal. ka), 630–530 (19.0–18.3 cal. ka), 480–430 (17.4–16.8 cal. ka), and 380/346–332 cm core depth (16.0/15.6–15.38 cal. ka). These $\delta^{18}O$ excursions can hardly be ascribed to short-term changes in global ice volume. Two $\delta^{18}O$ minima around 20.3 and 18.7 cal. ka match distinct negative $\delta^{13}C$ excursions of 0.4 and 0.7 ‰ (Fig. 2.3d), an equivalent of short-term warmings by ~3° and ~6°C [*Bemis et al*., 2000]. In contrast, the two excursions of ~0.8 ‰ (a potential equivalent to local warming by up to ~4°C) near 17.1 and 15.5 cal. ka may be assigned to local melt water advection during HS-1, since they do not match any negative $\delta^{13}C$ signal beyond the noise level nor any rise in Uk_{37}-based SST (Fig. 2.3c).

2.4.2 Planktic ^{14}C record

Our high-resolution planktic record of surface water ^{14}C shows raw ^{14}C ages that gradually dropped from 17.75 to 16.0 ^{14}C ka from 800 to 440 cm core depth. Between 332.5 and 251.5 cm the ages steeply dropped from 14.8 to 11.5 ^{14}C ka (Fig. 2.2a).

Very large analytical uncertainties ranging up to 800 yr occur between 270 and 500 cm depth. They are linked to samples that were subject to overly excessive CO_2 cleaning by re-combustion at the Leibniz Laboratory, Kiel, which resulted in samples, where the analytical

uncertainty was blown up by the blank uncertainty. Despite these high uncertainty ranges visual inspection reveals a ^{14}C record that depicts several broad intervals of constant ^{14}C ages extending over 15.5–104.5 cm sediment depth each (definition of plateau boundaries and the derivation of average ^{14}C ages in Table 2.2).

Table 2.2: Definition of planktic ^{14}C plateaus in MD08-3180 (defined by visual inspection) (Sarnthein et al. [2015], modified). Pla. res. age = Planktic reservoir age. Atm. fMC = Atmospheric ^{14}C concentration as fraction of modern carbon.

Plateau No.	Age top [cal yr]	Depth [cm]	Age base [cal yr]	Depth [cm]	MD08-3180 Ø ^{14}C yr	Suigetsu Plateau Ø ^{14}C yr	Pla. res. age [yr]	Pla. $\Delta\Delta^{14}C$ [‰]	1 σ error [yr]	1 σ error [‰]	Atm. fMC
1a	13640	272.5	13940	288	12370	12006	370	54	311	38	1.20
1	14050	291	14921	320	13110/13720	12471	640/1210	96/175	192/235	30/36	1.25
2a	15272	324.5	16050	376	14885	13426	1460	220	390	63	1.325
2b	16050	376	16400	417	15460	13850	1610	245	160	27	1.35
3	16900	434.5	17580	493.5	16090	14671	1420	227	308	53	1.40
Outlier	17025	447.5	17063	450.5	16840	14671	2170	331	800	133	1.40
4	18000	498.5	18980	603	16455	15851	605	102	407	69	1.40
5a	19130	625	19600	706.5	16990	16670	320	57	127	23	1.45
5b	19600	706.5	20150	769	17540	17007	535	93	227	39	1.45

2.4.3 Tuning of ^{14}C plateaus to atmospheric ^{14}C plateaus in Lake Suigetsu record

The planktic ^{14}C record of MD08-3180 was tuned to the atmospheric ^{14}C record and varve-based chronology of Lake Suigetsu (Table 2.2 and Fig. 2.2b). Two extreme outlier ages at 267.5–268.5 and 447.5–450.5 cm depth were not incorporated into any (non-weighted) average of the ^{14}C plateaus (details in Suppl. Text 2.4). In total, we identified a suite of six ^{14}C plateaus between Plateau 1a (top at ~13.6 cal. ka) and Plateau 5b (base at 20.26 cal. ka), thereby obtaining 10, possibly 13, age control points.

Per analogy to Suigetsu it was hard to identify Plateau 1, since it falls into an interval of strongly decreasing planktic ^{14}C reservoir ages from~14.7 to 11.5 ^{14}C ka between 330–260 cm core depth. However, a suite of two very short plateaus between 291 and 320 cm depth may represent ‘lobate’ fragments of Plateau 1. Surface water reservoir ages would become

negative (-316 yr, -170 yr), if the 'mini-' plateaus were tuned to the next-older Plateaus 2a and 2b. Our conclusion on a fragmented Plateau 1.1–1.2 is corroborated by (1) the planktic $\delta^{18}O$ record that appears continuous and (2) by sediment fabrics that do not reveal any stratigraphic gap, though long-term sediment rates were short-term reduced by 50% at the presumable position of Plateau 1.

Despite unusually large analytical uncertainties for ages between 270 and 500 cm core depth, the plateau boundaries derived by the 1st derivative (Fig. 2.2c) closely match the boundaries derived by visual inspection for Plateaus 2a, 2b, 3, 5a and 5b [*Sarnthein et al.*, 2015]. Plateau 4 shows an internal structure similar to its atmospheric counterpart, but is not depicted in the 1st derivative. Also, fragmented Plateau 1 is not reflected in the 1st derivative (details on plateau boundaries and corresponding calendar ages in Suppl. Text 2.4).

2.4.4 Sedimentation rates

Sedimentation rates for core MD08-3180 (Fig. 2.2a, Table S2.2) were estimated from the thickness of core sections between age-calibrated ^{14}C plateau boundaries. The rates vary between 168 and 59–70 cm/kyr over the upper LGM and HS-1. During the B/A they dropped to 28–45 cm/kyr, an estimate that closely agrees with rates derived by Schwab et al. [2012] on the basis of a U^{k}_{37}-based SST record tuned to the NGRIP $\delta^{18}O$ record. Reduced sedimentation rates during B/A may result from a reinforced AMOC that led to enhanced winnowing of fine grain sizes at the core site.

2.4.5 Planktic reservoir ages

Planktic ^{14}C reservoir ages ($\Delta\Delta^{14}C$ values) were separately deduced for each single ^{14}C plateau in our record (Table 2.2). During the LGM (Figs. 2.2a and 2.3a), they varied between 320 ± 125 yr and 600 ± 400 yr, in contrast to HS-1 where they ranged from 1215 ± 235 yr to

1610 ± 160 yr (at σ=1). These high surface-water reservoir ages were indirectly confirmed by four paired benthic ^{14}C ages that would produce extremely low, almost negative, hence physically impossible apparent benthic ventilation ages, in case the surface-water reservoir-ages were lower than those derived by our tuning technique (details in Suppl. Text 2.4). The ^{14}C outlier at 447.5–450.5 cm depth may even reflect a short excursion of reservoir ages up to 2170 ± 800 yr in the middle of HS-1. At the onset of the B/A planktic reservoir ages still were of 1210 ± 190 yr. Subsequently they dropped to 360 ± 240 yr at 13.9 cal. ka.

2.4.6 Benthic ^{14}C record and raw benthic ventilation ages

Raw benthic ^{14}C ages slowly drop from 17.6 to 15.3 ^{14}C ka from 750–340 cm core depth. Farther upcore, they quickly decrease from 15.3 to 11.7 ^{14}C ka. Striking young outliers mark core depths near 445, 373, 347, and 320 cm (Fig. 2.2a and Table 2.2).

Raw apparent benthic ventilation-ages (Fig. 2.3e; Table 2.1) were low all over the LGM, ranging between 180 ±160 and 740 ±350 ^{14}C yr. During HS-1 and the onset of B/A, they varied from 1150 ±210 to 2050 ±300 ^{14}C yr, but dropped to 340 ±200 yr during B/A at 14.0 cal. ka.

2.4.7 Benthic ventilation ages adjusted to past changes in atmospheric ^{14}C

As outlined above, ‘actual’ benthic ventilation ages incorporate short-term changes in atmospheric ^{14}C that have occurred since the time a water mass lost contact with the atmosphere (Fig. 2.4; Suppl. Text 5). These adjustments lead to ‘actual’ benthic ventilation ages of 340–740 ^{14}C yr for the LGM prior to 18 cal. ka (Table 2.2; Fig. 2.3e). From 18–17 cal. ka, they clearly increased to 990–1370 ^{14}C yr. During HS-1, these ages reached peak values of ~2170–2540 ^{14}C yr. After the onset of B/A they dropped from 1560 to 700 ^{14}C yr.

Low benthic ventilation ^{14}C ages form brief excursions near 17.0, 16.0 and 15.6 cal. ka, where paired planktic reservoir ages in part exceed the 'raw' benthic ventilation ages by ~430 ^{14}C yr (Figs. 2.2a and 2.3e; Table 2.2). A most extreme low in benthic ventilation age occurs at 14.9 cal. ka (373–375 cm depth) with ('raw' and 'actual') values of -180 ± 210 yr that are physically impossible and hard to explain. In this particular core section both sediment laminations [*Kissel et al.*, 2008] and a lack of any evidence for bioturbation refute an interpretation by downcore bioturbation. Note, the benthic low matches a likewise aberrant low in raw planktic ^{14}C age, 660 ^{14}C yr lower than expected from hypothetical ^{14}C age interpolation.

2.5 Discussion

2.5.1 Boundary conditions of ^{14}C plateau tuning that influence the age model

We are tuning the jumps and plateaus in our planktic ^{14}C record (Fig. 2.2a, 2.2c) to those in the varve-based atmospheric ^{14}C record of Lake Suigetsu [*Bronk Ramsey et al.*, 2012] (Fig. 2.2b). In this context, we need to consider the approximate depth range down to which short-term atmospheric ^{14}C signals are mixed into ocean surface waters and the time spans involved. Observations of the 'atomic-bomb effect' show that changes in surface ocean ^{14}C concentrations (top 10 m) closely reflect short-term variations in atmospheric ^{14}C activity within no more than a decade [*Nydal et al.*, 1980]. In the subtropics *G. bulloides* may serve as reliable tracer of surface-ocean conditions, since it preferentially inhabits the top 25–75 m of the upper mixed layer in the ocean (shown by the δ^{18}O signature [*Deuser et al.*, 1981; *Hemleben et al.*, 1989]; *Fairbanks et al.*, 1982; *Schmuker and Schiebel*, 2002]). Near the Azores *G. bulloides* seasonally reaches down to 300 m water depth during winter [*Schiebel et al.*, 2002], a vertical migration that leads to a ^{14}C record averaging the top 300 m. Nevertheless, our planktic ^{14}C record forms a suite of robust plateaus that closely mirror the

plateau structures recorded in the Lake Suigetsu atmospheric ^{14}C record, except for Plateau 1, hence justifies the use of the plateau tuning technique.

Furthermore, our age model for core MD08-3180 well compares to independent evidence such as the age model of Schwab et al. [2012] that is based on short-term SST oscillations. They were tuned to temperature-based tipping points in the $\delta^{18}O$ record NGRIP [*Andersen et al.*, 2004], here assuming that changes in topmost SST near the Azores were synchronous with temperature changes in North Greenland. Accordingly, the onset of B/A warming would begin at 320–315 cm depth. That was 7 cm (~200 yr) below DO event 1 as derived from both an abrupt 0.5-‰ reduction in planktic foraminifera-based $\delta^{18}O$ and ^{14}C plateau tuning, a record of the upper mixed layer of the ocean (Figs. 2.2a and 2.3b). Irrespective of differential bioturbational mixing of foraminifera and nannofossil biomarkers, the 200-yr offset lies within the uncertainty range, thus may largely support our age model based on plateau tuning. Moreover, there is a slight chance that the pronounced planktic $\delta^{13}C$-based warm spike we find near 20.5 cal. ka (Fig. 2.3) may correspond to a narrow-confined warm spike in GICC05 [*Andersen et al*., 2006] and a broad but modest warm oscillation in GISP2 [*Grootes and Stuiver*, 1997] at 20.52 cal. ka, a correlation that confirms the plateau-based chronology. However, in contrast to the scarce unequivocal climatic tie points in the ice cores, our ^{14}C plateau boundaries provide us with at least ten tie points, a yield clearly superior to that of the single warm spike at 20.5 ka. Moreover, Greenland temperature oscillations and SST near the Azores may even be anti-correlated by meridional shifts in the Azores Current in response to stadial events.

Indirect, though no stringent support may also come from the fairly uniform suite of sedimentation rates, with maximum rates during the LGM, medium high rates during HS-1, and minimum rates during early B/A (Fig. 2.2a).

2.5.2 Planktic stable isotopes and ventilation ages record HS-1 meltwater incursions

Low (~300–600 yr old) planktic reservoir ages mark both the LGM and B/A sections of MD08-3180 (Fig. 2.3a). We regard these ages as a record of well mixed, ventilated, thus ^{14}C enriched surface waters. In contrast, high planktic reservoir ages are encountered all over HS-1, a feature generally characteristic of upwelled subsurface waters and/or strong, ongoing meltwater-induced surface water stratification that leads to subsurface habitats of our planktic tracer species sealed-off from the atmosphere [*Sarnthein et al.*, 2007]. The latter scenario most likely applies to the high reservoir ages of open-ocean Site MD08-3180 far distant from any upwelling cell, also in absence of any IRD. Both model studies [*Hill and Condron*, 2014] and short-lasting deglacial negative anomalies in $\delta^{18}O$ of surface-waters [*Cortijo et al.*, 2005] indeed suggest an incursion of HS-1 meltwaters down to the subtropical North Atlantic (Fig. 2.1). To trace HS-1 meltwater pulses up to their periphery at Site MD08-3180 we now compare the (SST corrected) $\delta^{18}O$ signal of *G. bulloides* (Figs. 2.2 and 2.3; sampling resolution: 70–80 yr) with meltwater-specific trends in planktic ^{14}C reservoir-age (Fig. 2.3).

Immediately after the onset and during late HS-1 the $\delta^{18}O$ record shows two meltwater-induced 'bipartite' $\delta^{18}O$ minima at 17.4–16.8 and ~15.6–15.3 cal. ka. The latter also reappears in $\delta^{18}O$ minima of *G. truncatulinoides* and *G. ruber* [*Schwab et al.*, 2012; *Repschläger et al.*, 2015] (Fig. S2.1). The minimum at 17.4–16.8 cal. ka matches a unique extreme of 2170 yr in planktic reservoir age. A similar meltwater-induced reservoir age was reported for various other Heinrich events in the northern North Atlantic [*Sarnthein et al.*, 2001; *Waelbroeck et al.*, 2001; *Thornalley et al.*, 2011].

However, MD08-3180 does not contain any IRD as direct proof for meltwater advection. By comparison, Bard et al. [2000] monitored in Core Su81-18 two maxima in magnetic susceptibility (MS) and IRD deposition near 17.5 and 16.0 cal. ka, events they interpret as

major pulses of ice rafting off Portugal during HS-1. These ages, however, were deduced under the assumption of a constant surface water reservoir age near 400 yr. In case the planktic reservoir ages at Site Su81-18 had increased over HS-1 up to 1400–1600 ^{14}C yr per analogy to the ages we find in MD08-3180, the calibrated age of the IRD layers would drop to ~16.5/16.3 and 15.0/14.8 cal. ka, respectively. Thus, none of these events is matching the age of meltwater pulses found at MD08-3180, which may suggest major spatial variability of short-term meltwater incursions over HS-1.

Meltwaters near the Azores probably originated from the Labrador Sea. Hill and Condron [2014] simulated in their model a transport of icebergs and meltwaters from the Labrador Sea within a narrow coastal current alongshore North America up to 32.5°N, where icebergs mixed with Gulf Stream waters and eventually entered the subtropical gyre of the North Atlantic. Thus we indeed may conclude that Site MD08-3180 like site MD99-2334K off Portugal [*Skinner et al.*, 2014] were located within the southern periphery of Heinrich meltwater lids as documented by HS-1 reservoir age anomalies of >1000 yr in excess of planktic reservoir ages of the preceding LGM.

2.5.3 Benthic ventilation ages record glacial-to-deglacial changes of flow patterns in the deep Atlantic

Modern ventilation ages of deep waters at Site MD08-3180 amount to ~800 yr [*Matsumoto*, 2007]. By comparison, apparent benthic ^{14}C ventilation ages were as low as 340–740 ^{14}C yr during the LGM and terminal Bølling, in contrast to peak values of 2170–2540 ^{14}C yr during HS-1 and ~1500 ^{14}C yr in the early Bølling (Figs. 2.3e and 2.5c).

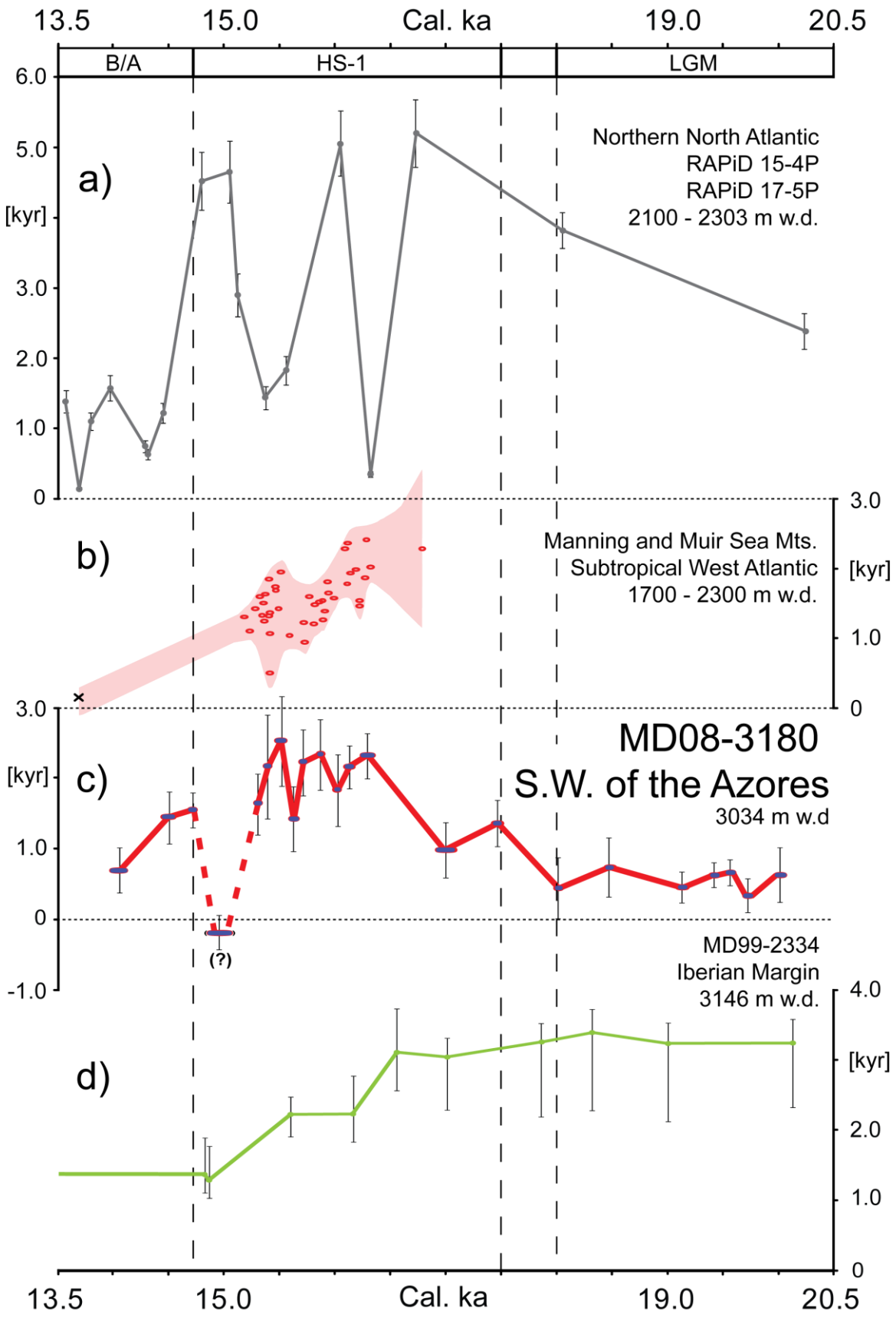

Figure 2.5: Comparison of short-term variations in Atlantic (apparent) deep-water ventilation ages (equivalent to $\Delta\Delta^{14}C$). a) Northern North Atlantic [*Thornalley et al.*, 2011]. b) Subtropical Western Atlantic; circles: coral ages of Robinson et al. [2005] and Adkins et al. [1998]; crosses: coral age of Azores Sea Mount; red shading = 1σ error range. c) 'Actual' apparent benthic ventilation ages and propagated error at Site MD08-3180 (details in Figs. 2.3 and 2.4). d) Iberian Margin [Skinner et al., 2014].

Accordingly, the LGM ventilation ages in the Azores region are unexpectedly low for 3060 m w.d.. They contrast with some high LGM deep-water ages reported from the South Iceland Rise [*Thornalley et al.*, 2011] and Iberian Margin [*Skinner et al.*, 2014], here amounting to ~2500–4000 and ~3250–3400, respectively (Fig. 2.5). In particular, our new age estimates conflict with the LGM model of Ferrari et al. [2014] postulating old deep waters all over the Atlantic for water depths >2000 m. As yet, the low LGM ventilation ages are confined to a narrow zone near the Azores, which suggests that LGM deep-water formed somewhere nearby in the central northern North Atlantic. This conclusion is supported by the large-scale ambient water mass with an elevated $\delta^{13}C$ value of 0.65 ‰ in the LGM paleoceanographic transect of Fig. 2.1b [*Sarnthein et al.*,1994]. The LGM deep-water source was possibly linked to a narrow S – N stretching belt of increased sea surface salinity [*Duplessy et al.*, 1991] and temperature during winter [*Pflaumann et al.*, 2003]. This belt may have extended from 50°N/40°W up to ~60°N/20°W, in part just west of the Mid-Atlantic ridge as semi-enclosed winter polynya [*Sarnthein et al.*, 2003b], an ideal location for brine water-supported seasonal deep-water formation.

Low LGM benthic ventilation ages continued at Site MD08-3180 until ~18 cal. ka. During subsequent HS-1 they increased to 1400 yr at 17.4 cal. ka and to >2500 yr near 15.5 cal. ka (Figs. 2.3e and 2.5c). The marked shift from low ventilation ages during LGM to high ages during HS-1 suggests a major change in deep water sources, that is a major reduction in NADW formation and an incursion of ‘old’ southern-source waters, as first inferred from benthic $\delta^{13}C$ transects [*Sarnthein et al.*, 1994] (Fig. 2.1b) and now confirmed by coral-based evidence of Thiagarajan et al. [2014]. Far more extreme ventilation ages of 4000–5000 yr were found by Thornalley et al. [2011] in the northeastern North Atlantic during HS-1, here ascribed to an increased advection of poorly ventilated Antarctic Intermediate Waters

(AAIW). This HS-1 scenario is in harmony with the LGM simulation of Ferrari et al. [2014], in contrast to that of our ventilation ages for the LGM.

As outlined above, the old deep waters of HS-1 probably stemmed from the Southern Ocean and Antarctic Circumpolar Current, where these waters had a ventilation age of 2200–3600 yr near the onset of HS-1 [*Skinner et al*., 2010]. Per analogy to the time span modern NADW needs to flow north–south [*Matsumoto*, 2007] the old deep waters of the Southern Ocean will need further ~700 yr to reach the Azores, in total leading to extreme age values that are indeed monitored in the northeast Atlantic by *Thornalley et al.* [2011] (Fig. 2.5a). However, we cannot reconcile potential deep-water ages of 3000–4500 yr with the ventilation age of only 2500-yr recorded for MD08-3180. Rather the latter age may reflect a mixture of old deep waters from the south with young waters that possibly originated during HS-1 from ongoing brine water formation nearby in the northwestern Atlantic.

Indeed, coral records from upper deep waters (1700–2300 m w.d.) in the subtropical northwest Atlantic [*Robinson et al.*, 2005; *Thiagarajan et al., 2014*] also show only medium old HS-1 ventilation ages that scatter from 1200 to 2400 yr (Fig. 2.5b), thus largely confirm the age range found near the Azores. Altogether, a basin-wide survey of deep-water ventilation ages in the subtropical North Atlantic (Fig. 2.5) suggests a large-scale east-west gradient for HS-1 times, that extends from high ventilation ages in the east to medium low values in the west. This zonal trend may suggest ‘old’ deep waters in the east, advected by Coriolis forcing from the south, and an influence of weak deep-water formation in the far northwest. By theory, signals of initial North Atlantic deep-water rejuvenation indeed should originate in the northwesternmost Atlantic.

However, in contrast to the gradual rise of densely resolved ventilation age maxima at MD08-3180, the ages at the Iberian east Atlantic margin dropped continuously over late HS-1 from ~3200 to ~1400 yr [*Skinner et al.*, 2014], though less well resolved (Fig. 2.5d). A similar general drop of ventilation age also applies to the coral record of Fig. 2.5b. In total, the gradual rejuvenation of deep waters in records from the eastern, central and western North Atlantic is difficult to explain.

During B/A benthic $\delta^{13}C$ records suggest a modern mode of AMOC [*Sarnthein et al.*, 2001]. Indeed, apparent deep-water ventilation ages at MD08-3180 have dropped to the modern level of 700 yr near 14.0 cal. ka, thus confirm a fast recovery of AMOC subsequent to HS-1 (Fig. 2.5).

2.5.4 Short-lasting drops in benthic ventilation age during HS-1

Near 16 and 15.6 cal. ka apparent benthic ventilation ages in MD08-3180 dropped abruptly from ~2250 to ~1800/1400 yr (Fig. 2.3c; Table 2.1). Both events occur subsequent and prior to local meltwater injections ($\delta^{18}O$ minima in Fig. 2.3b). The second event parallels similar oscillations in ventilation age in the northernmost North Atlantic [*Thornalley et al.*, 2011] and, possibly, in the subtropical western Atlantic [*Adkins et al.*, 1998; *Robinson et al.*, 2005] (Fig. 2.5a and b) within the range of age uncertainty linked to deep-water transit times.

The most prominent minimum in deep-water ventilation is centered at 14.9 cal. ka (Fig. 2.5c). The extreme minimum is tied to both a low planktic reservoir age and a negative (!) benthic-planktic age difference of 1400 ^{14}C yr. The benthic ^{14}C minimum does not present a rare outlier, since it was measured on a 4 cm thick sediment slice (at 118.5–121.5 cm core depth). Also, we exclude a bias of bioturbational mixing in view of ongoing fine sediment lamination (H. Kinkel, pers. comm.). Thus the benthic ventilation minimum may indeed document an

extreme pulse of deep-water formation not yet monitored at any other site in the North Atlantic.

On the basis of our ^{14}C plateau tuning that presents a record of the upper mixed layer in the ocean the minimum occurred about 250 yr prior to DO-1 dated at 14.67 cal. ka. On the basis of the most prominent warming in the Uk^{37}-based SST record (Fig. 2.3c), that is a record of the very ocean surface that Schwab et al. [2012] tuned to the NGRIP incremental time scale [Andersen et al., 2006], the ventilation minimum had an age of ~14.7 cal. ka. The difference between the two age estimates lies within the range of age uncertainty but may also record real differences in the sequence of events that marked one of the most dramatic incidents of climate change over the last 20 kyr. The model of Liu et al. [2009] suggests a major AMOC overshoot that finally induced the immense B/A warming subsequent to a reduction in the meltwater flow several centuries before. The succeeding renewal of AMOC is supported by a return to young surface water reservoir ages of 360–640 yr near 14.5 cal. ka, values similar to those of today.

In conclusion, the 14.9 cal. ka drop in ventilation ages close to the Azores may indeed present a first precursor and overshoot signal of the formation of ^{14}C enriched ventilated NADW right after HS-1. However, we still need supportive evidence from other sites to verify the extreme minimum in the benthic ventilation age.

2.6 Conclusions

Sediments in Core MD08-3180, 30-50 nautical miles southwest of the Azores, provided a record of short-term deglacial meltwater incursions to the Azores Current and of past changes

in North Atlantic Deep Water composition and origin near 3100 m water depth. On the basis of high-resolution planktic and benthic ^{14}C records we arrived at the following conclusions:

(1) We identified the equivalent of six atmospheric ^{14}C plateaus in the planktic ^{14}C record (Plateaus 2a – 5b; in addition, possibly a Plateau 1a and parts of Plateau 1). Tuning of ^{14}C plateau boundaries to pertinent plateau boundaries in the atmospheric ^{14}C record of Lake Suigetsu provided us with 10, possibly 13, age control points, the backbone of our calendar age model for the interval 23–13 cal. ka. It implies sedimentation rates of ~110–170 cm/ky for the late LGM, 60–70 cm/ky for HS-1, and ~30–45 cm/ky for early B/A.

(2) Between 17.5 and 14.7 cal. ka, planktic ^{14}C reservoir ages rose to ~1600 and briefly up to 2170 yr. The high values by far exceed the LGM level of 320–600 yr and record transient incursions of HS-1 meltwater as far south as 38°N, a feature also recorded by two prominent planktic $\delta^{18}O$ minima near 17.4–16.8 and 15.6–15.4 ka.

(3) A first continuous millennial-to-centennial-scale record of changes in apparent benthic ventilation ages (analogous to benthic $\Delta^{14}C_{0,adj}$ of Cook and Keigwin, [2015]) has been established by summing the planktic ^{14}C reservoir ages and the ^{14}C age difference of paired benthic and planktic foraminifera samples, a sum finally adjusted to past short-term changes in atmospheric ^{14}C between the time of deep-water formation and that of foraminifera deposition.

(4) During LGM apparent deep-water ventilation ages ranged from 340–740 yr, a robust record of glacial North Atlantic Deep Water formation, though constrained to a region near to the Azores. The origin of ‘young’ LGM deep waters may be linked to a narrow belt of open

waters in the North Atlantic, a semi-enclosed polynya that extended from 50°N/35°W to 60°N/20°W during LGM winter.

(5) During HS-1 peak benthic ventilation ages increased up to 2200–2550 yr. The high ages reflect incursions of old, southern-source deep waters. Their flow was interrupted by brief events of northern deep-water formation near 16.1 and 15.6 cal. ka, that alternated with meltwater incursions. At the onset of B/A we found a third, most prominent minimum in benthic ventilation age near 14.9/14.7 cal. ka, that probably introduced the renewal and may depict an overshoot of AMOC *sensu* [Liu et al., 2009].

2.7 Acknowledgments

We acknowledge fruitful suggestions and critique of Pieter M. Grootes, Kiel, that helped us to streamline our manuscript, moreover, the constructive and valuable critique of three anonymous reviewers, and discussions with J. Repschläger, C. Schwab, and M. Weinelt, Kiel, who kindly provided sediment samples of MD08-3180. Several students helped with careful sample preparation. We thank the Kiel Leibniz Laboratory for AMS ^{14}C and stable-isotope analyses, and J. Southon, University of California Irvine, for measuring AMS ^{14}C ages on extremely small foraminifera samples. The study was funded by Deutsche Forschungsgemeinschaft (DFG) grant Sa207-48.

2.8 Supplementary Information

2.8.1 S2.1 Core sampling and sample processing

Calypso square core MD08-3180 Cq was retrieved at MD Cruise 168 from 31°7.698’W, 37°59.99’N, and 3064 m water depth [Kissel et al., 2008]. The 10.5 m long core was sampled by 1-cm thick sediment slices of ~21cc volume each, that were freeze-dried, washed over a

63µm sieve, cleaned with deionized water, and finally split into subfractions of 63-150, 150-250, 250-315, 315-400, and >400 µm.

2.8.2 S2.2 Stable isotope measurements

An initial stratigraphic record of core MD08-3180 relied on wide-spaced $\delta^{18}O$ data of *Globigerina bulloides* [Schwab et al., 2012], that we augmented by 154 data between 160 and 1040 cm core depth. 5 to 20 foraminifera tests each were picked from the size fraction 315-400 µm. Where specimens were scarce we added specimens from the 250–315 µm size fraction (all data are stored at www.pangaea.de).

Beyond 350 cm core depth a general lack of *C. wuellerstorfi* and other epibenthic species prevented us from reconstructing a record of bottom water $\delta^{13}C$, except for a single sample from 506.5 cm core depth, where we analyzed three tests of *C. wuellerstorfi* from the 250–315 µm size fraction.

Prior to stable-isotope analysis, tests were carefully cracked to open the foraminifera chambers, subsequently submersed into ultrapure ethanol and ultrasonic-cleaned for three seconds. Ethanol and contaminants were decanted. Cleaned test fragments were dried at 40°C.

Stable isotopes ($\delta^{18}O$ and $\delta^{13}C$) were measured at the Leibniz Laboratory of Kiel University using a MAT 253 mass spectrometer. The system is equipped with a Carbo-Kiel Device (Type IV) for automated CO_2 preparation from carbonate samples for isotope analysis. Samples were reacted by individual acid addition (99% H_3PO_4 at 75°C). Precision was regularly checked using an internal Solnhofen limestone standard that was converted to the Vienna Pee Dee Belemnite (VPDB) standard using the National Bureau of Standards NBS-19

carbonate standard. External standard errors are better than ±0.08 ‰ for $\delta^{18}O$ and ±0.05 for $\delta^{13}C$.

2.8.3 S2.3 Analysis of ^{14}C ages

A planktic ^{14}C record for 251.5–800.5 cm core depth was established from 68 monospecific AMS ^{14}C measurements on *G. bulloides* from the size fraction >150µm (Table S2.1). The foraminifera samples spanned 1–7 cm thick sediment slices that contained 377–1057 specimens equal to 4–10 mg carbonate each.

Table S2.1: Planktic ^{14}C ages measured on *G. bulloides* in Core MD08-3180.

Sample No.	Centered at core depth [cm]	Assigned calendar age [yr]	Conventional ^{14}C age [yr]	Conventional ^{14}C age [‰]	Number of specimens	Weight ± 0.5 [mg]	Size fraction
KIA 47890	251.5 – 253.5	13233 – 13272	11540 ±140	762.3 ±17.3	515	7	>400-250µm
KIA 48058	259.5	13388	11500 ±55	761.1 ±6.8	547	5	>400-250µm
KIA 49281	262.5	13446	11850 ±70	771.3 ±8.7	531	4	>400-250µm
KIA 48438	267.5 – 268.5	13543 – 13562	14760 ±80	840.8 ±9.9	1349	8	250-150µm
KIA 49282	272.5	13640	12340 ±70	784.8 ±8.7	570	7	>400-250µm
KIA 47892	275.5 – 276.5	13689 – 13717	12750 ±180	795.5 ±22.2	424	6	>400-250µm
KIA 49283	280.5	13794	12160 ±70	779.9 ±8.7	317	6	>400-315µm
KIA 47893	283.5	13852	12440 ±160	787.5 ±19.7	429	7	>400-250µm
KIA 49284	287.5	13930	12160 ±70	779.9 ±8.7	851	9	>400-250µm
KIA 47894	291.5	14065	13160 +170/-160	805.7 +20.9/-19.7	443	6	>400-250µm
KIA 48059	298.5 – 299.5	14275 – 14305	13060 ±70	803.2 ±8.7	541	6	>400-250µm
KIA 49134	304.5	14455	13460 ±70	816.9 ±8.7	649	6	>400-250µm
KIA 47895	307.5	14545	13750 +210/-200	819.4 +25.8/-24.6	401	6	>400-250µm
KIA49133	310.5	14635	13680 ±70	817.9 ±8.7	638	10	>400-250µm
KIA 47896	315.5	14785	14080 +200/-190	826.7 +24.6/-23.5	368	6	>400-250µm
KIA 47910	319.5	14905	13630 ±120	816.7 ±14.8	724	7	>400-150µm

KIA 47897	324.5	15272	14560 +230/-220	836.8 +28.2/-27.0	377	6	>400-250µm
KIA 47907	329.5	15347	14820 ±190	842 ±23.4	403	6	>400-250µm
KIA 47898	334.5	15423	14500 +180/-170	835.5 +22.2/-20.9	467	6	>400-250µm
KIA 47899	339.5	15498	14860 +250/-240	842.7 +30.6/-29.4	382	6	>400-250µm
KIA 47912	344.5	15574	14790 +170/-160	841.4 +20.9/-19.7	647	6	>400-150µm
KIA 47900	349.5	15649	14780 +210/-200	841.2 +25.8/-24.6	429	6	>400-250µm
KIA 47913	354.5	15725	14940 +200/-190	844.3 +24.6/-23.4	614	6	>400-150µm
KIA 47905	359.5	15800	14870 +220/-210	842.9 +27.0/-25.8	416	7	>400-250µm
KIA 48521	362.5	15846	14900 +160/-150	843.5 +19.7/-18.5	448	6	>400-250µm
KIA 47901	364.5	15876	15060 +270/-260	846.6 +33.1/-31.8	331	5	>400-250µm
KIA 47902	369.5	15951	15100 +210/-200	847.4 +25.8/-24.6	447	6	>400-250µm
KIA 47903	374.5	16027	15110 +210/-200	847.6 +25.8/-24.6	505	8	>400-250µm
KIA 48522	378.5	16071	15420 +170/-160	853.3 +20.9/-19.7	514	7	>400-250µm
KIA 47914	380.5	16088	15330 ±170	851.7 ±20.9	541	7	>400-250µm
KIA 47915	387.5	16148	15420 +200/-190	853.3 +24.6/-23.4	579	6	>400-150µm
KIA 47916	394.5	16207	15460 ±170	854.1 ±20.9	582	7	>400-250µm
KIA 47906	401.5	16267	15640 +210/-200	857.3 +25.8/-24.6	608	6	>400-150µm
KIA 47863	407.5 – 409.5	16318 – 16335	15390 ±180	852.8 ±22.2	785	7	>400-150µm
KIA 47864	414.5 – 416.5	16378 – 16395	15540 +230/-220	855.5 +28.2/-27.0	563	6	>400-150µm
KIA 47904	420.5 – 424.5	16500 – 16614	15850 +250/-240	861 +30.6/-29.4	509	5	>400-150µm
KIA 47865	427.5 – 430.5	16700 – 16785	15730 +270/-260	858.9 +33.1/-31.8	643	5	>400-150µm
KIA 47866	434.5 – 437.5	16900	15960 ±250	862.9 ±30.6	658	6	>400-150µm
KIA 47867*	441.5 – 444.5	16950 – 16988	16270 +400/-390	868.1 +48.6/-47.4	491	4	>400-150µm
KIA 47868*	447.5 – 450.5	17025 – 17063	16840 +830/-760	877.1 +98.2/-90.3	708	5	>400-150µm
KIA 47869	456.5 – 458.5	17140 – 17164	15930 +220/-210	862.4 +27.0/-25.8	805	5	>400-150µm
KIA 47870	463.5 – 466.5	17227 – 17265	16140 +290/-280	865.9 -35.5/-34.3	668	6	>400-150µm
KIA 47871	470.5 – 472.5	17315 – 17340	15710 +200/-190	858.8 +24.6/-23.4	756	7	>400-150µm

KIA 47872	477.5 – 479.5	17403 – 17428	16170 +220/-210	866.4 +27.0/-24.6	539	6	>400-250µm
KIA 46873	484.5 – 485.5	17491 – 17504	16250 +200/-190	867.7 +24.6/-23.4	649	7	>400-250µm
KIA 47875	491.5 – 493.5	17580	16290 ±230	868.4 ±28.2	5567	6	>400-250µm
KIA 47874	498.5 – 499.5	18000	16440 +250/-240	870.8 +30.6/-29.4	752	5	>400-150µm
KIA 47909	505.5 – 507.5	18056 – 18075	15990 +170/-160	864 +20.9/-19.7	785	8	>400-250µm
KIA 47908	512.5 – 514.5	18123 – 18142	16500 +230/-220	871.8 +28.2/-27.0	814	6	>400-150µm
KIA 47876	519.5 – 521.5	18189 – 18208	16670 +250/-240	874.5 +30.6/-29.4	714	5	>400-150µm
KIA 47917	525.5 – 528.5	18246 – 18274	16470 ±240	871.3 ±29.4	769	5	>400-150µm
KIA 47877	533.5 – 535.5	18321 – 18340	16310 +270/-260	868.7 +33.1/-31.8	573	5	>400-150µm
KIA 49135	543.5 – 546.5	18416 – 18445	16310 ±90	868.7 ±11.1	787	5	>400-150µm
KIA 49136	551.5 – 557.5	18492 – 18551	16350 ±90	869.4 ±11.1	807	5	>400-150µm
KIA 49180	563.5 – 565.5	18605 – 18624	16600 ±100	873.4 ±12.4	1057	6	>400-150µm
KIA 49181	573.5 – 576.5	18700 – 18729	16450 ±100	871 ±12.4	940	6	>400-150µm
KIA 49182	582.5 – 586.5	18785 – 18823	16710 ±100	875.1 ±12.4	1026	7	>400-150µm
KIA 49183	592.5 – 596.5	18880 – 18918	16670 +110/-100	874.5 +13.6/-12.4	996	6	>400-150µm
KIA 49184	613.5 – 617.5	19051 – 19078	16810 +110/-100	876.6 +13.6/-12.4	672	5	>400-150µm
KIA 49285	634.5 – 635.5	19184 – 19190	16990 ±110	879.4 ±13.6	772	7	>400-150µm
KIA 49286	653.5 – 655.5	19294 – 19305	16880 ±110	877.7 ±13.6	868	7	>400-150µm
KIA 49287	673.5 – 675.5	19409 – 19421	17040 ±110	880.1 ±13.6	651	5	>400-150µm
UCIAMS 127528	696.5 – 699.5	19542 – 19559	17055 ±50	880.3 ±6.2	505	5	>400-150µm
KIA 49553	713.5 – 715.5	19661 – 19679	17420 ±110	885.7 ±13.6	647	7	>400-150µm
KIA 49554	733.5 – 745.5	19837 – 19855	17670 ±110	889.2 ±13.6	564	5	>400-150µm
KIA 49555	753.5 – 755.5	20013 – 20031	17530 ±110	887.2 ±13.6	634	7	>400-150µm
KIA 49565	782.5 – 787.5	20268 – 20312	17910 +130/-120	892.4 +16.1/-14.8	953	5	>400-150µm
KIA 49566	796.5 – 800,5	20392 – 20427	17750 ±110	890.3 ±13.6	645	5	>400-150µm

A benthic AMS ^{14}C record was measured on 23 samples from 255.5–756.5 cm core depth. 22 of them occur within the boundaries of one of the ^{14}C plateaus (Tables 2.2 and S2.2). Due to insufficient epibenthic specimens we analyzed mixed foraminifera assemblages of Hoeglundina elegans, Gyridinoida soldanii, Cibicides mundulus, Cibicidoides wuellerstorfi, Cibicides sp., Bulimina sp., Melonis sp., Pullenia bulloides, and Lenticulina sp. from 2–11 cm thick sediment sections that contained 81–1605 specimens each. We excluded infaunal Miliolid tests (e.g., Pyrgo sp.), since their low ^{14}C contents may significantly bias ^{14}C ages toward older values [*Magana et al*., 2010]. Because of high sedimentation rates (Fig. 2.2a) the (single) 11 cm thick sediment slice spans a time slice no longer than ~170 yr.

AMS ^{14}C ages of planktic and benthic samples were measured at the Leibniz Laboratory, University of Kiel (KIA numbers), and the Keck Carbon Cycle AMS facility (UCIAMS numbers), University of California, Irvine.

Sample processing in the Leibniz Laboratory included sample cleaning with 15% H_2O_2 in an ultrasonic bath to remove dust and detrital carbonate as well as organic surface coatings. CO_2 was released from the samples with 100% H_3PO_4 at 90°C and graphitized with H_2 using about 2 mg Fe powder as catalyst. The ^{14}C concentration was measured by comparison of simultaneously collected ^{14}C, ^{13}C, and ^{12}C beams of each sample with those of Oxalic Acid standard CO_2 and those of pre-Eemian planktic foraminifera [*Nadeau et al*., 1998]. Samples submitted to the KECK AMS Group were cleaned and leached prior to graphitization and hydrolyzed in H_3PO_4. Before ^{14}C analysis the released CO_2 was graphitized under H_2 on an iron catalyst [*Vogel et al*., 1984].

All ^{14}C values were converted into conventional ^{14}C ages following Stuiver and Pollach [1977] (Tables S2.1 and S2.2). ^{14}C ages were not corrected for a 400-yr reservoir age (all data available at www.pangaea.de under…).

Table S2.2: Benthic ^{14}C ages measured on mixed foraminifera assemblages in Core MD08-3180.

Sample No.	Centered at core depth [cm]	Assigned calendar age [yr]	Conventional ^{14}C age [yrs]	Conventional ^{14}C age [‰]	Number of specimens	Weight ± 0.5 [mg]	Size fraction	Species
UCIAMS 127524	255.5–262.5	13310 – 13427	11660±30	765.8±3.7	304	6	>400-150µm	*H. elegans, G. soldanii, C. wuellerstorfi, Bulimina spp., Melonis sp. C. mundulus, P. bulloides*
KIA 48392	289.5–292.5	13995 – 14095	12810±60	797±7.4	147	7	>400-250µm	*H. elegans, G. soldanii, C. wullerstorfi, C. mundulus, G. orbicularis*
KIA 48739	304.5–307.5	14455 – 14545	13620±60	816.5±7.4	349	9	>400-150µm	*H. elegans, C. wuellerstorfi, C. mundulus, Bulimina spp., Melonis sp., P. bulloides*
UCIAMS 127525	312.5–313.5	14695 – 14725	13730±30	819±3.7	255	8	>400-150µm	*H. elegans, G. soldanii, C. wuellerstorfi, Bulimina spp., Melonis sp.,C. mundulus, P. bulloides*
KIA 48393	318.5–321.5	14895 – 15038	12290±60	783.5±7.4	119	8	>400-250µm	*H. elegans, G. soldanii, C. wullerstorfi, C. mundulus, G. orbicularis*
UCIAMS 127527	325.5–326.5	15287 – 15302	14770±35	841±4.3	262	5	>400-150µm	*H. elegans, G. soldanii, C. wuellerstorfi, Bulimina spp., Melonis sp., C. mundulus, P. bulloides*
KIA48738	331.5–332.5	15377 – 15392	15010 +80/-70	845.7 +9.9/-8.7	344	11	>400-150µm	*H. elegans, G. soldanii, C. wuellerstorfi, Bulimina spp., Melonis sp., P. bulloides*
KIA 48394	338.5–341.5	15483 – 15528	15260±80	850.4±9.9	92	8	>400-250µm	*H. elegans, G. soldanii, C. wullerstorfi*
KIA 48737	346.5–348.5	15604 – 15623	14470±70	834.9±8.7	313	9	>400-150µm	*H. elegans, G. soldanii, C. wuellerstorfi, Bulimina spp., Melonis sp., P. bulloides*
KIA 48526	352.5–353.5	15694 – 15710	15370±160	852.4±19.7	209	6	>400-150µm	*H. elegans, G. soldanii, C. wuellerstorfi, Bulimina spp., Melonis sp., P. bulloides*
KIA 48525	363.5–364.5	15861 – 15876	15480±160	854.4±19.7	276	5	>400-150µm	*H. elegans, G. soldanii, C. wuellerstorfi, Bulimina spp., Melonis sp., P. bulloides*
KIA 48524	373.5–374.5	16012 – 16027	14980±160	845.1±19.7	186	5	>400-150µm	*H. elegans, G. soldanii, C. wuellerstorfi, Bulimina spp., Melonis sp., P. bulloides*
KIA 48395	382.5–387.5	16105 – 16148	15730±90	854.9±11.1	81	7	>400-250µm	*H. elegans, G. soldanii, C. wullerstorfi*
KIA 48523	400.5–408.5	16259 – 16372	15890 +180/-170	861.7 +22.2/-20.9	752	6	>400-150µm	*H. elegans, G. soldanii, C. wuellerstorfi, Bulimina spp., Melonis sp., P. bulloides*

UCIAMS 132993	440.5–450.5	16937 – 17063	15660±200	857.6±24.6	605	2	>400-150µm	*H. elegans, G. soldanii, C. wuellerstorfi, Bulimina spp., Melonis sp., C. mundulus, P. bulloides*
UCIAMS 132992	480.5–484.5	17441 – 17491	16040±60	864.2±7.4	1455	6	>400-150µm	*H. elegans, G. soldanii, C. wuellerstorfi, Bulimina spp., Melonis sp., P. bulloides Lenticulina sp.*
KIA 49727	498.5–502.5	18000 – 18028	16300±100	868.6±12.4	1244	5	>400-150µm	*H. elegans, C. wuellerstorfi, C. mundulus, Bulimina spp., Melonis sp., P. bulloides*
KIA 49728	547.5–552.5	18454 – 18501	16590±100	873.2±12.4	1605	5	>400-150µm	*H. elegans, C. wuellerstorfi, Bulimina spp., Melonis sp., C. mundulus, P. bulloides, Uvigerina sp., Cibicides sp.*
UCIAMS 127527	620.5–630.5	19066 – 19161	16850±60	877.2±7.4	1111	3	>400-150µm	*H. elegans,C. wuellerstorfi, Bulimina spp., Melonis sp., C. mundulus, P. bulloides,*
KIA 49730	671.5–678.5	19289 – 19438	17350±110	884.7±13.6	1482	5	>400-150µm	*H. elegans, C. wuellerstorfi, Bulimina spp., Melonis sp., C. mundulus, P. bulloides*
KIA 49731	697.5–703.5	19548 – 19582	17340±130	884.5±16.1	1368	6	>400-150µm	*H. elegans, G. soldanii, C. wuellerstorfi, Bulimina spp., Melonis sp., C. mundulus, P. bulloides*
UCIAMS 132991	718.5–723.5	19705 – 19749	17350±60	884.7±7.4	995	6	>400-150µm	*H. elegans, G. soldanii, C. wuellerstorfi, Bulimina spp., Melonis sp., P. bulloides, Lenticulina sp.*
UCIAMS 132990	750.5–756.5	19987 – 20040	17640±90	888.7±11.1	605	6	>400-150µm	*H. elegans, G. soldanii, C. wuellerstorfi, Bulimina spp., Melonis sp., P. bulloides, Lenticulina sp.*

2.8.4 S2.4 ^{14}C plateau tuning and derivation of planktic ^{14}C reservoir ages

Absolute calendar ages were estimated by visual correlation following the rules of Sarnthein et al. [2007; 2015]. A suite of six to seven plateaus in the planktic ^{14}C record of MD08-3180 (Fig. 2.2a) was tuned to an analogous suite of age calibrated atmospheric ^{14}C plateaus between 13 and 22 cal. ka, that are well defined in the Lake Suigetsu ^{14}C record of Bronk Ramsey et al. [2012] (Fig. 2.2b). The age-calibrated upper and lower plateau boundaries provided us with 12–14 age control points. Two of them (at 291 and 320 cm depth) are poorly established. In between, calendar ages were interpolated assuming constant sedimentation rates (details in Suppl. Text 2.6).

Planktic reservoir ages were separately calculated for each single ^{14}C plateau by subtracting the average ^{14}C age of an atmospheric plateau (estimated from ^{14}C dates of Bronk Ramsey et al. [2012]) from the (unweighted) average ^{14}C age of its planktic plateau counterpart. In this way, we take into account of the short-term oscillations and error range of raw ^{14}C ages within both the atmospheric and planktic ^{14}C plateaus. The tuning of the conjugate plateaus is superior to any subtraction of single ^{14}C ages one-by-one, the results of which could be very noisy and thus difficult to read. Reservoir age uncertainty was calculated by Gaussian error propagation of the errors of planktic and atmospheric ^{14}C ages within a plateau. On average, we accept for our ^{14}C plateaus 10% outlier dates. Thus, our uncertainty estimates correspond to 90 % probability or 1.68 σ. In case several choices of plateau tuning compete, we select the lowest possible estimates of planktic reservoir age. Exceptions are based on stringent findings (say, on the basis of paired benthic reservoir ages) that suggest a higher planktic reservoir age level as more plausible.

Sarnthein et al. [2015] introduced an objective statistical approach (Fig. 2.2c) to identify ^{14}C jumps and plateau boundaries in a ^{14}C record otherwise identified by visual inspection only. A test run for the atmospheric ^{14}C record of Lake Suigetsu yielded (varve counted) calendar ages of plateau boundaries with a deviation that does not exceed the range of decades to 100 yr. The resulting ‘calendar’ ages hardly differ from those established by visual inspection and corroborate the accuracy of ^{14}C plateau boundaries previously defined. Thus, we stick to the use of planktic plateau boundaries as age control points, that are correlated by visual inspection to ^{14}C plateau boundaries in the Lake Suigetsu record. (Fig. 2.2a).

The uncorrected planktic ^{14}C record of MD08 3180 shows two striking outliers at 267.5–268.5 cm and 447.5–450.5 cm with ^{14}C ages of 14,770 ± 80 and 16,840 +830/-760 yr, respectively (Fig. 2.2a). The first outlier suggests a reservoir age of ~2700 yr on top of Plateau 1a at the end of the B/A, a time span generally marked by low surface water reservoir ages (~ 500 yr) all over the North Atlantic [*Waelbroeck et al*., 2001; *Thornalley et al*., 2011; *Skinner et al*., 2014] (Fig. 2.5). The outlier matches an aberrant short-lasting peak in the content of fine fraction reaching 11.2 % as compared to 2–6 % further downcore (Fig. S2.1d). Hence we assume that this short-term injection of suspended allochthonous sediment also contained a lot of ancient foraminifera tests that biased the ^{14}C age accordingly.

The second outlier of 16,840 ^{14}C yr at 447.5–450.5 cm core depth has a broad analytical uncertainty of +830/-760 years, thus may be considered statistically insignificant. However, we tentatively assigned this age to a short-term 'true' culmination in surface water reservoir age of 2170 yr, since the paired benthic ^{14}C age (Figs. 2.2a, 2.3a and 2.3e) is 1180 yr lower than the planktic ^{14}C age under discussion. The apparent 'raw' benthic ventilation age that sums the planktic reservoir age of 2170 yr with the (negative) benthic-planktic age difference of -1180 (i.e., 15,660–16,840 yr) (details in Suppl. Text 2.5) finally amounts to ~1000 yr, a value that comes close to that of the next-older 'raw' benthic ventilation age of 1300 yr immediately below. Thus we may regard the extreme planktic ^{14}C age and the related extreme planktic reservoir age as real excursions, even more so as they match a marked planktic $\delta^{18}O$ minimum as tracer of meltwater incursions (Figs. 2.3b and main text).

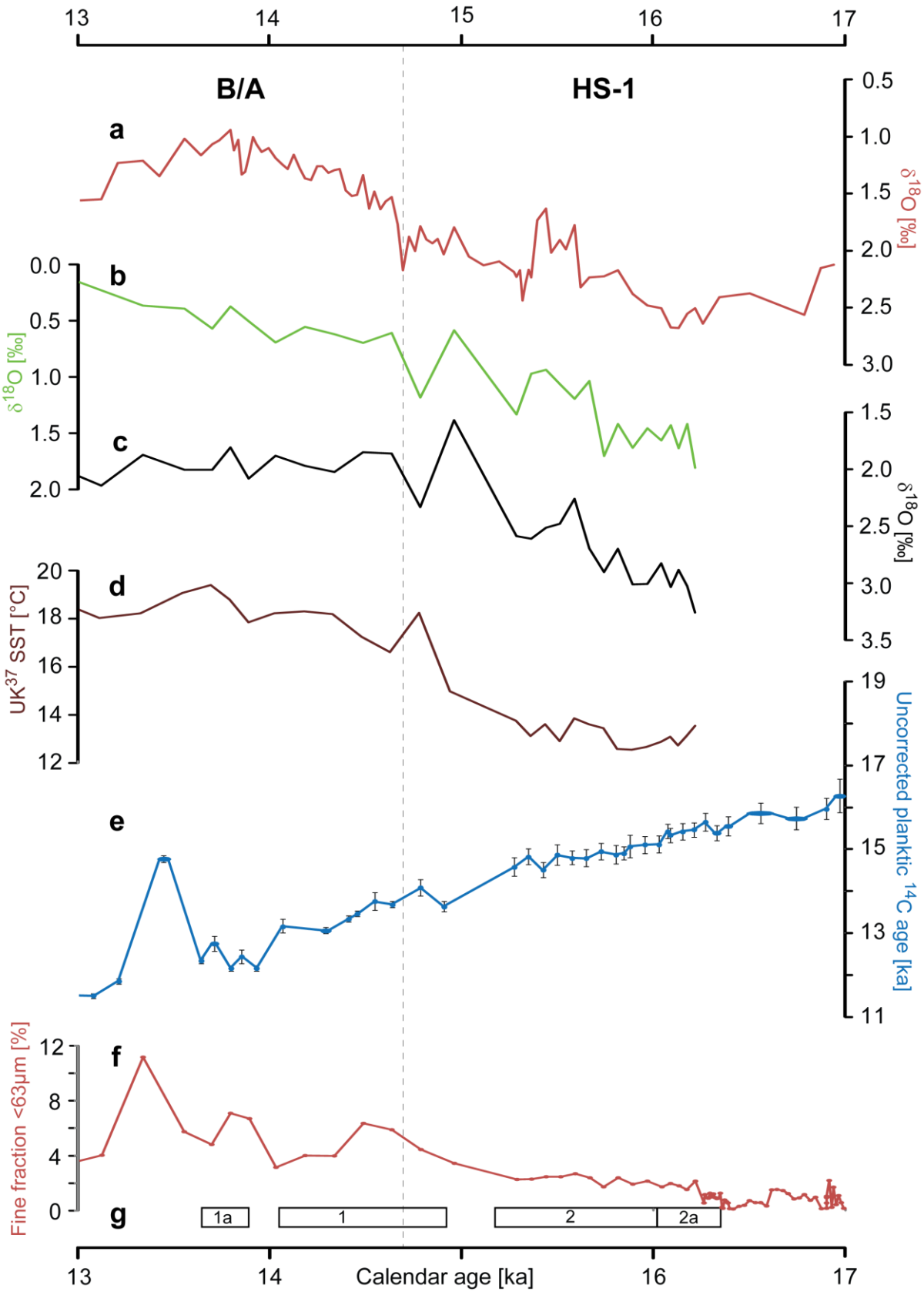

Figure S2.1: Stable isotope records, and sediment properties between 13 and 17 cal. ka from Site MD08-3180: (a) □^{18}O record of *G. bulloides*, (b) δ^{18}O record of *G. ruber* [Schwab et al., 2012], (c) δ^{18}O record of *G. truncatulinoides* [Repschläger et al., 2015], (d) Uk37-based SST estimates, (e) uncorrected planktic ^{14}C ages, (f) fine fraction (<63µm) (note the extreme at 13.55 ka equal to 265.5 cm core depth), and (g) boundaries of planktic ^{14}C plateaus 1 – 2b vs. age.

2.8.5 S2.5 Apparent benthic ventilation ages

'Raw' apparent benthic ventilation ages present the sum of (1) the ^{14}C age difference between paired benthic and planktic foraminifera dates and (2) the planktic reservoir age of the ^{14}C plateau that covers the pair of benthic and planktic dates (Figs. 2a, 3, and 4). Thus 'raw' ventilation ages (in ^{14}C yr) present the difference between an atmospheric and benthic ^{14}C level at the site and time of foraminifera deposition. As first shown by Adkins and Boyle [1997] and recently summarized by Cook and Keigwin [2015], our 'raw' ventilation ages need to be converted to 'actual' benthic ventilation ages by means of the 'projection' technique. Accordingly, we need to correct the 'raw' ages for changes in atmospheric ^{14}C over brief glacial-to-deglacial time spans that preceded sediment deposition (Fig. 2.4a). These intervals each start with the formation of deep waters that incorporated an initial ^{14}C signal from the sea surface and end with the growth of benthic foraminifera that finally incorporated the ^{14}C signal in deep-sea sediments, though somewhat modified by radioactive decay. Our approach disregards any mixing of water masses that originate from different source regions and contribute differential ^{14}C ventilation ages, thus justify the modifier 'apparent'.

Our approach (Fig. 2.4) slightly differs from the projection technique proper. In ^{14}C-based metrics we directly adjust the $\Delta\Delta^{14}C$ equivalent of our 'raw' benthic ventilation age to changes in atmospheric ^{14}C that occurred between the time of deep-water formation and that of sediment deposition. That means our conversion of ^{14}C ventilation ages into the $\Delta\Delta^{14}C$ value incorporates past changes in atmospheric ^{14}C concentration that have preceded the time of sediment deposition. To constrain the time of deep-water formation we sum the absolute age of foraminifera deposition as deduced from ^{14}C plateau tuning and the 'raw' ventilation age as proxy of the time span that passed since deep-water formation. In this way we implicitly assume that the initial (planktic) reservoir age of downwelled surface waters, a major unknown, was equal to that estimated for the site and time of benthic-foraminifera

deposition. Finally, we add the $\Delta^{14}C$ difference between the initial and final concentrations (fMC) of atmospheric ^{14}C to the $\Delta\Delta^{14}C$ equivalent of the 'raw' benthic ventilation age to obtain an 'actual' benthic $\Delta\Delta^{14}C$ value (Fig. 2.4), a robust product coming close to the values defined as $\Delta^{14}C_{0adj}$ or $\Delta^{14}C_{0\text{-}atm}$ by Cook and Keigwin [2015]. In Fig. 2.4 the slopes of the linear broken lines connecting the raw ventilation ages with the initial atmospheric fMC vary because of different raw ^{14}C ventilation ages added to the absolute age of foraminifera deposition.

Uncertainty estimates for our (apparent) benthic ventilation ages include the propagated error of benthic ^{14}C analyses, that of the surface water reservoir age contemporaneous with foraminifera deposition, and that of changes in average atmospheric $\Delta^{14}C$ between deep-water formation and foraminifera deposition.

2.8.6 S2.6 Sedimentation rate

Estimates of sedimentation rates are based on linear interpolation of sedimentation rates between age-calibrated ^{14}C plateau boundaries. Major jumps in sedimentation rate may be a mere artifact of too low sampling resolution responsible for insufficient precision in the definition of planktic ^{14}C plateau boundaries. To avoid these artifacts we did not specify distinct rates for the short sediment sections that separate the different ^{14}C plateaus and span 300-500 yr and less. These intervals are smaller than justified by our sampling resolution (details in Table S2.3). By incorporating these small inter-plateau sections into the next-following ^{14}C plateau each we obtained a smooth and realistic record of modest changes in sedimentation rate (Fig. 2.2a).

Table S2.3: Definition of age control points for the calculation of sedimentation rates.

^{14}C plateau boundaries used as tie points	Calendar age [yr]	Core depth [cm]	Sedimentation rate [cm/kyr]
Top 1a – Top 1	13640 – 14050	272.5 – 291	45.1
Top 1 – Top 2a	14050 – 15272	291 – 324.5	27.4
Top 2a – Base 2a/ Top 2b	15272 – 16050	324.5 – 376	66.0
Top 2b – Top 3	16050 – 16900	376 – 434.5	68.8
Top 3 – Top 4	16900 – 18000	434.5 – 498.5	58.1
Top 4 – Base 4	18000 – 18980	498.5 – 603	106.6
Base 4 – Base 5a / Top 5b	18980 – 19600	603 – 706.5	166.9
Top 5b – Base 5b	19600 – 20150	706.5 – 769	113.6

Chapter 3

Refined modeling and ^{14}C plateau tuning reveal consistent patterns of glacial and deglacial ^{14}C reservoir ages of surface waters in low-latitude Atlantic

Sven Balmer, Michael Sarnthein, Manfred Mudelsee, and Pieter M. Grootes

Submitted to *Paleoceanography*

3.1 Abstract

Modeling studies predict that changes in radiocarbon (^{14}C) reservoir ages of surface waters during the last deglacial episode will reflect changes in both atmospheric ^{14}C concentration and ocean circulation including the Atlantic Meridional Overturning Circulation. Tests of these models require the availability of accurate ^{14}C reservoir ages in well-dated Late Quaternary time series. We here test these models using plateau-tuned ^{14}C time-series in multiple well-placed sediment core age-depth sequences throughout the lower latitudes of the Atlantic Ocean. ^{14}C age plateau-tuning in glacial and deglacial sequences provides accurate calendar year ages that differ by as much as 500-2500 years from those based on assumed global reservoir ages around 400 years. This study demonstrates increases in local Atlantic surface reservoir ages of up to 1000 years during the last glacial maximum, ages that reflect stronger trades off Benguela and summer winds off southern Brazil. By contrast, surface water reservoir ages remained close to zero in the Cariaco Basin in the southern Caribbean due to lagoon-style isolation and persistently strong atmospheric CO_2 exchange. Later, during the early deglacial (16 ka) reservoir ages decreased to a minimum of 170-420 ^{14}C years throughout the South Atlantic, likely in response to the rapid rise in atmospheric pCO_2 and Antarctic temperatures occurring then. Changes in magnitude and geographic distribution of ^{14}C reservoir ages of peak glacial and deglacial surface waters deviate from the results of Franke et al. [2008] but are generally consistent with those of the more advanced ocean circulation models of Butzin et al. [2012].

3.2 Introduction

^{14}C reservoir ages of surface waters represent the difference between ^{14}C ages of the atmosphere and contemporaneous surface waters. Past reservoir ages can be derived from ^{14}C records of planktic foraminifers in comparison to past ^{14}C concentrations of the atmosphere. Changes in reservoir age may form an important tracer of past changes in ocean circulation [*Grootes*, 2015]. Franke et al. [2008] based their model simulation of spatial and temporal variations in glacial reservoir age on the assumption that these were controlled by changes in atmospheric ^{14}C concentration and a 30-% reduction of Atlantic Meridional Overturning Circulation (AMOC). They found changes that were fairly modest in the low-latitude Atlantic during present and peak glacial times, at most rising from 400 to 500 ^{14}C years in high latitudes (Table 3.1). Later, Butzin et al. [2012] used similar assumptions in testing four MOC scenarios of the Last Glacial Maximum (LGM). However, different from previous approaches (details of model design are listed in Table 3.2), their general circulation model (GCM) employed a 'self-consistent simulation' of ^{14}C, an LGM wind field controlled by LGM sea surface temperatures (SST), and a higher gas transfer velocity for the ^{14}C transfer from the atmosphere [*Sweeney et al.*, 2007]. On this basis changes in simulated reservoir age were far more distinct reaching 500 in low and 2200 ^{14}C years in high latitudes.

It is difficult to validate the different glacial reservoir ages simulated and their spatial and temporal gradients, since centennial-to-millennial-scale records of empiric ^{14}C reservoir ages are widely lacking both for modern and past ocean surface waters in the Atlantic, a gap now reduced in this study. Yet, some authors already took a step forward and employed the differential reservoir ages simulated by either one of the two models each as – possibly controversial – database to reconstruct past distribution patterns of deep-water ventilation ages and their underlying changes in AMOC [*Freeman et al.*, 2015; *Huang et al.*, 2015], which is a further incentive to test the significance of the model results.

Table 3.1: Changing ^{14}C reservoir ages [yr] of surface waters. ^{14}C reservoir ages present the difference in ^{14}C yr between coeval paired ^{14}C ages of the atmosphere and ocean surface waters. a) Skinner et al. [2010]; b) Sarnthein et al. [2015]; c) Little et al. [1997]; d) Vidal et al. [1999]; e) Came et al. [2003]; f) Sortor and Lund [2011]; g) Jaeschke et al. [2007]; h) Hughen et al. [2006]; i) Franke et al. [2008]; j) Butzin et al. [2012]; *Including *Zoophycos* outliers. C. = current; PD = preindustrial; w.d. = water depth.

	South Atlantic W. Wind Drift	**Benguela Current**	**Brazilian Margin South Brazil C.**	**Brazilian Margin Equatorial**	**Cariaco Basin**	**Azores C.**
	MD07 3076 [a] (44°4'S, 14°12'W) (3770 m w.d.)	GeoB 1711-4 (23°17'S, 12°23'W) (1976 m w.d.)	KNR 159-5-36-GGC (27°31'S, 46°48'W) (1268 m w.d.)	GeoB 3910-1 (4°15S, 36°21'W) (2361 m w.d.)	ODP 1002 [b] (10°42'N, 65°10'W) (893 m w.d.)	MD08-3180 [b] (38°N, 30°08'W) (3034 m w.d.)
No. of ^{14}C ages (23–12 cal. ka)	18	59 +3[c][d]	26 + 37[e][f]	44 + 5[g]	179[h]	68
Sediment slice/sample		1 cm	1.5 cm	1–2 cm		
Planktic species	*G. bulloides/ inflata /N. pachyderma* (s)	*G. bulloides*	*G. ruber*	*G. sacculifer*	*G. bulloides G. ruber*	*G. bulloides*
Number of tests/sample		318–944 (5–12 mg)	128–263 (1.6–5 mg)	66–299 (3–14 mg)		
Ø Sample res [yr]	~600	184	175 / 140*	134	104	105
B/A	700 – 1300	880	170 – 230	210 – 230	360	360 – 640
HS-1	700 – 1800	420 – 660	170 – 460	180 – 630	(-100 –) 90	1460 – 2170
LGM	1300 – 2400	730–1080	540 – 870	–	20 – 700	320 – 600
LGM (model) [i]	400 – 500	500 – 600	500 – 600	500 – 600	500 – 600	400 – 500
LGM (model[j])	At 50°S 2300 – 2700	1000 – 1300	800 – 1100	800 – 1100	500 – 800	600 – 900
LGM – PD [i] Model anomaly	100	100	200	100	100	100
LGM – PD [j] Model anomaly	At 50°S 1400 – 1800	400 – 600	400 – 600	200 – 400	200 – 400	200 – 400
LGM – B/A Empiric anomaly	600 – 1700	-150 – 200	370 – 640	–	-340 – 340	-40

Table 3.2: Model description for the reconstruction of changes in surface water reservoir age [*Franke et al., 2008; Butzin et al., 2012*]. * Use of an updated relationship between wind speed and gas transfer velocity for $^{14}CO_2$ air-sea exchange following Sweeney et al. [2007]. (a) Fanning and Weaver [1996]; (b) Bitz et al. [2001].

Study	Model	Coupled to other models	Resolution	Forcing	Parameters for PD	**Parameters for LGM**
Franke et al. [2008]	UVic ESCM v.2.7	– Two dimensional energy-moisture balance model of the atmosphere[(a)] – Dynamic-thermodynamic sea-ice model[(b)]	3,8° x 1,8°; 19 levels	– Top of the atmosphere solar insolation over a year; - Wind stress at ocean surface, monthly climatology	– Solar radiation (1950) – Land ice distribution (1950) – CO_2 = 280ppmv – Windfields: **recent** NCEP/NCAR	– Solar radiation (21kyr BP) – Land ice distribution (21kyr PB) – CO_2 = 200ppmv – Windfields: **recent** NCEP/NCAR
Butzin et al. [2012]	Hamburg LSG ocean circulation model (improved*)	– ECHAM3/T42	3.5° x 3.5° 22 levels	– Ten year averaged monthly fields of wind stress – Surface air temperature – Freshwater flux	– Present day SST – $\Delta^{14}C$ = 0‰ – CO_2 = 280ppmv	– GLAMAP SST as basis for ECHAM3/T42 simulation of AMOC – $\Delta^{14}C$ = 350‰ – CO_2 = 200ppmv – Modified freshwater balance in southern ocean mimics sea ice transport to the north

To allow testing of the model simulations we now provide a synthesis of six, partly published and partly new planktic ^{14}C reservoir age records from various key sectors of the low-latitude Atlantic (Fig. 3.1). Most records were established by means of the ^{14}C plateau tuning

technique [*Sarnthein et al.*, 2007, 2015]. In this way we generate a robust network of calendar age chronologies resolved at millennial-to-centennial age scales for last glacial and deglacial times: chronologies that may help in building global correlations of climate and atmospheric signals defined in ice cores, ocean sediments, and speleothems.

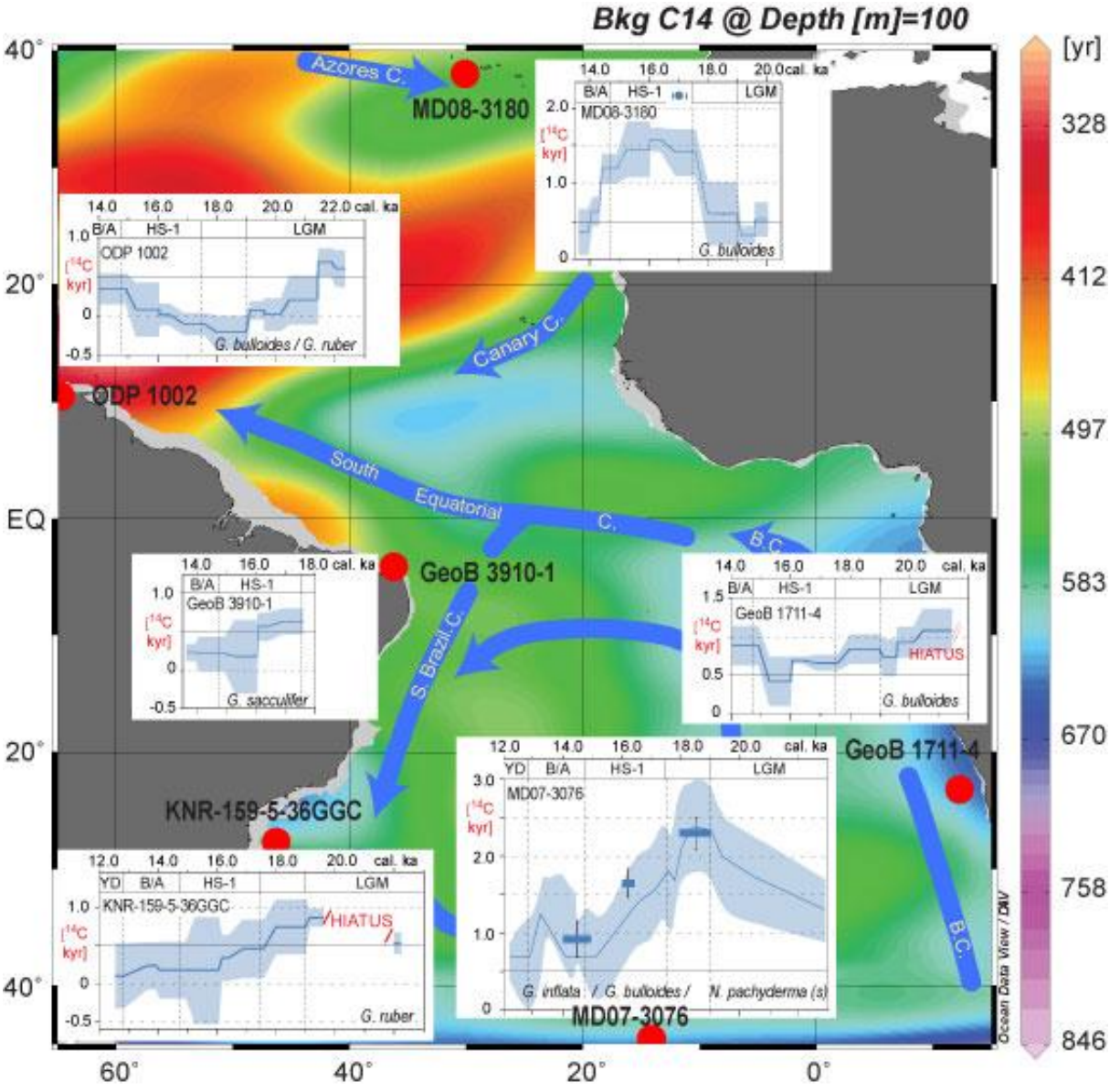

Figure 3.1: Distribution pattern of glacial-to-deglacial ^{14}C reservoir ages of surface waters at core sites in the tropical and subtropical-to-mid-latitude Atlantic vs. spatial variability of modern ^{14}C reservoir ages in top 100 m water depth modeled by Key et al. [2004]. Bkg = Background. Blue arrows show major surface currents (C.). B. = Benguela. Records of ODP1002 and MD08-3180 from Sarnthein et al. [2015], and MD07-3076 from Skinner et al. [2010], error ranges shaded in blue, compared to reservoir ages derived from *14*C plateau tuning (blue bars). Planktic foraminiferal species analyzed for 14C ages are given near bottom of age diagrams. Map based on R. Schlitzer [2015].

Our new records stem from three sites at the eastern and western continental margins of the South Atlantic (Table 3.1). Core GeoB 1711-4 was obtained from the Benguela Upwelling System off Namibia the intensity of which is linked to the strength of southeasterly trades [*Lütjeharms and Meeuwis*, 1987]. In part, the upwelled waters consist of South Atlantic Central Water (SACW) [*Shannon and Nelson*, 1996]. Cores GeoB 3910-1 and KNR 159-5-36GGC stem from the Brazilian Margin, where modern surface waters are widely stratified and belong to the North Brazil and South Brazil Currents (Fig. 3.1, Table 3.1). Moreover, Site KNR159-5 is partly influenced by a local cell of coastal upwelling of SACW, in particular during austral summer **[***Castelao et al.*, 2004].

To focus on the low-latitude and southern Atlantic, a major blank area in terms of ^{14}C reservoir ages, we supplement these ^{14}C records with the only planktic records of ^{14}C reservoir age published so far from the northern subtropical Atlantic (MD08-3180; *Balmer and Sarnthein*, resubm. after rev.; *Sarnthein et al*. [2015]) and subantarctic South Atlantic (MD07-3076; *Skinner et al*. [2010]), moreover, with one from the Cariaco Basin (OPD 1002; Sarnthein et al. [2015]) that formed an almost isolated deep lagoon, when sea-level dropped to the peak glacial and early deglacial low.

In total, these six empiric records provide a novel database for tracing changes in regional surface water circulation, stratification, and coastal upwelling with the transformation from the last glacial to the Bølling-Allerød episode that, in turn, have been controlled by past changes in seasonal wind strength. In particular, the records help us to test the consistency of data for the last glacial simulated by published GCMs and thus the underlying changes in ocean circulation the models are based on.

3.3 Methods

Initial age control of all cores was based on planktic oxygen isotope ($\delta^{18}O$) records (Fig. S.31a-c), in GeoB 1711-4 also on a benthic $\delta^{18}O$ record [*Little et al.*, 1997]. In GeoB 3910-1 we used an X-ray fluorescence (XRF) geochemical record to identify the Younger Dryas and Heinrich Stadial 1 (HS-1) by maxima in Ti/Ca that reflect humid conditions in nearby Eastern Brazil [*Jaeschke et al.*, 2007] (Fig. S3.2; details of method in Suppl. Text 3.1). The stratigraphic records served as guideline to focus our sediment sampling for ^{14}C dates of peak glacial and deglacial sediments. In total, we analyzed 59 samples of GeoB 1711-4 and 44 samples of GeoB 3910-1. Samples of 20 cm^3 each were spaced at 2.5 and/or 5 cm, and more closely near ^{14}C plateau boundaries (Tables 3.1 and S3.3). In core KNR-159-5-36GGC the glacial-to-deglacial section was first identified by wide-spaced ^{14}C ages of *G. ruber* [*Came et al.*, 2003; *Sortor and Lund*, 2011] (Table 3.1), now supplemented by 26 ^{14}C ages between 60 and 200 cm core depth (Table S3.3).

Sediment samples were freeze-dried, washed over a 63 µm sieve, and finally cleaned with deionized water. Monospecific planktic foraminifera tests for AMS ^{14}C analyses were picked in the 150–400 µm size fraction as detailed in Table 3.1.

Radiocarbon samples were analyzed at the facility for accelerator mass spectrometry (AMS) of the Leibniz Laboratory, University of Kiel, Germany (KIA numbers), and the Keck Carbon Cycle AMS facility (UCIAMS numbers), University of California, Irvine, USA (Table S3.3). In the Leibniz Laboratory samples were cleaned with 15% H_2O_2 in an ultrasonic bath to remove dust and detrital carbonate as well as organic surface coatings. CO_2 was released from the samples with 100% H_3PO_4 at 90°C and reduced with H_2 using Fe powder as catalyst. The ^{14}C concentration was measured by standard procedures, that is by comparing the

simultaneously collected ^{14}C, ^{13}C, and ^{12}C beams of each sample with those of oxalic acid standard CO_2 and those of pre-Eemian foraminifera [*Nadeau et al.*, 1998]. Samples at the Keck AMS Laboratory were cleaned and leached prior to hydrolyzation in 70% H_3PO_4. The released CO_2 was graphitized under H_2 on an iron catalyst before ^{14}C analysis [Vogel et al., 1984]. All ^{14}C values were converted into conventional ^{14}C ages following Stuiver and Pollach [1977], uncorrected for any reservoir age. Data are stored at www.pangaea.de.

3.3.1 Derivation of calendar ages

Both absolute calendar (cal.) ages and surface water reservoir ages were derived by means of the ^{14}C plateau-tuning technique following the definitions and rules defined by Sarnthein et al. [2007; 2015]. The suites of ^{14}C plateaus were identified in the planktic ^{14}C age-depth records by visual inspection and tuned to a suite of analogous plateaus in the atmospheric ^{14}C record of Lake Suigetsu between 22.5 and 12 cal. ka on the age scale based on varve counts [*Bronk Ramsey et al.*, 2012; *Sarnthein et al.*, 2015]. The locations of planktic ^{14}C plateau boundaries were objectively confirmed by inflection points (short-lasting maxima and/or the half-hight of steep slopes) in the 1st derivative record of all downcore changes in the ^{14}C age – depth relationship (details in Suppl. Text S3.2). Within each core the range of resulting sedimentation rates and their short-term variability (Fig. S3.1a-c) provides supportive information on the quality of plateau definitions.

For each ^{14}C plateau in each core planktic average reservoir ages were estimated from the difference between the average ^{14}C ages of coeval atmospheric and planktic ^{14}C plateaus. Uncertainties in planktic reservoir ages (uncertainty in Fig. 3.1, Table S3.1) were estimated by Gaussian error propagation and include the uncertainties of coeval atmospheric and marine ^{14}C plateaus (for 1.68σ, equivalent to a confidence interval of 90 % for Gaussian distribution).

Planktic ^{14}C reservoir ages were analyzed on various foraminifer species that represent different habitats and growth seasons (details in Suppl. Text S3.3). Oceanographic implications are discussed below.

In total, the suites of ^{14}C plateau boundaries provide us with 7–18 age control points in each core, depending on the time span of the ^{14}C record reconstructed (Fig. S3.1). These ages fully confirm the age estimates first deduced from δ^{18}O and XRF records (Figs. S3.1 and S3.2). The cal. ages derived by visual and mathematical methods of plateau definition hardly deviate by >50–100 yr [*Sarnthein et al.*, 2015]. In summary, we regard the suite of plateau boundary ages in each core as a robust estimate, in particular, since the series of reservoir ages appear fairly stable over a complete suite of plateaus and internally consistent within any particular ^{14}C record. They hardly reveal any abrupt rise that may result in an artificial plateau with boundaries that may mistakenly be picked as age tie points. An exception form reservoir ages in Core GeoB1711-4, which rise from 420 to 880 years between plateaus 2a and 1 (Fig. S3.1a).

Given that changes in atmospheric ^{14}C are short-term reflected by those of ocean surface waters [Sweeney et al., 2007] one may consider a simple test on this question: In case a ^{14}C age-depth plateau does not reflect any coeval atmospheric plateau defined at Lake Suigetsu but just reflects a temporary local rise in (upwelling and) reservoir age we may necessarily expect that the ^{14}C plateau immediately subsequent will record the elevated level of reservoir age reached during the increase of reservoir age over the antecedent 'pseudo'-plateau under discussion. This test case does not apply to any of the ^{14}C records employed in this study (Fig. S3.1). Moreover, the suites of ^{14}C plateaus employed each show a distinct atmospheric

analogue.

3.4 Results

Previous studies claimed that planktic reservoir ages were largely constant at ~400 ^{14}C yr in low-latitude surface waters [*Broecker et al.*, 2004; based on data of Stuiver and Braziunas, 1993]. By contrast, our new data reveal distinct spatial and temporal variations reasonably linked to major features of ocean circulation (Table 3.1, Fig. 3.1). Widely stratified surface waters along the west Atlantic continental margin (GeoB 3910-1; KNR 159-5-36GGC) show low reservoir ages ranging from 150–350 ^{14}C yr over Younger Dryas (YD)-to-late Heinrich Stadial 1 (HS-1) times, ages that rose up to 650–870 ^{14}C yr over early HS-1 and the terminal Last Glacial Maximum (LGM). By contrast, glacial-to-deglacial reservoir ages in the subtropical upwelling zone off Southwest Africa (GeoB 1711-4) ranged from 650 to 1100 ^{14}C yr, except for late HS-1, where reservoir ages shortly dropped to 420 ^{14}C yr. Reservoir ages were far more variable in both the mid-latitude Southern and Northern Atlantic. At 44°S (MD07- 3076), they almost reached 2500 ^{14}C yr at the end of the LGM as compared to 700–1200 ^{14}C yr during HS-1-to-YD times. Near the Azores they reached ~1600 ^{14}C yr during HS-1 as compared to ~500 ^{14}C yr and less before and after (MD08-3180).

It is interesting to compare our new age control points in GeoB 1711, GeoB 3910-1, and KNR 159-5-36 (Figs. 3.1 and S3.1a–c) to published age control points derived from both conventional ^{14}C dating and tuning of abrupt local changes in ocean climate to climate signals dated in Greenland or Antarctic ice core records. After all, the quality of our new plateau boundary-based ages appear superior to most age estimates that result from the widely used simple match of allegedly coeval oscillations in paleoclimate and paleoceanography, oscillations that actually do not need to be contemporaneous.

In Core GeoB 1711-4 Vidal et al. [1999] based their age model of glacial-to-deglacial climate events on four planktic ^{14}C ages, assuming that ^{14}C reservoir ages of 400 ^{14}C yr were constant. Moreover, they used conversion standards into calendar ages, that were based on a tuning of various benthic $\delta^{18}O$ oscillations in their core during MIS 1-3 to those of Core SU90-08 in the distant North Atlantic at 40°N. These oscillations were only coarsely dated by orbital tuning *sensu* Prell et al., [1986] and can hardly be coeval with those in GeoB 1711-4 on a millennial age scale because of transit times of deep waters exceeding many hundred years. Our new age interpolation between age-calibrated ^{14}C plateau boundaries (Tables S3.1 and S3.3; Fig. S3.1a) now results in calendar ages that exceed the former estimates as much as 1650 (late HS-1) to 2500 yr (top LGM).

Core GeoB 3910-1 was retrieved at the site of GeoB 3910-2 (core depths correlated in Supp. Table S3.2), the age model of which was based on 5–6 planktic ^{14}C ages, using a constant ^{14}C reservoir age of 400 ^{14}C yr [*Jaeschke et al*., 2007]. Our new reservoir age estimates (Table S3.1) and age interpolation between age-calibrated ^{14}C plateau boundaries (Fig. S3.1b) now lead to calendar ages that are much lower than the former age estimates, by up to 1000 yr for the time span of early ^{14}C Plateau 2a, 15.5–16 cal. ka. We tested our new age model by means of a salient Ti/Ca maximum during HS-1 (Fig. S3.2), which documents enhanced humidity on land [*Jaeschke et al*., 2007]. When compared to U/Th-dated periods of speleothem growth in Northeast Brazil, that likewise record this humid event [*Wang et al*., 2004], the new (interpolated) ages for the upper and lower boundaries of the Ti/Ca maximum indeed match those of the very onset and end of speleothem growth within the uncertainty range of age control.

As compared to the ^{14}C-based age model of Sortor and Lund [2011] ^{14}C plateau tuning at Core KNR-159-5-36 leads to a hiatus at 20.5 to ~21.5 cal. ka, formerly overlooked, moreover,

to significantly different calendar ages. Prior to ~16 cal. ka, the former age estimates exceed our new ages by 600–1300 yr, till 15 ka by 150–500 yr. From 15–13 cal. ka, both estimates are about equal and after 13 cal. ka, our new age numbers for the YD exceed the former estimates by 300–500 cal. yr (Table S3.3, Fig. 3.1c).

Finally, we used the youngest section of the planktic ^{14}C record and age model of MD07-3076 [*Skinner et al*., 2010] for a test of ^{14}C plateau tuning (Figs. 3.1 and S3.1d). It revealed a distinct Plateau 1, as expected, precisely coeval with the first part of the Antarctic Cold Reversal, where sedimentation rates are sufficiently high. However, we found nothing but fragments of plateaus 2 and 4, where sedimentation rates are 8 cm/cal. kyr and less. Note the ^{14}C reservoir ages revealed by fractional plateau tuning precisely match those derived by the approach of [Skinner et al., 2010] (Fig. 3.1).

In all cores we studied, planktic ^{14}C ages form coherent records of ^{14}C plateaus and jumps, except for two groups of ^{14}C age outliers in KNR-159-5-36, which spread over 40 cm core depth each (Fig. S3.1). The aberrant age populations closely gather around ages of 11.9 and 13.8 ^{14}C ka, that differ by 2000–3500 and 1500–2000 ^{14}C yr each from the remainder of the ^{14}C record which strictly follows the temporal pattern of the Suigetsu atmospheric ^{14}C record [*Bronk Ramsey et al*., 2012]. In harmony with Sortor and Lund [2011] we assign the age outliers to two Zoophycos burrowing events that now are precisely dated at 11.9 (planktic) ^{14}C kyr = ~13.5 cal. ka and 13.8 (planktic) ^{14}C kyr = 16.05–15.27 cal. ka (here extending over ^{14}C Plateau 2a).

The closely spaced age-calibrated ^{14}C plateau boundaries imply multiple centennial-scale changes in sedimentation rate, moreover, two millennial-scale stratigraphic gaps during late LGM, previously undetected (Figs. 3.1 and S3.1; details on Cores ODP1002 and MD08-3180

in Sarnthein et al. [2015]). In all cores sedimentation rates increase significantly over the YD, the second half of HS-1 (^{14}C Plateau 2a), and at terminal LGM (^{14}C Plateaus 4–5); in part, they rise by a factor >2. These short-term changes modify the age control formerly derived by linear interpolation of long-term sedimentation rates, thus may lead to major reassessments of paleoceanographic conclusions previously published. Re-evaluations are suggested in view of Dansgaard-Oeschger cycles as short as 1500 yr, the 2800-yr interval of HS-1, and the urgent need to trace centennial-to-millennial-scale leads and lags of climate signals either starting in the northern or southernmost high-latitude Atlantic.

3.5 Discussion

3.5.1 Modeled vs Empiric Reservoir Ages of LGM Surface Waters – a Comparison

Models of Franke et al. [2008] and Butzin et al. [2012] both assume that past reservoir age changes of tropical and subtropical-to-subpolar surface waters mainly result from changes in both atmospheric ^{14}C concentration and reductions in AMOC. According to Franke et al. [2008], using only atmospheric ^{14}C concentrations and a 30% AMOC reduction, LGM reservoir ages did hardly differ from preindustrial (PD) values by more than 100 ^{14}C yr, except for ~200 ^{14}C yr simulated off Southern Brazil and in the Caribbean. By contrast, Butzin et al. [2012], using a more refined and realistic model, simulate LGM anomalies that reach 200–600 ^{14}C yr in the low-latitude Atlantic and even 1400–1800 ^{14}C yr near ~50°S (Fig. 3.2; Table 3.1). In the Caribbean early deglacial age anomalies shortly reach 500 ^{14}C yr, though unspecified for the location precisely addressed by model simulation.

To compare the model data with our empiric monospecific records we ignore interspecies offsets and different seasonal signals of various planktic species (for details see Suppl. Text 3.3). Our empiric ^{14}C reservoir ages corroborate the main simulated patterns and trends of Butzin et al. [2012] (Table 3.1), but show discrepancies with model results of Franke et al.

[2008], mainly in the extremes in low latitudes. In the Benguela upwelling belt, empiric LGM reservoir ages are significantly higher than those of Franke et al. [2008], in contrast to modestly high ages in the west Atlantic, off Southern Brazil. In the LGM Cariaco Basin (ODP 1002), which then formed a semi-enclosed lagoon due to low sea level, empiric reservoir ages fell to close to zero at ~21–19 cal. ka. In this case the immediate exchange of atmospheric CO_2 dominated the LGM ^{14}C balance of Cariaco surface waters and stepwise replaced antecedent incursions of old surface waters from outside dominant prior to 21.5 cal. ka.

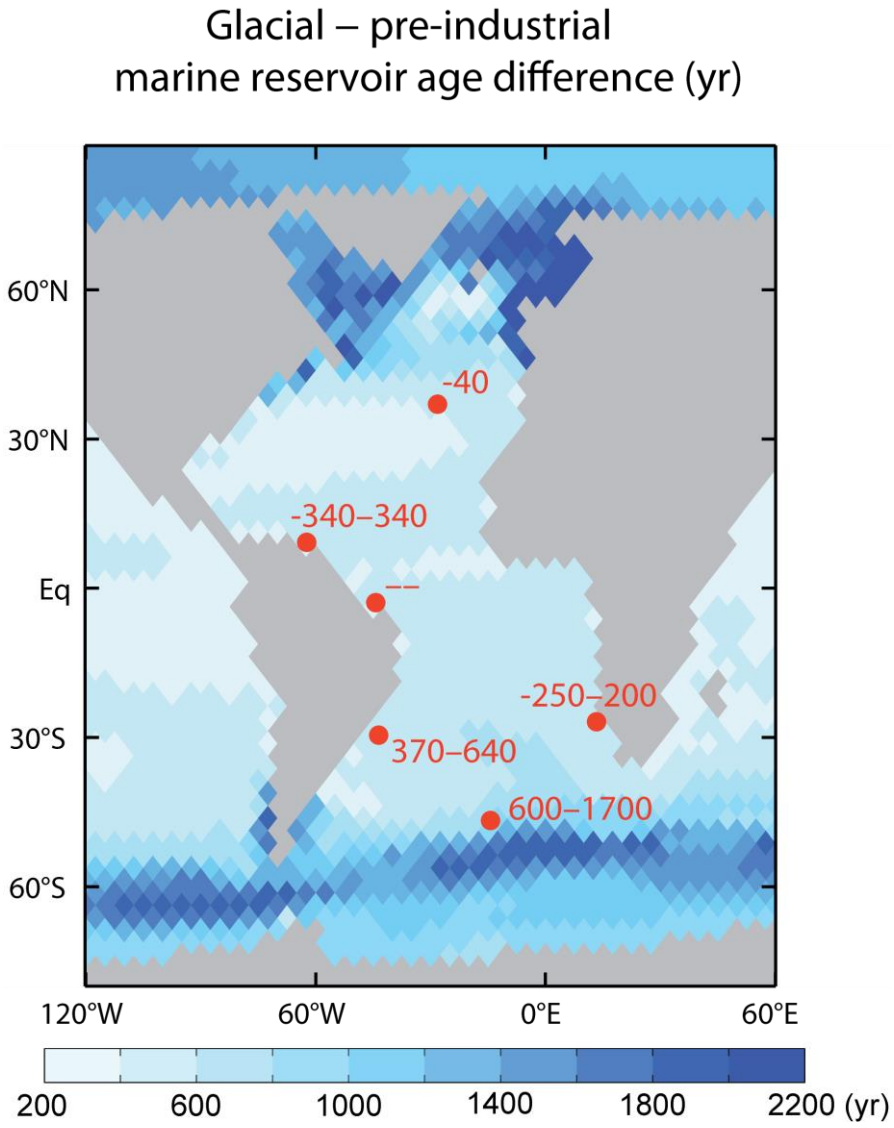

Figure 3.2: Simulated marine reservoir age difference between the glacial surface ocean (according to the spinup with LGM climate forcing, i.e. MOC scenario GS, $\Delta^{14}C_{atm}$ = 520‰ and atmospheric CO_2 = 185 ppmv) and the preindustrial (PD) surface ocean (control integration with present day climate forcing $\Delta^{14}C_{atm}$ = 0‰ and atmospheric CO_2 = 280 ppmv) [*Butzin et al.*, 2012, modified]. Red numbers are empiric LGM-to-B/A reservoir age anomalies regarded as in principle similar to those between the LGM and PD surface ocean.

At southern subpolar Site MD07-3076 LGM reservoir ages in part may present a subsurface signal because of meltwater stratification. These ages were reconstructed by tuning to Antarctic ice cores [*Skinner et al*., 2010] and by our technique of ^{14}C plateau tuning (Figs. 3.1 and S3.1d). Both lines of evidence produce reservoir ages that exceed the modeled age values of Franke et al. [2008] by 1000–2000 ^{14}C yr, but come fairly close to the estimates of Butzin et al. [2012] simulated for the major upwelling belt 4°-6° farther south. By contrast, empiric LGM reservoir ages at North Atlantic Site MD08-3180 match the age range predicted by both models (Table 3.1), as this site still belonged to the subtropics [*Pflaumann et al*., 2003]. Off Iberia, LGM reservoir ages of 400–500 yr modeled by Franke et al. [2008] likewise contrast with values modeled by Butzin et al. [2012] and empiric values of 1100–1700 yr of Skinner et al. [2014] (mainly based on *G. bulloides* and *N. pachyderma* s). The high local values probably resulted from LGM coastal upwelling [*Abrantes*, 1991].

In summary, the closer affinity of our empiric ^{14}C reservoir ages to the model ages of Butzin et al. [2012] versus those of Franke et al. [2008] may be linked to the more realistic model design of Butzin et al. (Table 3.2), which considered the LGM freshwater balance in the Southern Ocean and in particular, the LGM SST and wind fields, moreover, a more realistic gas transfer velocity for the exchange of ^{14}C of CO_2 of Sweeney et al. [2007].

3.5.2 High- vs. Low-Latitude Trends in Glacial-to-Deglacial Reservoir Age Records

Though Site MD08-3180 lies slightly south of the LGM subpolar front at 38°N, LGM-to-deglacial reservoir ages (Fig. 3.1) show a trend basically similar to that reported by Stern and Lisiecki [2013] for the ‘high-latitude North Atlantic’. Their results agree with ours in showing low reservoir ages of 300–600 yr for the LGM. They also agree for HS-1, when both high values of up to 1300–1600 yr and paired planktic $\delta^{18}O$ minima at MD08-3180 suggest major meltwater incursions (Balmer and Sarnthein, resubm.after rev.). In our record, however, these

events lasted from 18–14.5 cal. ka, but from 19.5–16 cal. ka in that of Stern and Lisiecki [2013]. The different timing may either record different meltwater events affecting different parts of the North Atlantic or suggest problems with the age model. By comparison, the deglacial, possibly meltwater-induced reservoir ages at South Atlantic Site MD07-3076 culminated as early as 19.2–18.0 cal. ka.

Trade winds are a major forcing of surface currents in the subtropical South Atlantic. As LGM trade winds intensified along the eastern continental margin during austral winter [*Little et a*l., 1997], coastal upwelling of ^{14}C-depleted intermediate waters was enhanced off Benguela, which resulted in maximum reservoir ages of surface waters (Figs. 3.1 and S3.1a), a feature promoted by the seaward shift of LGM coastlines. On the other hand, LGM reservoir ages and upwelling also increased at Site KNR-159-5-36 in the Southeast Brazil Bight, here probably controlled by enhanced winds during austral summer [*sensu Campos et al*., 2000] and by lowered sea-level.

Reservoir ages and upwelling dropped all over the subtropical South Atlantic over HS-1. In particular, reservoir ages dropped to 250–400 yr at ^{14}C Plateau boundary 2a–2b, 16.05 cal. ka. This marked drop immediately followed a distinct short-term rise in atmospheric pCO_2 and West Antarctic temperature at 16.3–16.05 cal. ka [Marcott et al., 2014], which probably induced a reduction of subtropical winds. The subsequent low in ^{14}C reservoir ages and Benguela upwelling already ended at the end of HS-1 (Fig. 3.1). In turn, Thornalley et al. [2015] demonstrated a clear feedback of the 16.2 ka event on AMOC with a strong pulse of deep-water convection that necessarily paralleled a widespread rejuvenation of surface waters as postulated by models and shown by our empiric records.

3.6 Conclusions

Glacial-to-deglacial planktic ^{14}C records were analyzed in the low- and mid-latitude Atlantic by means of the ^{14}C plateau-tuning technique. The results suggest significant spatial and temporal changes in the ^{14}C reservoir age of surface waters (Fig. 3.1) that imply a major step forward towards more accurate radiocarbon chronologies for the last deglaciation. In part, the changing reservoir ages are linked to changes in the habitat depth of planktic tracer species, taking into account differential monospecific ^{14}C records measured in parallel, and to changes in seasonal climate. These changes of climate affected the coastal upwelling belts off Southern Africa and Southern Brazil, where LGM reservoir ages reached 750-100 and almost 900 ^{14}C yr, respectively, suggesting an enhanced upwelling intensity as result of strengthened long-shore winds and seaward shoreline shift. Both changing reservoir ages and the interpolation of calendar ages between age-calibrated ^{14}C plateau boundaries lead to new age assignments that precisely match correlated U/Th-dated events in speleothems, but strongly differ from previous ^{14}C-based chronologies, thus imply the need of a re-evaluation of paleoceanographic correlations.

In the tropics and subtropics our empiric ^{14}C reservoir ages are largely consistent with model-based estimates of Butzin et al. [2012] for the LGM, also with extremes found in southern mid latitudes, but disagree with model estimates of Franke et al. [2008] that underestimate our mid-latitude values by up to ~2000 ^{14}C yr. The differences of the two models imply that realistic boundary conditions of SST and wind fields, moreover, the freshwater balance and past ^{14}C concentrations are needed to obtain realistic ^{14}C reservoir ages. Thus ^{14}C reservoir ages form a highly sensitive record and present an important tracer of past changes in ocean surface conditions and ocean circulation.

In summary, our new estimates of ^{14}C reservoir ages provide a novel basis to improve centennial-to-millennial-scale chronologies of the last glacial and deglaciation. They facilitate a series of new insights into past changes of climate and the spatial details and leads and lags of ocean circulation over short time scales by highlighting the importance of using detailed realistic boundary conditions in modeling.

3.7 Acknowledgments

We acknowledge valuable discussions with Gerrit Lohmann, and Birgit Schneider, moreover, helpful suggestions of reviewers on an earlier version of this manuscript. We thank the Kiel Leibniz Laboratory for AMS ^{14}C ages and John Southon, University of California Irvine, for measuring AMS ^{14}C ages on extremely small foraminifera samples, moreover, various students for careful help in sample preparation. Samples from South Atlantic cores were kindly provided by Delia Oppo, Woods Hole, and MARUM, Bremen, that also gave access to an XRF facility. Our study was supported by DFG grant Sa207/48.

3.8 Supplementary Information

3.8.1 S3.1 XRF-based Ti/Ca measurements

XRF measurements on GeoB 3910-1 were conducted at MARUM, Bremen University, Germany, using an XRF Core Scanner II (AVAATECH Serial No. 2). XRF data were collected every 4 mm using generator settings of 10 kV, a current of 0.5 mA, and a sampling time of 20 seconds. The surface of the sediment core was covered with a 4-micron thin SPEXCerti Prep Ultralenel foil to avoid contamination of the XRF measurement unit and desiccation of the sediment. The reported data was acquired by a Canberra X-PIPS Silicon Drift Detector (SDD; Model SXD 15C-150-500) with 150 eV X-ray resolution, the Canberra Digital Spectrum Analyzer DAS 1000, and an Oxford Instruments 50W XTF5011 X-Ray tube

with Rhodium (Rh) target material. Raw data spectra were processed by the analysis of X-ray spectra by iterative square software (WIN AXIL) package from Canberra Eurisys.

3.8.2 S3.2 1st Derivative

To identify plateaus in the curve of y = radiocarbon years against x = core depth in the sedimentary records (Fig. S3.1) we used the statistical method of Sarnthein et al. [2015]. It is based on the first derivative or slope of the curve over time, y'(x) = dy(x)/dx. Plateaus have by definition a slope of zero, while jumps in the curve have large slope values.

We use a running window, mathematically denoted as kernel, that is running along the x-axis and estimate the slope y' for x equal to the window's center using the points inside the window. This nonparametric technique is called kernel estimation. For example, we may consider the case of the running mean for estimating the zeroth derivative or mean trend, which uses a non-smooth uniform kernel. The first derivative is estimated via the first derivative of the kernel's trend estimate. The kernel method can be adjusted at the boundaries of the x-interval by using a smaller kernel width ("boundary kernel"). Details of the kernel method for derivative estimation are mathematically described by Gasser and Müller [1979; 1984], and described in a manner accessible to climatologists by Mudelsee [2014]. Both these papers and the book also contain the mathematical formulas and further references.

To construct a 1-sigma error band around the slope curve, we used bootstrap resampling [*Mudelsee*, 2014]. A resample y* is obtained by

(1) calculating the residuals (the differences between trend and data points),

(2) resampling point-wise random residuals, and

(3) adding the random residuals back to the trend. In case of our data, autocorrelation effects ("memory" of x-values) were negligible. A new first derivative is re-estimated on the

resample, yielding y*'(x). The procedure resampling–re-estimation is repeated until B = 10000 copies of y*'(x) are available. The standard error band results from the standard deviation over the B copies of y*'(x).

There is room for subjectivity in two dimensions. First, selection of the bandwidth (i.e., the width of the kernel function) determines the bias and variance properties of the slope estimate. Gasser and Müller [1984] defined objective guidelines to optimizing the bandwidth. However, we preferred some degree of 'undersmoothing' that is a smaller bandwidth that helps to better uncover the fine details (at the cost of these details being less significant). Second, a threshold value needs to be selected for defining plateaus and jumps in the ^{14}C record. Adopting a threshold value close to zero led to too many plateaus, while a more liberal, larger threshold value clearly led to a better agreement with the plateau boundaries previously identified by visual inspection.

The 1st derivative confirms the visual tuning of core GeoB 1711-4. Due to low data density we rely on jumps to identify ^{14}C plateau boundaries, except for the top of Plateau 4a. Plateau 3 appears smaller than suggested by the Suigetsu reference record (Fig. 3.2), because of decreasing reservoir ages. An outstanding jump at 210 cm core depth represents the hiatus identified by visual inspection. The 1st derivative of core GeoB 3910-1 is in line with the visual tuning of Plateaus 1a–3. Visual plateau boundaries are verified by jumps (Fig. 3.2). The plateau tuning of Core KNR 159-5-36GG is strongly confirmed by the 1st derivative, where the half heights of slopes constrain the boundaries of the YD Plateau. All other plateau boundaries are marked by jumps in the core depth – ^{14}C age relationship. A jump at 185 cm core depth reflects the hiatus identified by visual inspection.

3.8.3 S3.3 Interspecies Offsets and Inferred Seasonal Record of ^{14}C Signals

Cryptospecies IIb of *G. bulloides sensu* Darling and Wade [2008] is abundant in mid-latitudes and subtropical upwelling belts. It is widely regarded as 'gourmand' tracing maximum nutrition of upwelling seasons, but less dependent on changes in sea surface temperature (SST) [*Ganssen and Sarnthein*, 1983; *Sautter and Sancetta*, 1992; *Fraile et al*., 2009]. Thus ^{14}C variations of *G. bulloides* form a robust record of upwelling changes at Site GeoB1711-4 off Namibia, likewise of surface waters nutrient-enriched at Azores Site MD08-3180 during winter and spring [*Schwab et al*., 2012].

At ODP Site 1002 in the Cariaco Basin (and Cariaco 'lagoon' during LGM) most ^{14}C ages of *G. bulloides* exceed those of *G. ruber* by 100–200 ^{14}C yr, in rare cases by up to 600 ^{14}C yr. These anomalies imply that *G. bulloides* forms in waters more enriched in (slightly aged) dissolved inorganic carbon (DIC) than the surface waters where *G. ruber* is living with its symbionts [*Hemleben et al*., 1989]. During LGM and early HS-1 we find rare groups of samples where ^{14}C ages of *G. ruber* significantly exceed those of *G. bulloides*. These 'old' *G. ruber* samples are possibly enriched in reworked specimens admixed from outside to the sediments of the Cariaco lagoon through a shallow inlet channel (~25 m) during times of low sea level stand. In turn, ^{14}C ages analyzed on *G. ruber* and *G. sacculifer trilobus* give perennial records near the equator (GeoB 3910-1), but rather reflect summer conditions in the southern subtropics such as at Site KNR-159-5-36GGC [*Ganssen and Sarnthein*, 1983; *Mulitza et al*., 1998].

At Site MD07-3076, ^{14}C reservoir ages for sections older than 16.5 cal. ka were deduced from ^{14}C ages of *Neogloboquadrina pachyderma* (s). Though probably a different cryptospecies [*Darling and Wade*, 2008], the ^{14}C signal of South Atlantic *N. pachyderma* (s) may be ascribed to subsurface habitats per analogy to northern high latitudes [*Simstich et al*., 2003],

which in part may explain the elevated reservoir ages shown in Fig. 3.2. Likewise, the ^{14}C signal of *Globorotalia inflata* may stand for subsurface waters in transitional latitudes [*Groeneveld and Chiessi*, 2011].

3.8.4 Supplementary Tables

Table S3.1a: Definition of planktic ^{14}C plateaus in the ^{14}C record of GeoB 1711-4 (defined by visual inspection and confirmed by 1st derivative technique).

Plateau No.	TOP		BASE		AVERAGE ^{14}C yr		Pla. res. age [yr] (1.68 σ)	Pla. ΔΔ^{14}C [‰] (1.68 σ□	ATM fMC
	Depth [cm]	Age [cal yr]	Depth [cm]	Age [cal yr]	GeoB 1711-4	Suigetsu			
1	115	14050	125	14921	13357	12471	880±255	130±40	1.25
2a	127.5	15272	143.5	16050	13844	13426	420±320	67±51	1.325
2b	143.5	16050	150	16400	14543	13850	690±45	111±8	1.35
3	151.5	16900	156.5	17580	15335	14671	660±195	110±28	1.40
Comment:	By comparison with Suigetsu Plateau 3 the short length of Plateau 3 may be explained by a ~200-yr drop in local ^{14}C reservoir age over Plateau 3. Its actual range, 156.5–160.5 cm, is given by a dotted line in Fig. S3.1a.								
4	170	18000	175	18980	16690	15851	840±190	139±33	1.40
5a	177.5	19130	188.5	19600	17399	16670	730±240	126±43	1.45
5b	188.5	19600	195	20150	17936	17007	930±200	158±36	1.45
6a	197.5	20450	208.5	21420	18744	17667	1080±290	186±52	1.475
Comment:	Below Plateau 6a a ^{14}C jump of 2000 yr reflects a hiatus at 210–212 cm depth on top of sediments older than Plateau 7 (23 cal. ka).								

Table S31b: Definition of planktic ^{14}C plateaus in the ^{14}C record of GeoB 3910-1 (defined by visual inspection and confirmed by 1st derivative technique).

Plateau No.	TOP		BASE		AVERAGE ^{14}C yr		Pla. res. age [yr] (1.68 σ)	Pla. ΔΔ^{14}C [‰] (1.68 σ□	ATM fMC
	Depth [cm]	Age [cal yr]	Depth [cm]	Age [cal yr]	GeoB 3910-1	Suigetsu			
1a	83.5	13640	88.5	13940	12236	12006	230±110	34±2	1.20
1	89.5	14050	105	14921	12680	12471	210±220	32±34	1.25
2a	106	15272	136.5	16050	13602	13426	176±470	29±76	1.325
2b	136.5	16050	143.5	16400	14412	13850	560±180	91±30	1.35
3	145	16900	151.5	17580	15303	14671	630±160	106±27	1.40
Comment	Very low sedimentation rates below Plateau 3 suggest hiatus.								

Table S3.1c: Definition of planktic ^{14}C plateaus in the ^{14}C record of KNR 159-5-26GGC (defined by visual inspection and confirmed by 1st derivative technique).

Plateau No.	TOP		BASE		AVERAGE ^{14}C yr		Pla. res. age [yr] (1.68 σ)	Pla. ΔΔ^{14}C [‰] (1.68 σ□	ATM fMC
	Depth [cm]	Age [cal yr]	Depth [cm]	Age [cal yr]	KNR-159-5-36GGC	Suigetsu			
YD	70.5	12570	78.5	13000	10848	10747	100±425	15±62	1.20
1a	82.5	13640	88.25	13940	12240	12006	230±310	34±45	1.20
1	88.25	14050	100.5	14921	12650	12471	180±370	28±56	1.25
2a	102.5	15272	131	16050	13600	13426	170±700	28±111	1.325
2b	131	16050	140.75	16400	14190	13850	340±300	56±50	1.35
3	146.5	16900	162.5	17580	15130	14671	460±380	78±65	1.40
4	164.75	18000	176	18980	16600	15851	750±360	125±61	1.40
5a	177.5	19130	182.5	19600	17540	16670	870±120	149±21	1.45
Comment	Two suites of ^{14}C outliers with approximately uniform ^{14}C age each are ascribed to two events of *Zoophycos* burrowing (Fig.3.1c). Below Plateau 5a a ^{14}C jump of ~1200 yr reflects a hiatus at 182.5–185.5 cm depth.								
7	190.5	22010	-	-	19380	18843	540±140	98±26	1.50

Table S3.2: Correlation of ^{14}C ages in GeoB 3910-2 to core depths in GeoB 3910-1 by means of tuning high-resolution Ti/Ca records. 1) Jaeschke et al. [2007].

Raw ^{14}C ages[1)]		GeoB 3910-2[1)]	GeoB 3910-1
KIA No.	^{14}C age [yr]	Depth [cm]	Depth [cm]
KIA6813	12840±110	88	97
KIA25825	13550±70	103	111,8
KIA25824	14000±70	113	129
KIA6812	15780±110	148	153
KIA6811	20000±170	173	170
KIA25822	20580±150	183	175,4
KIA6808	22480±220	193	201

Table S3.3: Results of ^{14}C measurements for three cores from the tropical and subtropical South Atlantic. The ages of plateau boundaries were tuned to the calendar ages of (Suigetsu) atmospheric plateau boundaries (see text). In between, calendar ages were deduced by linear interpolation. Beyond our suite of ^{14}C plateaus ^{14}C ages (marked in red) were converted using Calib 7.0.4 [*Stuiver and Reimer*, 1993] with the Marine13 dataset [*Reimer et al*., 2013] and extrapolating the reservoir age of the next closest ^{14}C plateau up- or downcore (accepting potential errors of this extrapolation). Note that raw ^{14}C ages from three different laboratories, measured on closely spaced neighbor samples over almost two decades, closely agree, thus reflect true ^{14}C concentrations.

S3.3a) GeoB 1711-4: ^{14}C ages measured on *G. bulloides.*

KIA and UCI Laboratory numbers	Core Depth [cm]	Conventional ^{14}C age [yr]	1σ error	Plateau No.	Reservoir age [yr]	Calendar age [yr]
UCI 127536	105	12355	±30	-	-	13336
UCI 127537	107.5	12640	±25	-	-	13604
UCI 127538	110	12930	±25	-	-	13928
UCI 127539	112.5	13050	±30	-	-	14056
KIA 47685	115	13220	+70/-60	1	880±255	14050
UCI 127540	117.5	13215	±30	1	880±255	14268
KIA 47679	120	13410	±110	1	880±255	14486
KIA 49307	122.5	13460	±70	1	880±255	14703
KIA 47687	125	13480	+70/-60	1	880±255	14921
KIA 49305	127.5	13660	±70	2a	420±140	15272

KIA 47680	130	13740	±120	2a	420±140	15394
KIA 49399	132.5	13700	±70	2a	420±140	15515
KIA 47688	135	13870	±70	2a	420±140	15637
†KIA 4109	137.5	14060	±60	2a	420±140	15758
KIA 47681	140	14030	±120	2a	420±140	15880
KIA 49308	142.5	13850	±70	2a	420±140	16000
KIA 47689	145	14560	±70	2b	690±45	16131
KIA 49309	147.5	14520	±80	2b	690±45	16265
KIA 47682	150	14550	±130	2b	690±45	16400
KIA 49353	152.5	15500	±90	3	660±195	16971
KIA 47686	155	15170	±90	3	660±195	17174
UCI 140160	156.5	15580	±60	3	660±195	17296
KIA 49354	157.5	15720	±90	-	-	17377
UCI 140161	158.5	15830	±60	-	-	17458
KIA 47683	160	15880	±110	-	-	17580
KIA 49355	162.5	16070	±110	-	-	17685
KIA 47684	165	16220	±160	-	-	17790
KIA 49356	167.5	16390	+100/-90	-	-	17895
KIA 47622	170	16680	±140	4	840±190	18000
KIA48699	175	16700	±90	4	840±190	18980
UCI 140162	176.5	16850	±70	-	-	19070
KIA 49357	177.5	17160	±110	5a	730±240	19130
KIA 47664	180	17590	+ 180/-170	5a	730±240	19237
KIA 49365	182.5	17410	+120/-110	5a	730±240	19344
KIA 47665	185	17610	±190	5a	730±240	19450
UCI 127542	187.5	17225	±40	5a	730±240	19557
KIA 47666	190	17950	±170	5b	930±200	19727
KIA 49366	192.5	17870	±130	5b	930±200	19938
KIA 47667	195	17990	+190/-180	5b	930±200	20150
UCI 140163	196.5	18350	±70	-	-	20330
KIA 49367	197.5	18650	±140	6a	1080±290	20450
KIA 47668	200	18760	±180	6a	1080±290	20670
KIA 49368	202.5	18890	±140	6a	1080±290	20891
KIA 47669	205	18690	±190	6a	1080±290	21111
KIA 49369	207.5	18730	±150	6a	1080±290	21332
KIA 47670	210	19250	±190	-	-	22046
KIA 49398	212.5	21250	±160	-	-	24233
KIA 47671	215	20810	+250/-240	-	-	23755
KIA 49306	217.5	21290	+170/-160	-	-	24272
KIA 47672	220	21290	+280/-270	-	-	24280
KIA 49400	222.5	20200	+150/-140	-	-	23032
KIA 47673	225	21630	+310/-300	-	-	24755
KIA 49401	227.5	21490	+170/-160	-	-	24563
KIA 47674	230	21800	+280/-270	-	-	24916
KIA 49414	232.5	21580	±170	-	-	24683
KIA 47675	235	22640	+370/-350	-	-	25816
KIA 49415	237.5	23510	+220/-210	-	-	26742
KIA 47676	240	23580	+420/-400	-	-	26785
*KIA 555	242.5	18740	±130	-		21348
KIA 47677	245	25040	+490/-460	-	-	28080

KIA 47678	250	25490	+490/-460	-	-	28396
†KIA 4110	288	29130	±240	-	-	31814

*Little et al., 1997; † Vidal et al., 1999

S3.3b: GeoB 3910-1: ^{14}C ages measured on *G. sacculifer*.

KIA and UCI Laboratory numbers	Core Depth [cm]	Conventional ^{14}C age [yr]	1σ error	Plateau No.	Reservoir age [yr]	Calendar age [yr]
KIA 48760	50.5	9885	±45	-	-	11071
KIA 48761	60.5	10075	±45	-	-	11224
KIA 48762	70.5	10550	50/-49	-	-	12127
KIA 48763	80.5	11810	±50	-	-	13418
KIA 49429	81.5	11890	±60	-	-	13496
KIA 49430	83.5	12150	±60	1a	230±110	13640
KIA 49431	85.5	12360	±60	1a	230±110	13760
KIA 49432	87.5	12200	±60	1a	230±110	13880
UCI 128554	89.5	12460	±30	1	210±220	14050
KIA48764	90.5	12865	±60	1	210±220	14106
†KIA 6813	97	12840	±110	1	210±220	14471
KIA48765	100.5	12620	±60	1	210±220	14668
UCI 128555	102.5	12615	±30	1	210±220	14781
UCI 128556	104.5	12335	±35	1	210±220	14893
KIA 49433	106.5	13840	+80/-70	2a	176±470	15285
KIA 49527	108.5	13200	±70	2a	176±470	15336
KIA48766	110.5	13190	±70	2a	176±470	15387
†KIA 25825	111.8	13550	±70	2a	176±470	15412
UCI 128557	114.5	12855	±30	2a	176±470	15489
KIA 49528	117.5	13800	±70	2a	176±470	15565
KIA 48767	120.5	13820	±70	2a	176±470	15642
KIA 49529	124.5	13760	±80	2a	176±470	15744
†KIA 25824	129	14000	±70	2a	176±470	15859
KIA 49530	133.5	13330	±70	2a	176±470	15973
UCI 128558	134.5 – 135.5	13530	±35	2a	176±470	15999 – 16024
KIA 49531	137.5	14320	±80	2b	560±180	16100
UCI 128559	139.5	14600	±35	2b	560±180	16200
KIA 49567	141.5	14250	±70	2b	560±180	16300
UCI 128560	142.5	14480	±40	2b	560±180	16350
KIA 49568	145.5	15240	±80	3	630±160	16943
UCI 128561	147.5	15185	±40	3	630±160	17155
KIA 49569	149.5	15370	±90	3	630±160	17368
UCI 140169	151.5	15420	±50	3	630±160	17580
†KIA 6812	153.4	15780	±110	-	-	18416
UCI 140170	153.5	15750	±45	-	-	18379
UCI 144777	154.5	15795	±40	-	-	18426
KIA 49570	156.5	16640	±100	-	-	19324
UCI 140171	157.5	16700	±60	-	-	19391
UCI 144778	158.5	16765	±45	-	-	19497
KIA 49571	161.5	17590	±100	-	-	20447

UCI 140172	163.5	17670	±70	-	-	20550
UCI 144779	164.5	18090	±60	-	-	21068
KIA 49572	165.5	18280	±120	-	-	21335
UCI 140174	167.5	18480	±70	-	-	21635
KIA 49573	170.5	19050	±120	-	-	22293
UCI 140173	172.5	19220	±70	-	-	22447
KIA 49574	174.5	19520	+140/-130	-	-	22733
†KIA 6811	175.4	20000	±170	-	-	23310
UCI 132989	182.5	20510	±90	-	-	23923
†KIA 25822	183	20580	±150	-	-	24000
†KIA 6808	201	22480	±220	-	-	25908

†Jaeschke et al., 2007; ^{14}C ages from GeoB 3910-2, depths are correlated based on tuned Ti/Ca ratios (see Table S3.2)

S3.3c: KNR 159-5-36GGC: ^{14}C ages measured on *G. ruber*.

UCI and NOS Laboratory numbers	Core Depth [cm]	Conventional ^{14}C age [yr]	1σ error	Plateau No.	Reservoir age [yr]	Calendar age [yr]
*OS-27350	60	9450	±50	-	-	10644
†UCI 64771	60.5	9115	±20	-	-	10232
*OS-25479	64	10750	±90	-	-	12590
†UCI 92828	65.5	9425	±20	-	-	10620
†UCI 77922	67.5	10425	±25	-	-	12120
*OS-23210	68	10600	±45	-	-	12469
†UCI 64783	70.5	10705	†30	YD	100±425	12570
UCI 144785	72.5	10860	±45	YD	100±425	12640
†UCI 77923	75.5	10990	±25	YD	100±425	12745
UCI 144786	77.5	10835	±35	YD	100±425	12815
*OS-23211	80	11400	±50	-	-	13161
UCI 140175	80.5	12260	±90	-	-	13245
†UCI 64784	80.5	11485	±30	-	-	13245
UCI 144787	82.5	12200	±35	1a	230±310	13640
†UCI 77924	85.5	12460	±30	1a	230±310	13797
UCI 140176	87.5	12105	±40	1a	230±310	13901
*OS-23212	88	12200	±50	1a	230±310	13927
UCI 144788	88.5	12770	±60	1	180±370	14068
†UCI 64785	90.5	12705	±35	1	180±370	14210
*OS-22677	92	12450	±60	1	180±370	14317
UCI 144789	92.5	12600	±80	1	180±370	14352
†UCI 77925	95.5	12275	±30	1	180±370	14565
UCI 140177	97.5	6925	±25	1	180±370	14708
†UCI 64786	100.5	12710	±30	1	180±370	14921
UCI 140178	102.5	13235	±50	2a	170±700	15272
*OS-23318	104	13550	±60	2a	170±700	15313
UCI 144790	104.5	13560	±60	2a	170±700	15327
†UCI 77926	105.5	13295	±35	2a	170±700	15354
†UCI 64787	110.5	13465	±35	2a	170±700	15490
*OS-23317	112	13650	±60	2a	170±700	15331
†UCI 77927	115.5	13630	±30	2a	170±700	15627

UCI 144791	117.5	13945	±50	2a	170±700	15682
†UCI 64788	120.5	13350	±40	2a	170±700	15763
UCI 140179	122.5	13740	±50	2a	170±700	15818
UCI 144794	123.5	11800	±55	2a	170±700	15845
†UCI 77928	125.5	13765	±35	2a	170±700	15900
UCI 140181	127.5	11360	±45	2a	170±700	15956
†UCI 64789	130.5	13955	±35	2a	170±700	16036
UCI 144795	132.5	11905	±45	2b	340±300	16104
†UCI 92829	134.5	14340	±70	2b	340±300	16176
†UCI 64790	140.5	14045	±35	2b	340±300	16391
*OS-23213	141	14850	±120	-	-	16421
†UCI 77929	142.5	11975	±25	-	-	16549
UCI 140182	144.5	13500	±60	-	-	16720
†UCI 92906	146.5	15240	±90	3	460±380	16890
*OS-22678	148	12350	±65	3	460±380	16955
†UCI 64791	150.5	15500	±70	3	460±380	17063
UCI 140183	155.5	14090	±60	3	460±380	17278
UCI 140184	157.5	15220	±90	3	460±380	17364
†UCI 64792	160.5	12055	±30	3	460±380	17494
UCI 144796	162.5	15590	±110	3	460±380	17580
UCI 140185	165.5	16790	±120	4	750±360	18066
UCI 144797	166.5	16480	±140	4	750±360	18155
†UCI 64793	170.5	14365	±35	4	750±360	18510
UCI 144798	173.5	13450	±60	4	750±360	18775
UCI 140186	175.5	16530	±90	4	750±360	18953
UCI 140187	177.5	17520	±100	5a	870±120	19130
†UCI 77930	180.5	17510	±60	5a	870±120	19412
†UCI 92910	182.5	17590	±80	5a	870±120	19600
†UCI 77931	185.5	18780	±70	-	-	20504
UCI 140188	187.5	18930	±120	-	-	21106
†UCI 77932	190.5	19340	±60	7	540±140	22010
UCI 140189	195.5	19420	±100	-	-	22723
† UCI 77933	200.5	15525	±50	-	-	18210

*Came et al., 2003; †Sortor and Lund, 2011

Table S3.4: Age control points for estimates of sedimentation rate.

S3.4a: GeoB 1711-4

^{14}C Plateau boundaries used as tie points	**Calendar age [yr]**	**Core depth [cm]**	**Sedimentation rate [cm/kyr]**
Top 1 – Base 1	14050 - 14921	115 – 125	11.4
Base 1 – Base 2a / Top 2b	14921 - 16050	125 – 143.5	16.3
Top 2b – Top 3	16050 - 16890	143.5 – 151.5	9.5
Top 3 – Base 3	16890 - 17580	151.5 – 160	12.3
Base 3 – Base 4	17580 - 18980	160 – 175	10.7
Base 4 – Base 5a / Top 5b	18980 - 19600	175 – 188.5	21.7

Top 5b – Base 5b	19600 - 20150	188.5 – 208.5	11.8
Base 5b – Base 6a	20150 - 21420	195 – 208.5	10.6

S3.4b: GeoB 3910-1

^{14}C Plateau boundaries used as tie points	Calendar age [yr]	Core depth [cm]	Sedimentation rate [cm/kyr]
Top 1a– Base 1a	13640 - 13940	83 – 88.5	16.7
Base 1a – Base 1	13940 - 14921	88.5 – 105	16.8
Base 1 – Base 2a / Top 2b	14921 - 16050	105– 136.5	27.9
Top 2b – Top 3	16050 - 16890	136.5– 145	10.1
Top 3 – Base 3	16890 - 17580	145 – 151.5	9.4

S3.4c: KNR 159-5-36GGC

^{14}C Plateau boundaries used as tie points	Calendar age [yr]	Core depth [cm]	Sedimentation rate [cm/kyr]
Top YD– Base YD	12570 - 13000	70 – 78.5	18.6
Base YD – Base 1a	13000 - 13940	78.5 – 88.25	10.3
Base 1a – Base 1	13940 - 14921	88.25– 100.5	12.4
Base 1 – Base 2a / Top 2b	14921 - 16050	100.5– 131	27
Top 2b – Top 3	16050 - 16890	131 – 146.5	18.4
Top 3 – Top 4	16890 – 18000	146.5 – 164.75	16.4
Top 4 – Top 5a	18000 – 19130	164.75 – 177.5	11.2
Top 5a – Base 5a	19130 - 19600	177.5 – 182.5	10.6

3.8.5 Supplementary Figures

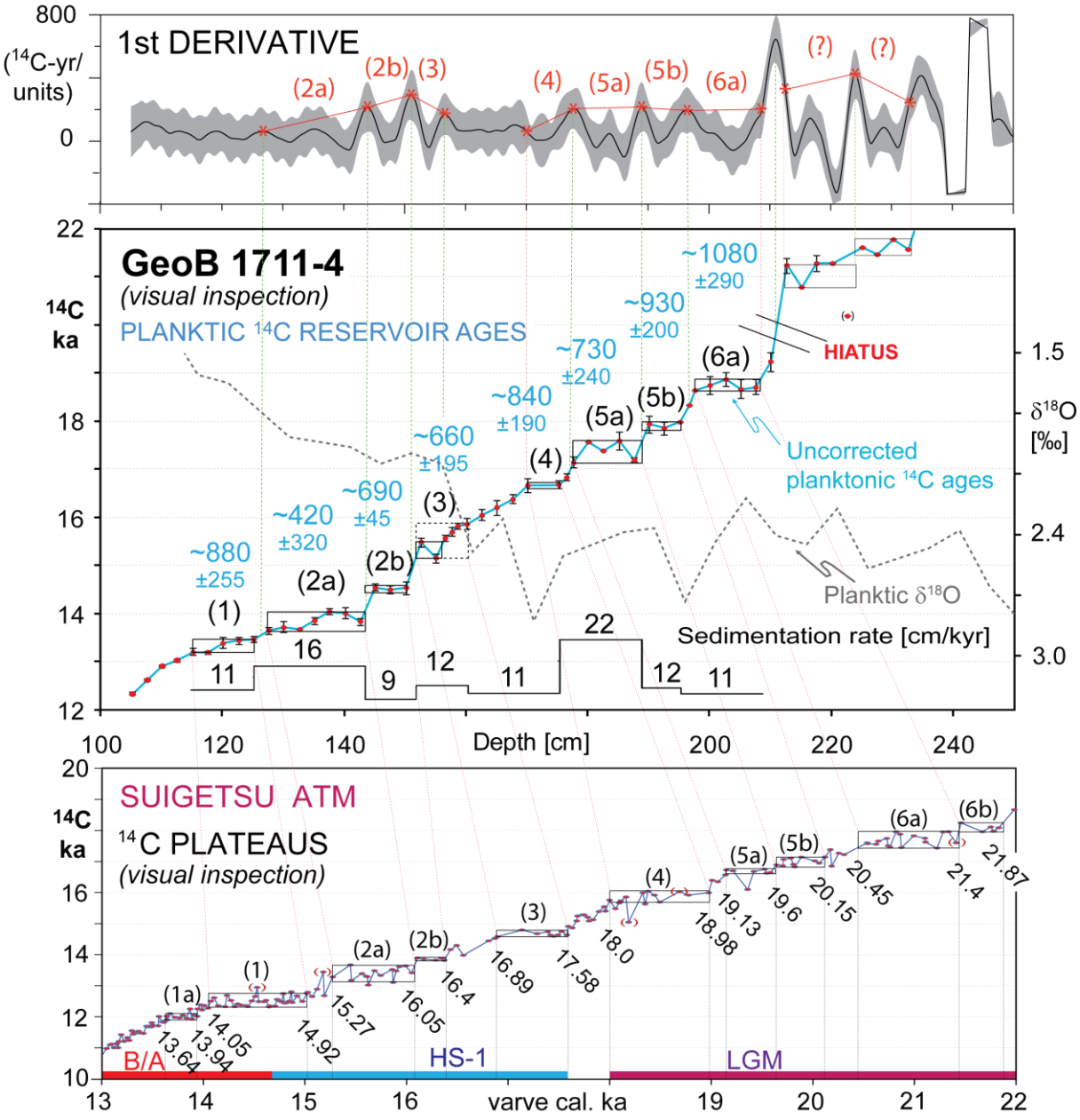

Figure S3.1a: Mid panel: Planktic ^{14}C records of core GeoB1711-4 (Table S3.3a) plotted vs. core depth, moreover, vs. planktic δ^{18}O records [*Little et al.*, 1997], finally, vs. sedimentation rates. In panels below, planktic ^{14}C plateaus (horizontal boxes) and/or ^{14}C jumps are tuned to atmospheric (atm) ^{14}C plateau suite of Lake Suigetsu [*Bronk Ramsey et al.*, 2012], with varve-based calendar ages given below. Local planktic reservoir ages (in blue) result from difference between the average uncorrected ^{14}C age of planktic ^{14}C plateaus measured in a core and the ^{14}C age of equivalent atmospheric ^{14}C plateaus numbered 1 – 7 (numbers in brackets). Topmost panel each shows 1st derivative units (^{14}C yr per cm core depth; bandwith: 1/3 optimum smoothing at 2.5 cm sample spacing) and 1-sigma uncertainty range (shaded). High values indicate ^{14}C jumps (linked by green correlation lines). Low values ^{14}C plateaus (correlation lines and numbers in red) constrained at "half-height" by asterisks. YD = Younger Dryas, B/A = Bølling-Allerød, H1 = Heinrich Stadial 1, LGM = Last Glacial Maximum. Sedimentation rates interpolated between plateau boundary ages (Table S3.4a).

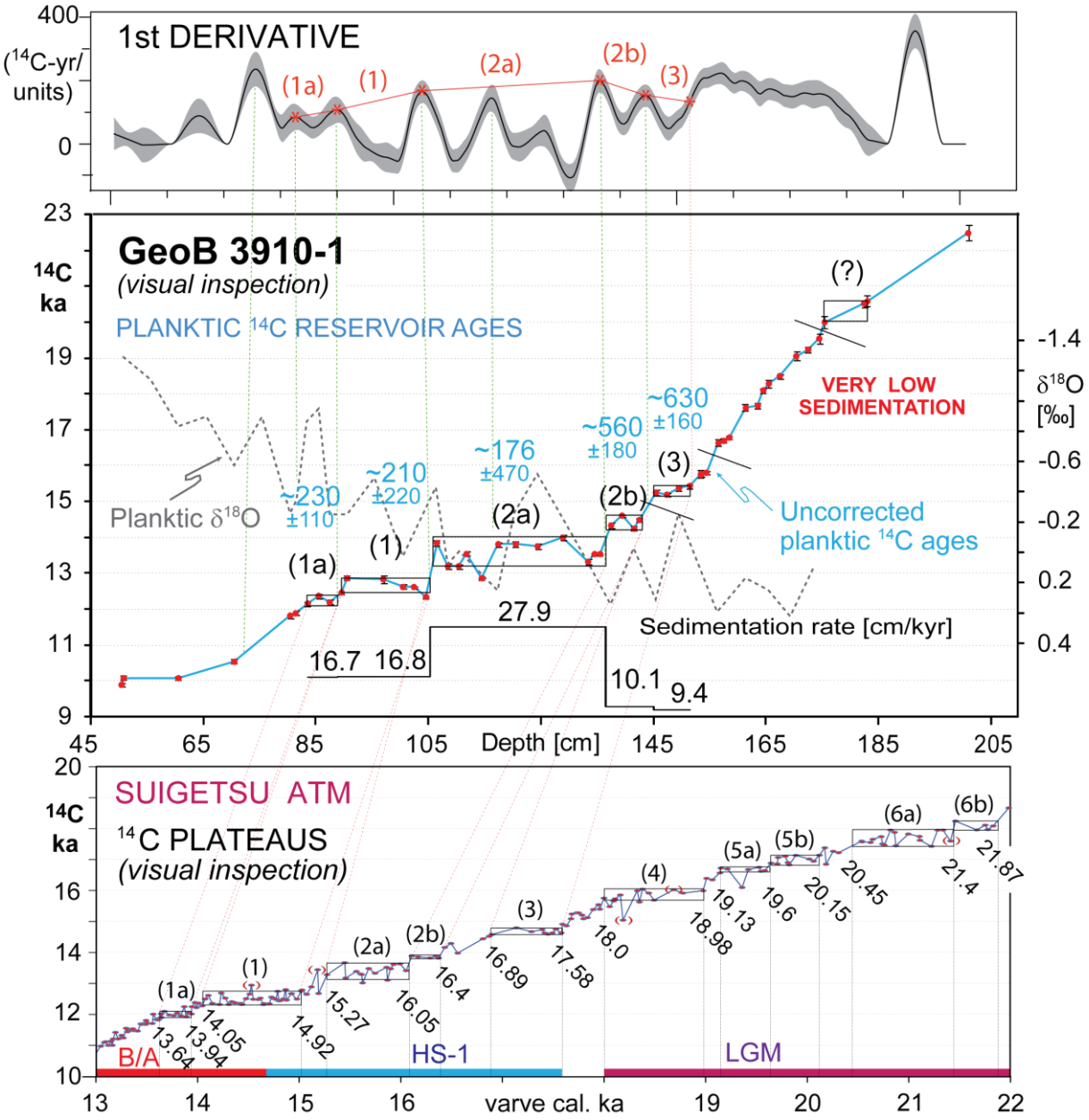

Figure S3.1b: Mid panel: Planktic ^{14}C records of cores GeoB3910-1 (Table S3.3b) plotted vs. core depth, moreover, vs. planktic δ^{18}O (this study), finally, vs. sedimentation rates. In panels below, planktic ^{14}C plateaus (horizontal boxes) and/or ^{14}C jumps are tuned to atmospheric (atm) ^{14}C plateau suite of Lake Suigetsu [*Bronk Ramsey et al*., 2012], with varve-based calendar ages given below. Local planktic reservoir ages (in blue) result from difference between the average uncorrected ^{14}C age of planktic ^{14}C plateaus measured in a core and the ^{14}C age of equivalent atmospheric ^{14}C plateaus numbered 1 – 7 (numbers in brackets). Topmost panel each shows 1st derivative units (^{14}C yr per cm core depth; bandwith: 1/3 optimum smoothing at 2.5 cm sample spacing) and 1-sigma uncertainty range (shaded). High values indicate ^{14}C jumps (linked by green correlation lines). Low values ^{14}C plateaus (correlation lines and numbers in red) constrained at "half-height" by asterisks. YD = Younger Dryas, B/A = Bølling-Allerød, H1 = Heinrich Stadial 1, LGM = Last Glacial Maximum. Sedimentation rates interpolated between plateau boundary ages (Table S3.4b).

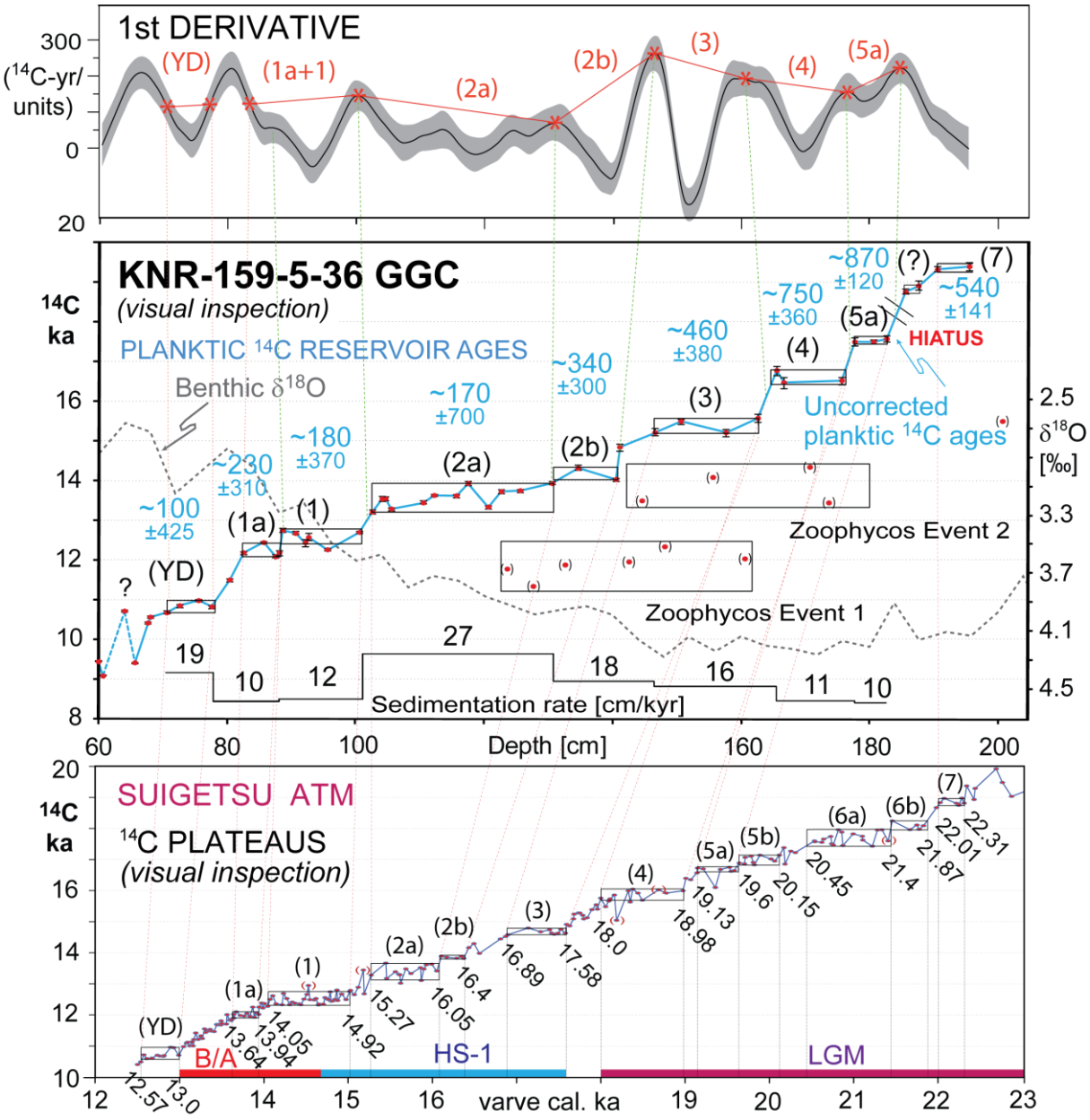

Figure 3.1c: Mid panel: Planktic ^{14}C records of core KNR-159-5-36 GGC (Table S3.3c) plotted vs. core depth, moreover, vs. benthic δ^{18}O [*Curry and Oppo*, 2005], finally, vs. sedimentation rates. In panels below, planktic ^{14}C plateaus (horizontal boxes) and/or ^{14}C jumps are tuned to atmospheric (atm) ^{14}C plateau suite of Lake Suigetsu [*Bronk Ramsey et al*., 2012], with varve-based calendar ages given below. Local planktic reservoir ages (in blue) result from difference between the average uncorrected ^{14}C age of planktic ^{14}C plateaus measured in a core and the ^{14}C age of equivalent atmospheric ^{14}C plateaus numbered 1 – 7 (numbers in brackets). Topmost panel each shows 1st derivative units (^{14}C yr per cm core depth; bandwith: 1/3 optimum smoothing at 2.5 cm sample spacing) and 1-sigma uncertainty range (shaded). High values indicate ^{14}C jumps (linked by green correlation lines). Low values ^{14}C plateaus (correlation lines and numbers in red) constrained at "half-height" by asterisks. YD = Younger Dryas, B/A = Bølling-Allerød, H1 = Heinrich Stadial 1, LGM = Last Glacial Maximum. Sedimentation rates interpolated between plateau boundary ages (Table S3.4c).

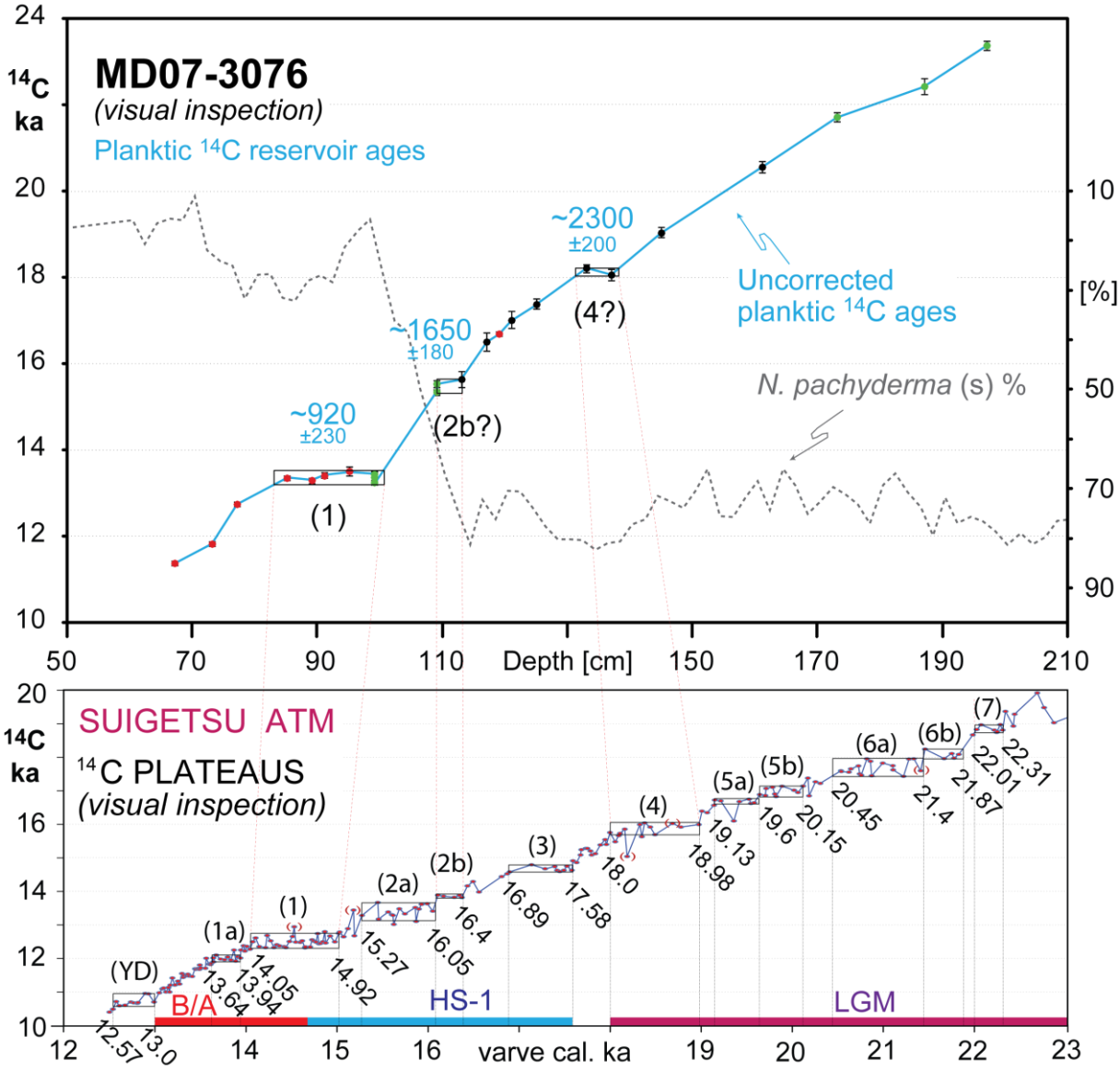

Figure 3.1d: Mid panel: Planktic ^{14}C records of core MD07-3076 plotted vs. core depth, moreover, vs. planktic species counts [*Skinner et al.*, 2012]. In panel below, planktic ^{14}C plateaus (horizontal boxes) and/or ^{14}C jumps are tuned to atmospheric (atm) ^{14}C plateau suite of Lake Suigetsu [*Bronk Ramsey et al.*, 2012], with varve-based calendar ages given below. Local planktic reservoir ages (in blue) result from difference between the average uncorrected ^{14}C age of planktic ^{14}C plateaus measured in a core and the ^{14}C age of equivalent atmospheric ^{14}C plateaus numbered 1 – 7 (numbers in brackets). YD = Younger Dryas, B/A = Bølling-Allerød, H1 = Heinrich Stadial 1, LGM = Last Glacial Maximum.

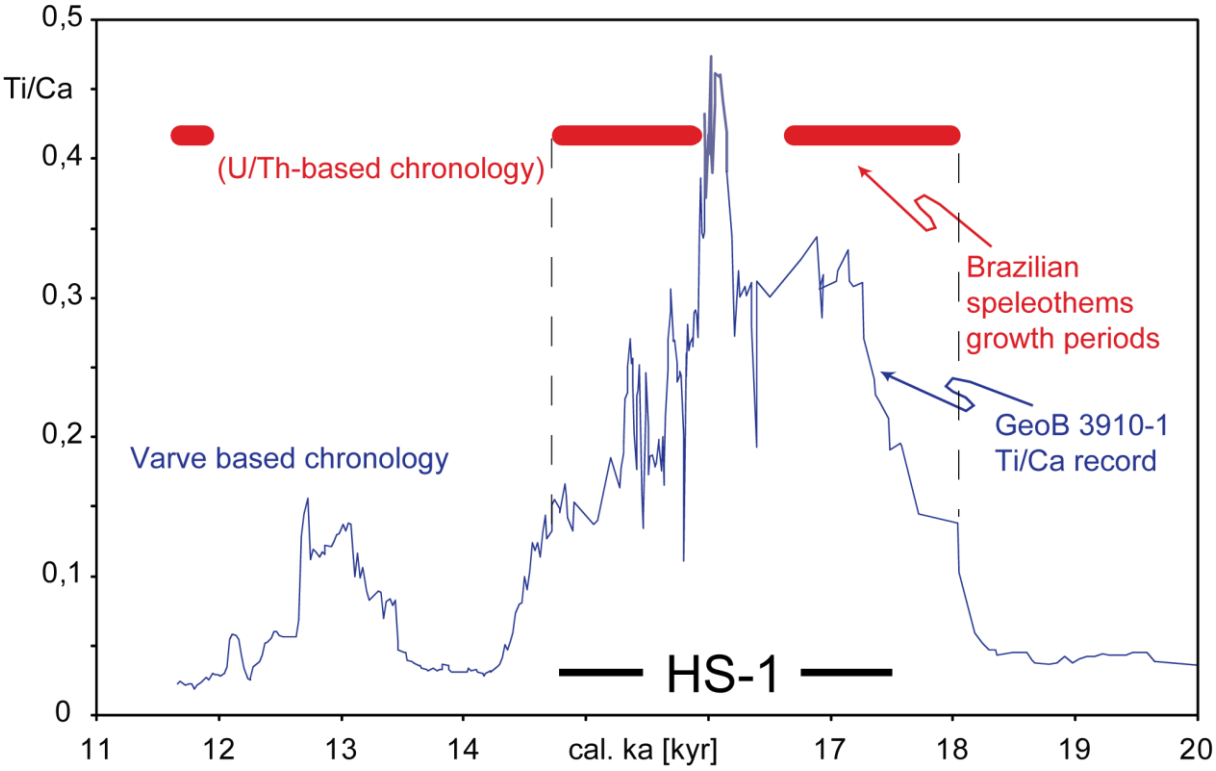

Figure S3.2: Deglacial Ti/Ca record of Core GeoB3910-1 vs. Suigetsu varve-based calendar age [*Bronk Ramsey et al.*, 2012], compared to growth periods of speleothems in Northeast Brazil [*Wang et al.*, 2004].

Chapter 4

Planktic ^{14}C plateaus, a result of short-term sedimentation pulses?

Sven Balmer and Michael Sarnthein

Submitted to *RADIOCARBON*

4.1 Abstract

The tuning of plateaus in glacial and deglacial planktic ^{14}C records to pertinent structures in the atmospheric ^{14}C record of Lake Suigetsu results in both a record of surface water reservoir ages and a centennial-scale absolute age model. However, the atmospheric origin of planktic ^{14}C plateaus may be questioned. Alternatively, plateaus may result from short pulses of increased hemipelagic sediment deposition, which challenges the technique of ^{14}C plateau tuning. To test the two rationales for the interval 23–12 cal. ka we calculated hypothetical sedimentation rates for all ^{14}C plateaus identified in five Atlantic sediment cores assuming sediment pulses that either span 10, 100, 200, or 300 years each. These rates were compared to rates derived by ^{14}C plateau tuning that assumes an atmospheric origin of the plateaus.

In each plateau suite our hypothetical sedimentation rates result in at least one or two cases in extreme values that exceed the rates reported for short lasting pulses of sediment deposition in contourites by a factor of 50 and therefore appear unrealistic. Moreover, they result in entire suites of plateau structures that ‘incidentally’ appear closely aligned to the pattern of atmospheric ^{14}C plateau suites rather than to any pulses of climate-controlled sediment discharge.

4.2 Introduction

Over the last 40 kyr, changes in atmospheric ^{14}C concentration are best recorded in laminated sediments of Lake Suigetsu, Japan [*Bronk Ramsey et al*., 2012]. The record includes numerous distinct centennial-to-millennial-scale periods of constant ^{14}C ages called ^{14}C plateaus, where the short-term scatter of ^{14}C ages hardly exceeds 100–300 ^{14}C yr. In the age–depth profile of Lake Suigetsu ^{14}C plateaus show a ratio of ^{14}C years versus calendar years with an overall gradient of less than 1. [*Sarnthein et al*., 2015]. Atmospheric ^{14}C signals are transferred to ocean surface waters within a decade [*Nydal et al*., 1980; *Sweeney et al*., 2007]. Accordingly, ^{14}C plateaus may likewise be documented in the planktic ^{14}C record of marine sediments.

Indeed, some 14 sediment cores from various parts of the ocean (Fig. 4.1) already record pertinent glacial and deglacial ^{14}C plateaus with approximately constant ^{14}C ages that extend over ~5–50 cm and up to 200 cm sediment thickness, where long-term average rates of hemipelagic sedimentation exceed 10 cm/kyr [*Sarnthein et al*., 2007; 2015]. The atmospheric ^{14}C plateau boundaries have been age-calibrated to the incremental time scale of the Suigetsu record (Fig. 4.2A) that is based on varve counts independent of any radiometric dating [*Bronk Ramsey et al*., 2012]. The boundaries may thus provide a suite of narrow-spaced age control points for marine sediment records [*Sarnthein et al*., 2015].

However, planktic ^{14}C plateaus may also have an alternative origin in marine sedimentation processes. Plateau-like structures each may derive from a short-lasting massive rise in sedimentation rate, in the extreme, from instantaneous turbidite deposition, a question addressed in this study. By contrast, periods of reduced hemipelagic sedimentation rate may

shorten ^{14}C plateaus down to a length below sampling resolution, which may lead to minor and/or major "jumps" in ^{14}C age. In particular, jumps may apply to hiatuses, periods of non-

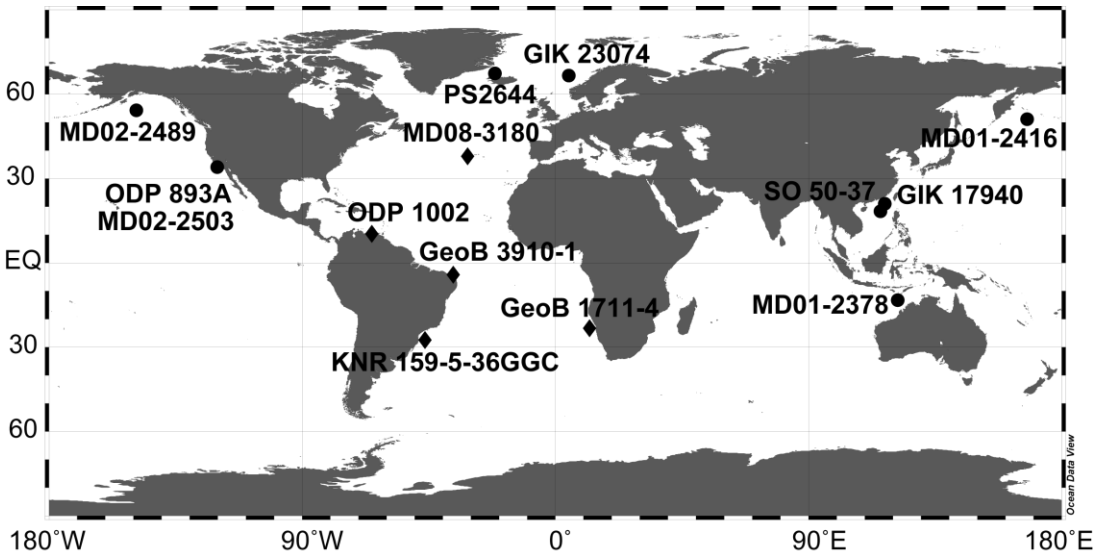

Figure 4.1: Locations of ^{14}C plateau-tuned sediment cores [*Sarnthein et al., 2015,* supplemented]. Diamonds mark locations of cores cited in this study.

deposition and/or sediment erosion, the frequency of which necessarily rises with the time resolution established by our densely spaced age control points and with the increase of average sedimentation rates [following *Sadler*, 1999].

To cope with these sources of uncertainty various rules have been defined for ^{14}C plateau tuning [*Sarnthein et al.*, 2007]. In particular, all sediment sections are ignored, where visual inspection indicates any small-scale turbidite-related structures that necessarily result in ^{14}C plateaus independent of atmospheric ^{14}C signals. As compared to average sedimentation rates of 0.1–2 cm/kyr that prevail over large regions in the deep sea [*Seibold and Berger*, 1996] ^{14}C plateau tuning is restricted to (hemi-) pelagic sedimentation rates >10 cm/kyr of sediment drifts, where short plateaus of >300/400 yr can still be resolved. The tuning technique strictly

excludes sediment sections from shallow-sea regions, where changes in eustatic sea-level result in incoherent stratigraphic records [*Sadler*, 1999].

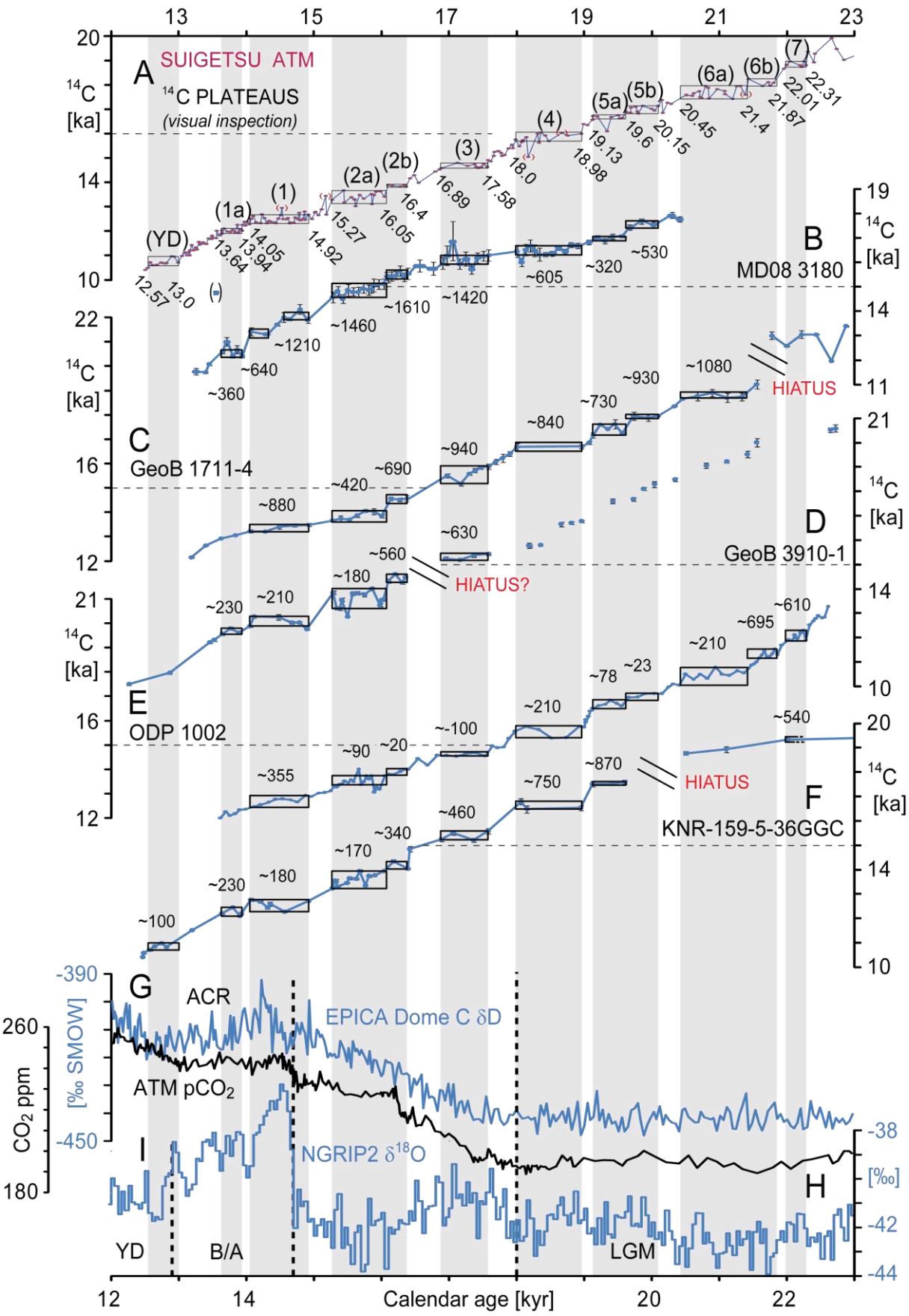

Figure 4.2: Comparison of marine ^{14}C plateaus in five Atlantic sediment cores (B–F) with atmospheric (ATM) ^{14}C plateaus of Lake Suigetsu (A) [*Bronk Ramsey et al.*, 2012], and climate signals from southern and northern high latitudes at 12 to 23 cal. ka (G–I). Black boxes, grey vertical bars, and numbers in brackets in ^{14}C record of Lake

Suigetsu (A) mark atmospheric ^{14}C plateaus defined by visual inspection. Numbers below boxes show calendar ages of plateau boundaries [Sarnthein et al., 2015]. Horizontal dashed lines show 15 ^{14}C ka age for reference. Numbers above or below plateaus in ^{14}C records B – F show surface water reservoir ages deduced by ^{14}C plateau tuning [Sarnthein et al., 2015; Balmer and Sarnthein, resubm. after rev.]. In ^{14}C record D (GeoB 3910-1) the tuning does not extend beyond Plateau 3; further back ages of ^{14}C dates are extrapolated using the sedimentation rate of Plateau 3. (G) δD record of EPICA Dome C [*Jouzel et al.*, 2007]; ACR = Antarctic Cold Reversal. (H) Deglacial rise in atmospheric pCO_2 [Marcott et al., 2014]. (I) $\delta^{18}O$ record of NGRIP2 at 50-yr resolution [*Rasmussen et al.*, 2014]; YD: Younger Dryas, B/A: Bølling–Allerød, LGM: Last Glacial Maximum.

Irrespective of these constraints, the potential origin of marine ^{14}C plateaus still remains a matter of discussion, that is, whether it may result from changes in sedimentation rate. In this study we test the relationship between any individual ^{14}C plateau and sedimentation rate in five sediment cores, where detailed age models have been first developed from plateau tuning [*Sarnthein et al*., 2015; *Balmer et al*., resubm. after rev.]. We focus on sediment records from the tropical and subtropical Atlantic each representing a different depositional environment between 12 and 23 cal. ka (Table 4.1). For each core we compare the published short- and long-term average sedimentation rates deduced from plateau tuning with a set of different hypothetical short-term depositional scenarios of enhanced sedimentation pulses affecting each single ^{14}C plateau (Fig. 4.3).

Table 4.1: Plateau-tuning derived and hypothetical ranges of sedimentation rate [cm/kyr] for ^{14}C plateaus in sediment cores MD08 3180, GeoB 1710-4, GeoB 3910-1, ODP 1002, and KNR-159-5-36GGC. MAR = Mid Atlantic Ridge.

Core Number and Core Location	MD08 3180 (38°N / 30°08'W) 3064 m w.d.			GeoB 1711-4 (23°17'S / 12°23'W) 1976 m w.d.			ODP 1002 (10°42'N / 65°10'W) 893 m w.d.			GeoB 3910-1 (04°15'S / 36°21'W) 2361 m w.d.			KNR 159-5-36GGC (27°31'S / 46°28'W) 1268 m w.d.		
Depositional environment	Narrow, steep-flanked sediment pockets at MAR[a)]			Cape Basin, upwelling induced high productivity[b)]			Marginal basin / Lagoon, restricted deep-water circulation, high productivity[c)]			Continental slope[d)]			Sao Paulo Plateau, intermittent coastal upwelling[e, f)]		
Stratigraphic unit	B/A	HS-1	LGM	B/A	HS-1	LGM	B/A	HS-1	LGM	B/A	HS-1	LGM	B/A	HS-1	LGM
Plateau tuning derived sed. rates [cm/ kyr] [f) g) h)]	28 – 45	28 – 70	110 – 167	11	9 – 16	11 – 22	50	35 – 90	40 – 110	17	9 – 28	–	11 – 19	12 – 27	10
Average rate	80			13			62			17			16		
Sedimentation rates as result of hypothetical pulses in sediment discharge															
10 yr plateau deposition	1550	2900 – 5900	6250 – 10450	1000	650 – 1600	500 – 1100	2100	2670 – 9830	2230 – 6100	500	700 – 3050	–	575 – 800	975 – 2850	500 – 1125
100 yr plateau deposition	155	290 – 590	625 – 1045	100	65 – 160	50 – 110	210	267 – 983	223 – 610	50	70 – 305	–	58 – 80	98 – 285	50 – 113
200 yr plateau deposition	78	145 – 295	313 – 523	50	33 – 80	25 – 55	105	134 – 492	112 – 305	25	35 – 152.5	–	29 – 40	49 – 143	25 – 56
300 yr plateau deposition	52	97 – 196	265 – 348	33	22 – 53	17 – 37	70	90 – 326	73 – 203	17	23 – 102	–	19 – 27	33 – 95	17 – 38

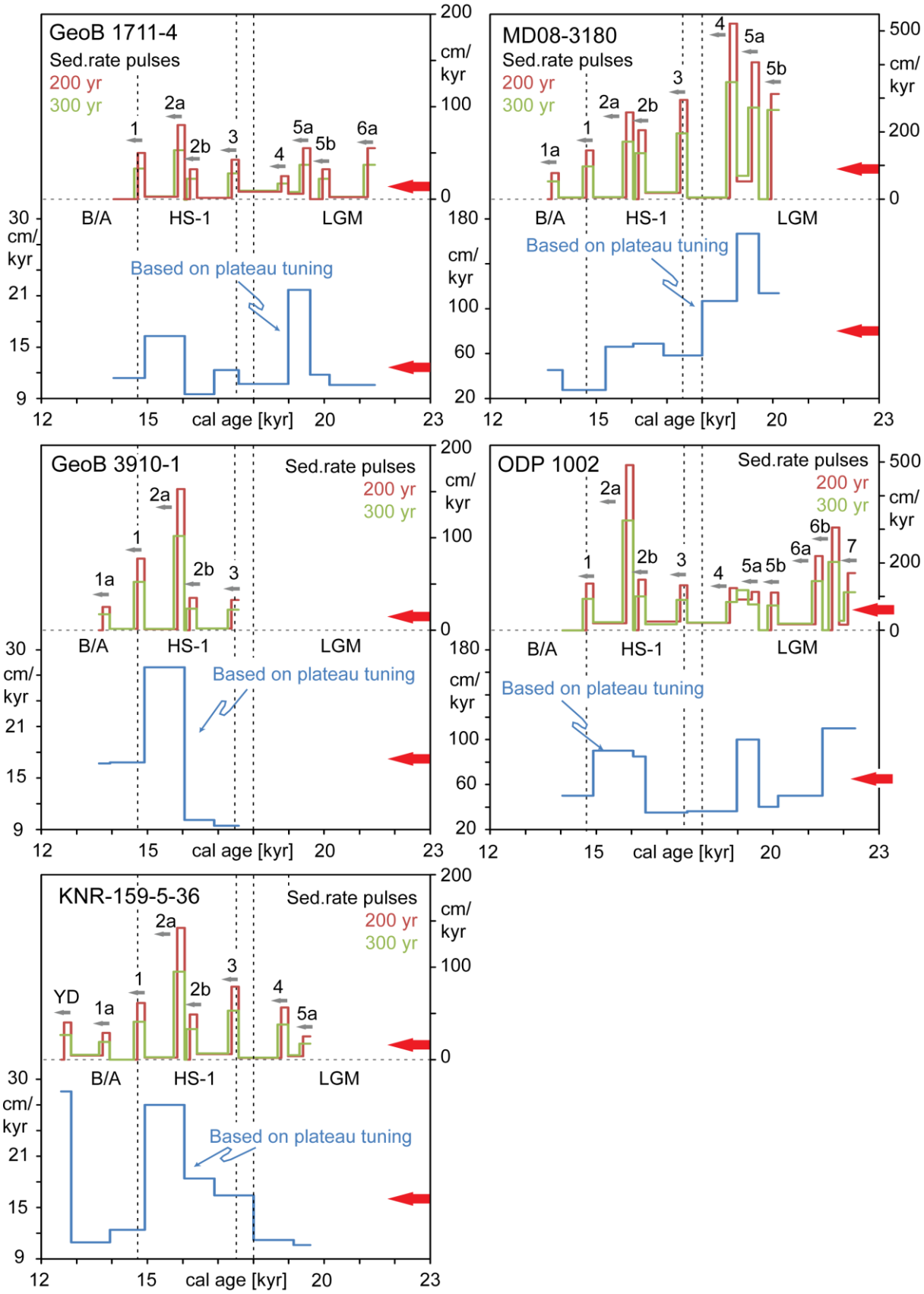

Figure 4.3: Sedimentation rates based on ^{14}C plateau tuning (blue lines) versus hypothetical pulses of sedimentation rate estimated for 200 and 300 yr-long pulses and differential ^{14}C plateau lengths in Atlantic sediment cores GeoB 1711-4, MD08 3180, GeoB 3910-1, ODP 1002, and KNR-159-5-36GGC. Red arrows mark long-term average in sedimentation rate for total plateau suite. Grey arrows mark direction of sediment discharge. B/A: Bølling–Allerød, HS-1: Heinrich Stadial 1, LGM: Last Glacial Maximum.

4.3 Materials and Methods

For this theoretical study we started by using published ^{14}C records as well as published age models and sedimentation rate data derived by means of the ^{14}C plateau tuning technique [*Sarnthein et al*., 2007] for Atlantic cores MD08 3180, GeoB 1711-4, GeoB 3910-1, ODP 1002, and KNR 159-5-36GGC (Fig. 4.2, Table 4.1) [*Sarnthein et al*., 2015; *Balmer and Sarnthein*, resubm. after rev.; *Balmer et al*., resubm. after rev.] (Details in Suppl. Texts S4.1–S4.2). To test whether the atmospheric age calibration is a necessary and best-possible rationale to explain the planktic ^{14}C plateau suite or might be replaced by a sequence of climate-controlled sedimentation pulses we established several hypothetical depositional scenarios for each ^{14}C plateau in each core.

We tested 10, 100, 200, and 300-yr long pulses of increased but non-turbiditic sediment accumulation starting right at the base of each ^{14}C plateau. We derived the atmospheric calendar age of the plateau base from the Suigetsu atmospheric ^{14}C record, hence arbitrarily considered these ages as "firm" reference levels for the lack of any other appropriate age markers. On top of them the differential sedimentation rates are estimated from the sediment thickness of each plateau section and the hypothetical length of the differential sedimentation pulses. The rates necessarily produce a hypothetical 'new' age for the plateau top, that differs from that derived by plateau tuning. The sedimentation rates of sediment sections that separate two subsequent ^{14}C plateaus each are estimated from the 'new' age of the plateau top now based on the end of the sedimentation pulse and the "firm" age of the next-following plateau base, moreover, from the sediment thickness deposited in between.

For the stratigraphic definition of the Last Glacial Maximum (LGM) we use the time slice of the 'Last Isotope Maximum' (23–18 cal. ka) defined by GLAMAP [*Sarnthein et al*., 2003b]. We follow Denton et al. [2006] and Sarnthein et al. [2011] for Heinrich Stadial 1 (HS-1)

(17.5–14.7 cal. ka), Svensson et al. [2008] for the Bølling-Allerød (B/A), and Jouzel et al. [2007] for the Antarctic Cold Reversal (ACR).

4.4 Results

We calculated for each ^{14}C plateau in each core four different hypothetical sedimentation rates derived for time spans of 10, 100, 200, and 300 yr each. The results show for each core a succession of up to 10 short lasting pulses of increased sedimentation rate with maxima ranging from 17 to 350 cm/kyr for the 300-yr scenario and ranging from 500 to 10450 cm/kyr for the 10-yr scenario (Fig. 4.3, Table S4.1).

On top of each plateau the hypothetical sedimentation rates need to drop to zero or less, that means, we need to postulate significant sediment erosion to keep balanced the long-term average sedimentation rate. In all cores the rates by far exceed the average sedimentation rates deduced from atmospheric plateau tuning by a factor of 6 to 180. Also, these rates exceed hemipelagic sedimentation rates of 97–200 cm/kyr as listed for contourites along the Mid-Norwegian Margin, in the Gulf of Cadiz [*Hernández-Molina et al*., 2015], and in the South China Sea [*Bühring et al*., 2004; *Bryn et al*., 2005; *Shao et al*., 2007; *Toucanne et al*., 2007] by a factor of 3.5–50.

In our test series (Fig. 4.3), Cariaco Basin ODP core 1002, Namibia core GeoB1711-4, and Brazilian Margin cores GeoB 3910-1 and KNR 159-5-36GGC show the highest hypothetical sedimentation rates during HS-1 (Plateau 2a), then reaching from 1600–9800 cm/kyr in the 10-yr and 50–325 cm/kyr in the 300-yr interval of ^{14}C plateau deposition. By comparison, Azores core MD08 3180 shows hypothetical sedimentation rates of 270–8150 cm/kyr for all four scenarios of the late LGM (Plateau 5a) and a maximum of 350–10450 cm/kyr for Plateau 4 in between LGM and HS-1 (Fig. 4.3, Table S4.1).

In contrast to the suite of odd sedimentation rate 'chimneys' that may result from short-lasting deposition pulses used to explain the suites of ^{14}C plateaus, the sedimentation rates derived from plateau tuning (lower panels in Fig. 4.2) show far more uniformity over time spans of 1000–4000 yr in all five Atlantic sediments cores analyzed.

When derived by means of ^{14}C plateau tuning, the changes from high to low and low to high rates may each be ascribed to specific climatic scenarios. For example, cores MD08-3180, GeoB 1711-4 and ODP 1002 show relatively enhanced sedimentation rates during the late LGM, which are attributed to an increased discharge of aeolian dust and terrigenous clay to the Atlantic basins [*Bacon*, 1984; *Harrison et al*., 2001], to increased primary productivity [*Sarnthein et al*., 1988], and/or to the lowered sea level [*Wallmann et al*., 2016], implying an enhanced sediment transport across shallow-water regions down to the deep sea. In all cores, the LGM rates dropped toward the HS-1 by a factor of 0.2–2.7. In part, the drop possibly resulted from global warming and decreasing wind gradients [*Shakun et al*., 2012], in part from the global sea level rise [*Wallmann et al*., 2016], both of which led to a reduced sediment discharge to the ocean. However, toward the end of HS-1 the rates in all cores rose from 9–35 to 16–90 cm/kyr, except for MD08 3180, where they dropped from 70 to 28 cm/kyr. Along the Brazilian margin and at ODP Site 1002 this rise may be ascribed to a wet period in the Brazilian North East [*Wang et al*., 2004] that induced an increase in river discharge [*Jaeschke et al*., 2007]. Later on, at the onset of B/A, sedimentation rates were widely reduced, except for a rise in cores MD08-3180 and KNR 159-5-36GGC.

4.5 Dicussion

Planktic ^{14}C plateaus were tuned to a pertinent suite of ^{14}C plateaus in the atmospheric record of Lake Suigetsu [Bronk Ramsey et al., 2012] to derive both an absolute age model and ^{14}C

reservoir ages for ocean sediment records. In effect, planktic ^{14}C plateaus in marine sediments are considered as direct reflection of the suite of atmospheric ^{14}C plateaus (Hypothesis 1). Alternatively, we may assume that planktic ^{14}C plateaus merely result from a series of short transient pulses of extremely high sedimentation rates (Hypothesis 2). The rationales of the two hypotheses will be discussed below.

4.5.1 Transfer of atmospheric ^{14}C signals to sediments of marine plankton

The time it takes until a ^{14}C signal is transferred from the atmosphere into ocean surface waters needs to be considered, when assuming an atmospheric control of ^{14}C plateau structures in planktic records of marine sediments. Nydal et al. [1980] first traced the marine contamination by bomb ^{14}C, thereby showing that an atmospheric signal is reflected in ocean surface waters within no more than a decade, with an oceanic uptake of 1.8 ± 0.5 PgCyr^{-1} at modern average wind speeds [*Sweeney et al*., 2007]. Accordingly, surface dwelling foraminifera (e.g., *Globigerinoides ruber*) may rapidly incorporate this signal into their test chemistry to be preserved in the sediment record. Thus, our records may resolve without any problems even short-lasting plateaus with a time span of 300 yr, if documented by at least two data points, given an average sampling resolution of 85–190 yr.

4.5.2 Bioturbational bias in ^{14}C age records

Bioturbation implies a vertical transport of sediment particles and, in turn, a potential repetition of ^{14}C ages. The bioturbational mixed layer represents a section of homogeneous sediment mixing near to the sediment water interface, that averages ^{14}C ages. Its thickness and the biogenic mixing intensity range from 2 to >10 cm and depend on the nutrient flux to the sea floor and the reactivity of particulate organic carbon [*Trauth et al*., 1997; *Smith and Rabouille*, 2002]. Furthermore, large burrowing organisms such as *Zoophycos* have been reported to reach depths of more than half a meter [*Wetzel and Sarnthein*, 1981; *Came et al*.,

2003]. To cope with these sources of bias in the ^{14}C age, Sarnthein et al. [2007] confined ^{14}C plateau tuning to sediment cores with average sedimentation rates >10 cm/kyr. Furthermore, ^{14}C ages from sediment cores that show clear signs of perturbation by burrows were also excluded from ^{14}C plateau tuning. Accordingly, these distortions were taken into account when discussing the origin of ^{14}C plateau structures in the five Atlantic sediment cores studied.

4.5.3 Hemipelagic sediment features that pretend a record of atmospheric ^{14}C plateaus

The sediments of our Atlantic core locations consist of neritic carbonate (GeoB 1711-4, GeoB 3910-1, KNR 159-5-36GGC, ODP 1002) and calcareous ooze (MD08 3180, MD07 3076) [*Thurman and Burton*, 2001]. In these sediment facies turbidites may reflect events of instantaneous sediment deposition that may result in artificial ^{14}C plateaus in the sediment record, independent of any change in atmospheric ^{14}C. However, none of the sediment cores shows any structure (e.g., a Bouma sequence) and/or any other proxy records (e.g., stable isotopes, XRF-data) that might indicate an influence of intermittent turbidite deposition [*Vidal et al.*, 1999; *Hughen et al.*, 2000; *Came et al.*, 2003; *Repschläger et al.*, 2015; *Balmer et al.*, resub. after rev.], which necessarily would exclude that sediment section from ^{14}C plateau tuning *sensu* Sarnthein et al. [2007].

However, we also need to consider potential short-term, non-turbiditic pulses and suites of pulses of enhanced hemipelagic sediment deposition that may produce ^{14}C plateaus in a sediment record. For example, short periods of extreme sedimentation rates were indeed found as a result of short-lasting events of long-slope suspended sediment transport, such as contourites. These short pulses reached up to 180 cm/kyr in the South China Sea (Core ODP 1144) during Marine Isotope Stage 2 and 3 [Bühring et al., 2004], an Early Holocene maximum of 123 cm/kyr in the Gulf of Cadiz (MD99-2341) [*Toucanne et al.*, 2007], and

some 120 cm/kyr along the Mid Norwegian Margin over the last 5300 years [*Bryn et al*., 2005].

In general, increased sedimentation rates lead to an enhanced resolution of the sediment record. In turn, however, they also imply a higher variance of these rates. Thus, sections of very high rates will alternate with small-scale hiatuses [Sadler, 1999]. In this way, we may indeed expect short-term abrupt changes between high and low sedimentation rates in each core for each of the four hypothetical time spans of depositional pulses under discussion as shown in Fig. 3. Minimum rates (0 cm/kyr) may depict a suite of stratigraphic gaps and/or erosion for which, however, we did not find any textural evidence in the sedimentary record. Also, at a pulse duration of 100-300 years many of the hypothetical maxima in sedimentation rate still exceed by far, that is by a factor of three to 50, the rates actually reported for contourite deposits (Fig. 4.3; Tables 4.1, S4.1). Hence these hypothetical extreme rates may be considered unrealistic. This holds true as long as at least one or two odd extremes occur in a glacial-to-deglacial suite of ^{14}C plateaus, suites that always need to be explained in their entirety, though other plateaus correspond to rates that appear realistic in coming close to and/or falling below those reported for contourites (Fig. 4.3, Table S4.1).

To distinguish any 'artificial' ^{14}C plateau structures that might have formed by mere sedimentary processes and, in particular, complete suites of such hypothetical sedimentation-controlled structures from atmosphere-controlled ^{14}C plateaus, we follow the rules defined by Sarnthein et al. [2007]. More specifically, we employed ^{14}C plateau tuning to complete plateau suites only. Moreover, our approach started with tuning some well-defined key structures such as plateaus 1, 2a, and 2b that suggest close parallels to structures in the atmospheric ^{14}C record (though offset by the local ^{14}C reservoir age). To further corroborate our results of plateau tuning we employed additional stratigraphic evidence such as stable

isotope records. In this way Balmer and Sarnthein [resub. after rev.] also identified a dichotomy of Plateau 1 in Core MD08 3180 (Fig. 4.2B) as result of a temporary fast decrease in local reservoir age. On the basis of these reasonings we preferentially tuned the uncorrected ^{14}C age records of the five cores under discussion to the atmospheric ^{14}C record of Lake Suigetsu (Fig. 4.1). Thus we accepted a dominantly atmospheric control of planktic ^{14}C plateaus and discarded the hypothesis that ^{14}C plateau suites as entirety result from a series of short-term intermittent sediment pulses. Minor deviations in the plateau suite such as jumps in the ^{14}C record were ascribed to local variations in surface water reservoir age [*Sarnthein et al., 2015*; *Balmer et al*., res. afer rev.].

4.5.4 Short-lasting sediment pulses as record of climate change

Climate changes imply several factors that in a specific way will result in significant changes in sedimentation rate as derived from our preferred ^{14}C plateau tuning (Fig. 4.2, lower panels), given the absence of any turbidite deposition. These changes include, for example, a wet period and increased river discharge in (northeastern) Brazil during HS-1 [*Wang et al*., 2004; *Jaeschke et al*., 2007] that indeed is reflected in the records from the Brazilian margin (ODP 1002; GeoB 3910-1; KNR159-5-36). In other cores sedimentation rate changes match climatic events documented in stable-isotope, temperature, and atmospheric pCO_2 records from Antarctica and Greenland (Figs. 4.1G and H). Necessarily, our theoretical approach includes an internal feedback, as extremes in the sediment thickness of a ^{14}C plateau will also induce extremes in the rates estimated for the pertinent hypothetical pulse that each starts from the base of a plateau that in turn is tuned to the calendar age of the base of an atmospheric plateau. Thus the hypothetical sedimentation rates may also appear as an artifact of atmospheric ages deduced for the ^{14}C plateau base each, that we needed to employ for our calculations in the absence of any other narrow spaced age control points.

4.6 Conclusions

We tested two different hypotheses that attempt to explain the origin of ^{14}C plateaus in marine sediment records, namely, whether these plateaus are the result of short transient pulses of extremely high sedimentation rates or that of intermittent changes in atmospheric ^{14}C. In this context we considered four different durations of sediment discharge (10, 100, 200, and 300 yr) that resulted in four hypothetical hemipelagic sedimentation rates for every ^{14}C plateau encountered in five Atlantic sediment cores. These hypothetical rates were compared to rates derived by ^{14}C plateau tuning that assumes an atmospheric control of ^{14}C. Based on our results we arrived at the following conclusions.

Sedimentation rates for pulse lengths of 10 to 300 yr may largely exceed the sedimentation rates reported for contourites – the best possible facies analogue – by a factor of up to 50 and thus are considered unrealistic. This conclusion holds true though some sedimentation rate pulses within a plateau suite may come close or lie below the maximum rates of contourites, thus may indeed be realistic.

The rules for ^{14}C plateau tuning [*Sarnthein et al*., 2007] enable us to ascribe complete suites of plateaus to direct atmospheric forcing, moreover, to identify some sedimentary-process controlled plateau structures in the sediment record. In turn, they enable us to discard the hypothesis claiming that a couple of sedimentation pulses have possibly induced the complete suites of ^{14}C plateau structures in five Atlantic sediment cores, since the sediment pulses closely follow the atmospheric ^{14}C record of Lake Suigetsu, though in part possibly the result of circular reasoning (since based on the assumption of atmospheric ^{14}C plateau base ages).

Sedimentation rates derived from ^{14}C plateau tuning show regional differences that reasonably resemble changes in climate on nearby continents in contrast to the hypothetical rates that largely vary without noticeable links to regional climate change.

4.7 Acknowlegements

We acknowledge with thanks valuable comments and critical discussion of an initial version of this manuscript by Ann Holbourn, Wolfgang Kuhnt, and Pieter M. Grootes. This study was supported by DFG grant SA207/48-1.

4.8 Supplementary Information

4.8.1 S4.1 ^{14}C Plateau Tuning

A correlation of plateau structures in glacial-to-deglacial planktic ^{14}C records to pertinent structures in the atmospheric ^{14}C record of Lake Suigetsu [*Bronk Ramsey et al.*, 2012] provides up to 21 age tie points between 23 and 12 cal. ka. In this way ^{14}C plateau tuning provides a robust and narrow spaced age model for all sediment cores discussed in this study, moreover, a quasi-continuous record of surface water reservoir ages for glacial-to-deglacial marine sediments (details in: Sarnthein et al. [2015], Balmer and Sarnthein [resubm. after rev.; Balmer et al. resubm. after rev.].

To tune a planktic ^{14}C record to the atmospheric ^{14}C curve several prerequisites need to be met following Sarnthein et al. [2007; 2015]:

(1) Sedimentation rates should exceed 10 cm/kyr to enable the identification of short plateaus of ~300 yr marked by no more than two or three ^{14}C dates each.

(2) The sampling resolution should be better than 100–150 yr to even identify ^{14}C plateaus as short as 300 yr.

(3) In addition to a visual identification of plateaus and jumps in ^{14}C records, a more objective mathematical method should be employed which applies the first derivative of all downcore changes in the ^{14}C age – core depth relationship.

(4) To identify the individual ^{14}C plateaus, the entire suite of plateaus and their internal structures need to be considered. In case of alternative tuning choices the lowest possible estimates of planktic ^{14}C reservoir ages need to be accepted, in case no other stringent evidence is suggesting a higher age value. For example, paired benthic ^{14}C ages that are lower than coeval planktic ^{14}C ages may necessarily imply an increased ^{14}C reservoir age to provide an apparent benthic ^{14}C ventilation age larger than ~400 yr [*Matsumoto*, 2007], since smaller and negative values are physically impossible.

4.8.2 S4.2 Plateau tuning derived estimates of hemipelagic sedimentation rate

Sedimentation rate estimates are based on the sediment thickness between age-calibrated ^{14}C plateau boundaries. Major jumps in hemipelagic sedimentation rates may form an artifact of too low sampling resolution that leads to insufficient precision in the definition of ^{14}C plateau boundaries. To avoid this bias we did not specify the rates for the short sediment sections that occur in between subsequent ^{14}C plateaus, sections that span 300–500 yr and less (Figs. 4.1a–e) and are smaller than resolved by our sampling density. When incorporating these small inter-plateau sections to the next subsequent or preceding ^{14}C plateau (Table S4.2) we obtained a generally smooth and realistic record of modest changes in sedimentation rate.

4.8.3 Supplementary Tables

Table S4.1a: Hypothetical sedimentation rates for the 10, 200, 200, and 300-yr long ^{14}C plateau deposition cycles in Core MD08 3180.

Plateau No./ Plateau length [cm]	10 yr cycle		100 yr cycle		200 yr		300 yr	
	Time span	Sed.rate [cm/kyr]	Time span	Sed. rate [cm/kyr]	Time span	Sed. rate [cm/kyr]	Time span	Sed. rate [cm/kyr]
1a (15.5)	13640 – 13930	0	13640 – 13840	0	13640 – 13740	0	-	-
	13930 – 13940	1550	13840 – 13940	155	13740 – 13940	77.5	13640 – 13940	52

1 (29.0)	13940 – 14911	3.08	13940 – 14821	3.4	13940 – 14721	3.84	13940 – 14621	4.4
	14911 – 14921	2900	14821 – 14921	290	14721 – 14921	145	14621 – 14921	97
2a (51.5)	14921 – 16040	4.02	14921 – 15650	4.37	14921 – 15850	4.84	14921 – 15750	5.42
	16040 – 16050	5150	15950 – 16050	515	15850 – 16050	257.5	15750 –16050	171
2b (41.0)	16050 – 16390	0	16050 – 16300	0	16050 – 16200	0	16050 – 16100	0
	16390 – 16400	4100	16300 – 16400	410	16200 – 16400	205	16100 – 16400	136
3 (59.0)	16400 – 17570	14.95	16400 – 17480	16.2	16400 – 17380	17.85	16400 – 17280	19.88
	17570 – 17580	5900	17480 – 17580	590	17380 – 17580	295	17280 – 17580	196
4 (104.5)	17580 – 18970	3.59	17580 – 18880	3.84	17580 – 18780	4.16	17580 – 18680	4.54
	18970 – 18980	10450	18880 – 18980	1045	18780 – 18980	522.5	18680 – 18980	348
5a (81.5)	18980 – 19590	36.06	18980 – 19500	42.3	18980 – 19400	52.38	18980 – 19300	68.75
	19590 – 19600	8150	19500 – 19600	815	19400 – 19600	407.5	19300 – 19600	272
5b (62.5)	19600 – 20140	0	19600 – 20050	0	19600 – 19950	0	19600 – 19850	0
	20140 – 20150	6250	20050 – 20150	625	19950 – 20150	312.5	19850 – 20150	265

Table S4.1b: Hypothetical sedimentation rates for the 10, 200, 200, and 300-yr long ^{14}C plateau deposition cycles in Core GeoB 1711-4.

Plateau No./ Plateau length [cm]	10 yr cycle		100 yr cycle		200 yr		300 yr	
	Time span	Sed. rate [cm/ky]	Time span	Sed. rate [cm/ky]	Time span	D Sed. rate [cm/ky]	Time span	Sed. rate [cm/ky]
1 (10.0)	14050 – 14911	0	14050 – 14821	0	14050 – 14721	0	14050 – 14621	0
	14911 – 14921	1000	14821 – 14921	100	14721 – 14921	50	14621 – 14921	33
2a (16.0)	14921 – 16040	2.23	14921 – 15950	2.42	14921 – 15850	2.69	14921 – 15750	3.01
	16040 – 16050	1600	15950 – 16050	160	15850 – 16050	80	15750 – 16050	53
2b (6.5)	16050 – 16390	0	16050 – 16300	0	16050 – 16200	0	16050 – 16100	0
	16390 –16400	650	16300 – 16400	65	16200 – 16400	32.5	16100 –16400	22
3 (8.5)	16400 – 17570	1.28	16400 – 17480	1.38	16400 – 17380	1.53	16400 – 17280	1.7
	17570 – 17580	850	17480 – 17580	85	17380 – 17580	42.5	17280 – 17580	28
4 (5.0)	17580 – 18970	7.19	17580 –18880	7.69	17580 – 18780	8.33	17580 – 18680	9.09
	18970 – 18980	500	18880 – 18980	50	18780 – 18980	25	18680 – 18980	17
5a (11.0)	18980 – 19590	4.09	18980 – 19500	4.8	18980 – 19400	5.95	18980 – 19300	7.91
	19590 – 19600	1100	19500 – 19600	110	19400 – 19600	55	19300 – 19600	37
5b (6.5)	19600 – 20140	0	19600 – 20050	0	19600 – 19950	0	19600 – 19850	0
	20140 – 20150	650	20050 – 20150	65	19950 – 20150	32.5	19850 – 20150	22
6a (11.0)	20150 – 21410	1.98	20150 – 21320	2.13	20150 – 21220	2.33	20150 – 21120	2.57
	21410 – 21420	1100	21320 – 21420	110	21220 – 21420	55	21120 – 21420	37

Table S4.1c: Hypothetical sedimentation rates for the 10, 200, 200, and 300-yr long ^{14}C plateau deposition cycles in Core GeoB 3910-1.

Plateau No./ Plateau length [cm]	10 yr cycle		100 yr cycle		200 yr cycle		300 yr cycle	
	Time span	Sed. rate [cm/ky]	Time span	Sed. rate [cm/ky]	Time span	Sed. rate [cm/ky]	Time span	Sed. rate [cm/ky]
1a (5.0)	13640 – 13930	0	13640 – 13840	0	13640 – 13740	0	-	-
	13930 – 13940	500	13840 –13940	50	13740 – 13940	25	13640 – 13940	17
1 (5.5)	13940 – 14911	1.02	13940 – 14821	1.13	13940 – 14721	1.28	13940 – 14621	1.46
	14911 – 14921	1550	14821 – 14921	155	14721 –14921	77.5	14621 – 14921	52
2a (30.5)	14921 – 16040	0.89	14921 – 15950	0.97	14921 – 15850	1.07	14921 –15750	1.2
	16040 – 16050	3050	15950 – 16050	305	15850 – 16050	152.5	15750 – 16050	102
2b (7.5)	16050 – 16390	0	16950 – 16300	0	16050 – 16200	0	16050 – 16100	0
	16390 – 16400	700	16300 – 16400	70	16200 – 16400	35	16100 –16400	23
3 (6.5)	16400 – 17570	1.28	16400 – 17480	1.38	16400 – 17380	1.53	16400 – 17280	1.7
	17570 – 17580	650	17480 – 17580	65	17380 – 17580	32.5	17280 – 17580	22

Table S4.1d: Hypothetical sedimentation rates for the 10, 200, 200, and 300-yr long ^{14}C plateau deposition cycles in Core KNR 159-5-36GGC.

Plateau No./ Plateau length [cm]	10 yr cycle		100 yr cycle		200 yr		300 yr	
	Time span	Sed. rate [cm/ky]	Time span	Sed. rate [cm/ky]	Time span	Sed. rate [cm/ky]	Time span	Sed. rate [cm/ky]
YD (8.0)	12570 – 12840	0	12570 – 12750	0	12570 – 12650	0	-	-
	12840 –12850	800	12750 – 12850	80	12650 – 12850	40	12550 – 12850	26.6
1a (5.75)	12850 – 13930	3.7	12850 – 13840	4.04	12850 – 13740	4.49	12850 – 13640	5.06
	13920 – 13940	575	13840 – 13940	57.5	13740 – 13940	28.75	13640 – 13940	19
1 (2.25)	13940 – 14911	0	13940 – 14821	0	13940 – 14821	0	13940 – 14621	0
	14911 – 14921	1225	14821 – 14921	122.5	14821 –14921	61.25	14621 – 14921	41
2a (28.5)	14921 – 16040	1.78	14921 – 15950	1.94	14921 – 15850	2.15	14921 – 15750	2.41
	16040 – 16050	2850	15950 – 16050	285	15850 – 16050	142.5	15750 – 16050	95
2b (9.75)	16050 – 16390	0	16050 – 16300	0	16050 – 16200	0	16050 – 16100	0
	16390 –16400	975	16300 – 16400	97.5	16200 – 16400	48.75	16100 – 16400	33
3 (16.0)	16400 – 17570	4.91	16400 – 17480	5.32	16400 – 17380	5.86	16400 – 17280	6.53
	17570 – 17580	1600	17480 – 17580	160	17380 – 17580	78.75	17280 – 17580	53
4 (11.25)	17580 – 18970	1.79	17580 – 18880	1.73	17580 – 18780	1.87	17580 – 18680	2.04
	18970 – 18980	1125	18880 – 18980	112.5	18780 – 18980	56.25	18680 – 18980	38
5a (5.0)	18980 – 19590	2.45	18980 – 19500	2.88	18980 – 19400	3.57	18980 – 19300	4.68
	19590 – 19600	500	19500 – 19600	50	19400 – 19600	25	19300 – 19600	17

Table S4.1e: Hypothetical sedimentation rates for the 10, 200, 200, and 300-yr long ^{14}C plateau deposition cycles in ODP Core 1002.

Plateau No./ Plateau length [cm].	10 yr cycle		100yr cycle		200 yr		300 yr	
	Time span	Sed. rate [cm/ky]	Time span	Sed. rate [cm/ky]	Time span	Sed. rate [cm/ky]	Time span	Sed. rate [cm/ky]
1a (21.0)	13640 – 13930	0	13640 – 13840	0	13640 – 13740	0	–	–
	13930 – 13940	2100	13840 – 13940	210	13740 – 13940	105	13640 – 13940	70
1 (28.0)	13940 – 14911	17.5	13940 – 14821	19.29	13940 –14721	21.76	13940 – 14621	24.96
	14911 – 14921	2770	14821 – 14921	277	14721 – 14921	138.5	14621 – 14921	93
2a (98.0)	14921 – 16040	16.97	14921 – 15950	18.46	14921 –15850	20.45	14921 – 15750	22.91
	16040 – 16050	9830	15950 – 16050	983	15850 – 16050	491.5	15750 – 16050	326
2b (30.0)	16050 – 16390	0	16050 – 16300	0	16050 – 16200	0	16050 – 16100	0
	16390 – 16400	3000	16300 – 16400	300	16200 – 16400	150	16100 – 16400	100
3 (27.0)	16400 – 17570	12.82	16400 – 17480	13.88	16400 – 17380	25.51	16400 – 17280	17.04
	17570 – 17580	2670	17480 – 17580	267	17380 – 17580	133.5	17280 – 17580	90
4 (25.0)	17580 – 18970	17.98	17580 – 18880	19.23	17580 – 18780	20.83	17580 – 18680	22.72
	18970 – 18980	2500	18880 – 18980	250	18780 – 18980	125	18680 – 18980	83
5a (23.0)	18980 – 19590	62.29	18980 – 19500	73.07	18980 – 19400	90.47	18980 – 19300	118.75
	19590 – 19600	2270	19500 – 19600	227	19400 – 19600	113.5	19300 – 19600	76
5b (22.0)	19600 – 20140	0	19600 – 20050	0	19600 – 19950	0	19600 – 19850	0
	20140 – 20150	2230	20050 – 20150	223	19950 – 20150	111.5	19850 – 20150	73
6a (70.0)	20150 – 21390	14.51	20150 – 21300	15.65	20150 – 21200	17.14	20150 – 21100	18.94
	21390 – 21400	4400	21300 – 21400	440	21200 – 21400	220	21100 – 21400	146
6b (35.0)	21400 – 21860	0	21400 – 21770	0	21400 – 21670	0	21400 – 21570	0
	21860 – 21870	6100	21770 – 21870	610	21670 –21870	305	21570 – 21870	203
7 (34.0)	21870 – 22305	9.19	21870 – 22215	11.59	21870 – 22115	16.32	21870 – 22015	27.58
	22305 – 22315	3400	22215 – 22315	340	22115 – 22315	170	22015 – 22315	113

Table S4.2a: Age control points for sedimentation rates estimated by means of ^{14}C plateau tuning in Core GeoB 1711-4 [*Balmer et al.*, resubm. after rev.].

^{14}C Plateau boundaries used as tie points	Calendar age [yr]	Core depth [cm]	Sedimentation rate [cm/kyr]
Top 1 – Base 1	14050 - 14921	115 – 125	11.4
Base 1 – Base 2a / Top 2b	14921 - 16050	125 – 143.5	16.3
Top 2b – Top 3	16050 - 16890	143.5 – 151.5	9.5
Top 3 – Base 3	16890 - 17580	151.5 – 160	12.3
Base 3 – Base 4	17580 - 18980	160 – 175	10.7
Base 4 – Base 5a / Top 5b	18980 - 19600	175 – 188.5	21.7
Top 5b – Base 5b	19600 - 20150	188.5 – 208.5	11.8
Base 5b – Base 6a	20150 - 21420	195 – 208.5	10.6

Table S4.2b: Age control points for sedimentation rates estimated by means of ^{14}C plateau tuning in Core GeoB 3910-1[*Balmer et al*., resubm. after rev.].

^{14}C Plateau boundaries used as tie points	Calendar age [yr]	Core depth [cm]	Sedimentation rate [cm/kyr]
Top 1a– Base 1a	13640 - 13940	83 – 88.5	16.7
Base 1a – Base 1	13940 - 14921	88.5 – 105	16.8
Base 1 – Base 2a / Top 2b	14921 - 16050	105– 136.5	27.9
Top 2b – Top 3	16050 - 16890	136.5– 145	10.1
Top 3 – Base 3	16890 - 17580	145 – 151.5	9.4

Table S4.2c: Age control points for sedimentation rates estimated by means of ^{14}C plateau tuning in Core KNR 159-5-36GGC [*Balmer et al*., resubm. after rev.].

^{14}C Plateau boundaries used as tie points	Calendar age [yr]	Core depth [cm]	Sedimentation rate [cm/kyr]
Top YD– Base YD	12570 - 13000	70 – 78.5	18.6
Base YD – Base 1a	13000 - 13940	78.5 – 88.25	10.3
Base 1a – Base 1	13940 - 14921	88.25– 100.5	12.4
Base 1 – Base 2a / Top 2b	14921 - 16050	100.5– 131	27
Top 2b – Top 3	16050 - 16890	131 – 146.5	18.4
Top 3 – Top 4	16890 – 18000	146.5 – 164.75	16.4
Top 4 – Top 5a	18000 – 19130	164.75 – 177.5	11.2
Top 5a – Base 5a	19130 - 19600	177.5 – 182.5	10.6

Table S4.2d: Age control points for sedimentation rates estimated by means of ^{14}C plateau tuning in Core MD08 3180 [*Balmer and Sarnthein*, resubm. after rev]

^{14}C plateau boundaries used as tie points	Calendar age [yr]	Core depth [cm]	Sedimentation rate [cm/kyr]
Top 1a – Top 1	13640 – 14050	272.5 – 291	45.1
Top 1 – Top 2a	14050 – 15272	291 – 324.5	27.4
Top 2a – Base 2a/ Top 2b	15272 – 16050	324.5 – 376	66.0
Top 2b – Top 3	16050 – 16900	376 – 434.5	68.8
Top 3 – Top 4	16900 – 18000	434.5 – 498.5	58.1
Top 4 – Base 4	18000 – 18980	498.5 – 603	106.6
Base 4 – Base 5a / Top 5b	18980 – 19600	603 – 706.5	166.9
Top 5b – Base 5b	19600 – 20150	706.5 – 769	113.6

Table S4.2e: Age control points for sedimentation rates estimated by means of ^{14}C plateau tuning in ODP Core 1002[*Sarnthein et al.*, 2015]

^{14}C plateau boundaries used as tie points	Calendar age [yr]	Core depth [cm]	Sedimentation rate [cm/kyr]
Top 1 – Base 1	14050 – 14921	526 – 554	46.7
Base 1 – Base 2a / Top 2b	14921 – 16050	554 – 671	98.3
Base 2a/ Top 2b – Base 2b	16050 – 16400	671 – 701	30
Base 2b – Base 3	16400 – 17580	701– 743	41.7
Base 3 – Base 4	17580 – 18980	743 – 793	50
Base 4 – Base 5a / Top 5b	18980 – 19600	793 – 854	61
Base 5a / Top 5b – Base 5b	19600 – 20150	854 – 876	22.3
Base 5b– Base 6a / Top 6b	20150 – 21400	876 – 938	61.7
Base 6a / Top 6b – Base 6b	21400 – 21870	938 – 999	52
Base 6b – Base 7	21870 – 223315	999 – 1039	49

Chapter 5

Intermediate- and deep-water ventilation ages as a record of glacial-to-deglacial AMOC flow patterns

Sven Balmer and Michael Sarnthein

5.1 Abstract

During Heinrich Stadial 1 (HS-1) (17.5–14.7 cal. ka) the deep Atlantic was filled by low $\delta^{13}C$ and ^{14}C-depleted waters. As widely accepted these waters originated from Southern Source Waters (SSW). However, recent evidence also suggests a major contribution of Arctic Mediterranean (AM) waters. To better constrain the different deep-water sources with supplementary evidence we established two apparent ventilation age records in the South Atlantic off Namibia and off Northeast Brazil, that cover glacial-to-deglacial times (22/18–13 cal. ka). The two sites show incoherent deep-water signals, since they represent opposed continental margins and different water depths. Today Namibia core GeoB 1711-4 (1970 m w.d.) records North Atlantic Deep Water (NADW) with a significant admixture of Southern Intermediate Water (SIW). During LGM and B/A ventilation ages amounted to ~2000 yr. At the onset of HS-1 they dropped to 500 yr, but subsequently rose to ~3000 yr at 16.0 cal. ka in waters showing geochemical characteristics of SSW. Brazilian margin core GeoB 3910-1 records ventilation ages of ~2800 yr in the early HS-1 and a maximum of 4600 yr in the middle of HS-1 (16.3–16.1 cal. ka). These waters either present a tongue of (Coriolis forced) ^{14}C-depleted SSW that move northward or a terminal advance of AM waters. Vice versa, B/A values of ~200 yr record a pulse northern deep waters at 13.8–13.4 cal. ka, possibly also at 15.4 cal. ka. Sampling density in the two South Atlantic cores is insufficient to constrain more precisely millennial- to centennial-scale ventilation changes. Accordingly the records cannot precisely constrain the contribution of AM waters to the ^{13}C- and ^{14}C-depleted waters in the deep Atlantic during HS-1.

5.2 Introduction

The Earth‘s climate and Atlantic Meridional Overturning Circulation (AMOC) during peak glacial times are generally considered as fairly stable over several thousand years with a circulation pattern possibly similar to that of today (benthic $\delta^{13}C$ records of Duplessy et al. [1988]; Sarnthein et al. [1994], and Curry and Oppo [2005]. In the northern North Atlantic peak glacial North Atlantic Deep-Water (NADW) penetrated down to almost 3600 m up to south of the Azores [*Sarnthein et al*., 1994; *Balmer and Sarnthein,* resub. after rev.]. In contrast, deglacial circulation (18–8 cal. ka) was marked by millennial-scale climate events in the North Atlantic that include a cooling during Heinrich Stadial 1 (HS-1), 17.5–14.7 cal. ka, and abrupt warming of subpolar sea surface and air temperatures near and over Greenland at the onset of the Bølling-Allerød (B/A) interstadial (14.7–13 cal. ka) [*Grootes and Stuiver*, 1997; *Waelbroeck et al*., 1998; *Bard et al*., 2000; *Steffensen et al*., 2008]. These events, in turn, led to major reorganizations of AMOC [*Sarnthein et al*., 1994; *McManus et al*., 2004; *Thiagarajan et al*., 2014]. During HS-1 vast portions of the deep Atlantic were dominated by nutrient-enriched abyssal waters that replaced NADW up to <1800 m water depth and probably originated from the Southern Ocean as inferred from low benthic $\delta^{13}C$ values [*Sarnthein et al*., 1994], in this way contrasting with modern and LGM AMOC geometries. Recently, this conceptual model was modified/questioned by Thornalley et al. [2015]. They presented ventilation ages of 7–10 kyr for the Arctic Mediterranean (AM) and Norwegian Sea. These estimates suggest that AM waters possibly contributed to the top of the low-$\delta^{13}C$ and ^{14}C-depleted Atlantic deep waters during HS-1. The glacial-to-deglacial changes in AMOC need to be better constrained by paleoceanographic evidence from southern parts of the Atlantic.

Centennial-to-millennial-scale changes in apparent deep-water ^{14}C ventilation ages help to trace modern flow directions of abyssal (>1500 m) water masses, since they increase with growing distance from the sites of deep-water formation [*Matsumoto*, 2007]. Per analogy, changes in apparent deep-water ventilation ages may be used to unravel past changes in the flow direction of glacial-to-deglacial water masses, in particular, millennial-scale reversals in deep-water flow that result from short-lasting melt water incursions in the North Atlantic [*Thornalley et al*., 2011].

As to be documented further below the subpolar South Atlantic shows a decrease in apparent deep-water ventilation ages over HS-1 from peak glacial values of 4000 yr to ~1500 at the onset of B/A [*Skinner et al*., 2010]. In contrast, the northeastern-most North Atlantic shows extreme ventilation ages of ~5000 yr right during HS-1. An ocean region in general assumed to be a 'dead-end' road at that time. Whereas a major drop to 630 yr is reported after the onset of the B/A [*Thornalley et al*., 2011], a trend somewhat weaker also reflected near the Azores [*Balmer and Sarnthein*, resubm. after revision], the Iberian Margin [*Skinner et al*., 2014] and in coral records from the eastern equatorial Atlantic [*Chen et al*., 2015].

Apparent ventilation ages from both coral and sediment records reveal an AMOC overshoot at the onset of the B/A [*Thiagarajan et al*., 2014; *Chen et al*., 2015; *Balmer and Sarnthein*, resub. after rev.] that is in line with the model simulations of Liu et al. [2009]. Likewise, the authors already show short-term pulses of potential NADW formation that preceded during HS-1. Also, these pulses were possibly reflected by short-term excursions in a εNd record from the southern Cape Basin, variations correlated to changes in northern hemispheric sea ice cover [*Piotrowski et al*., 2004].

Huang et al. [2015] made a first attempt to reconstruct the glacial-to-deglacial history of AMOC by means of two N–S transects integrating past ^{14}C ages of West and East Atlantic deep waters each. However, their attempt was hampered by unknown reservoir ages of surface waters in the source areas of the various deep and intermediate water masses, that define the initial ^{14}C age of these waters. Accordingly, glacial-to-deglacial records of South Atlantic ventilation ages and related deglacial patterns of deep-water flow remain largely unknown. To partly fill this gap and to uncover the glacial-to-deglacial history of deep-water ventilation history, and, in turn, that of deep-water circulation in the tropical and subtropical South Atlantic we now established two apparent ventilation age records from the benthic ^{14}C records of GeoB 1711-4 and GeoB 3910-1.

5.3 Materials

5.3.1 Core locations and hydrographic setting

For this study we used sediment cores from the eastern and western South Atlantic continental margins (Fig.5.1). Core GeoB 1711-4 was retrieved south of the Walvis Ridge (23°17'S, 12°23'W) at 1976 m water depth. Both, today [*Warren and Speer*, 1991] and during LGM [Sarnthein et al., 1994] the site is located near the upper periphery of the southward flow of upper NADW. Site GeoB 3910-1 (04°15'S, 36°21'W) is located at the Brazilian continental slope at a water depth of 2361 m, a position today bathed in NADW.

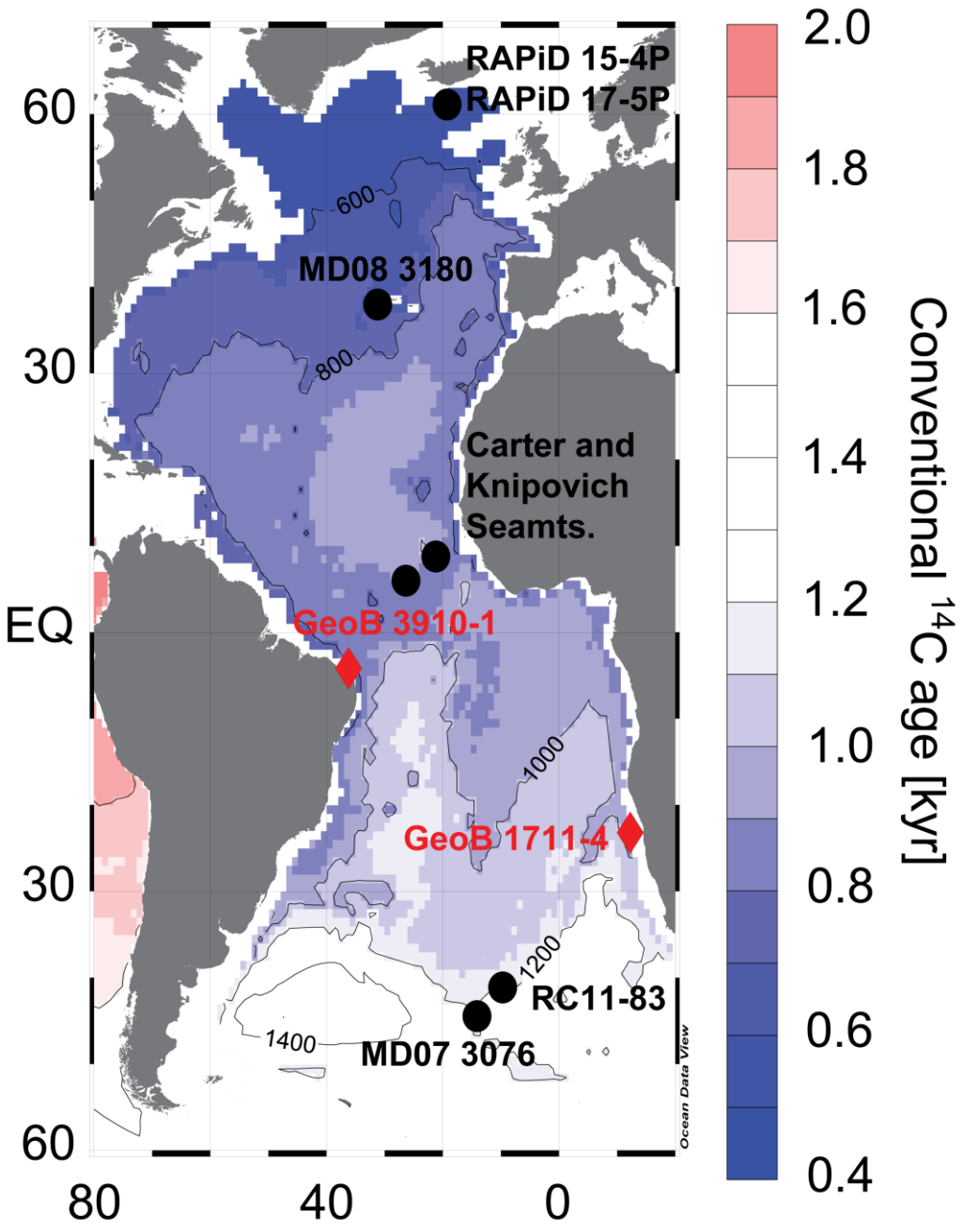

Figure 5.1: Objectively mapped conventional Atlantic ^{14}C age of natural radiocarbon below 1500 m, modified after Matsumoto [2007]. Red diamonds show sites of sediment records analyzed in this study, Circles show further core sites cited in this study.

5.3.2 Analysis of benthic ^{14}C ages

In both cores the age model for the glacial-to-deglacial section was deduced by means of the ^{14}C plateau tuning technique that provided 9–15 age control points each between 22 and 12 cal. ka [*Balmer et al.*, resubm. after rev.].

Raw benthic AMS ^{14}C records are shown in Figs. 5.2a+b and Table S5.1a+b. In Core GeoB 1711-4 18 samples were measured between 115 and 222.5 cm core depth, 14 of them falling within the range of planktic ^{14}C plateaus (Fig. 2a). Average sampling resolution is 6 cm. 32–298 benthic specimens, equal to 4–12 mg $CaCO_3$ were picked from the >150µm size fraction of 1 cm thick sediment slices each. In Core GeoB 3910-1 eight samples were measured between 80.5 and 177.5 cm core depth (Fig. 5.2b) equal to an average sampling resolution of 11 cm. 2–11 thick sediment slices provided sufficient benthic carbonate for AMS ^{14}C dating. All benthic samples are centered within the range of planktic ^{14}C plateaus. 74–337 specimens of mixed benthic species were picked from the size fractions >150µm, sufficient to obtain 3–6 mg $CaCO_3$.

Epibenthic species (e.g. *Cibicidoides wuellerstorfi*) were preferentially used for AMS ^{14}C dating. However, numbers of epibenthic specimens were insufficient in three samples of GeoB 1711-4 (147.5, 155 and 192.5 cm) and in all samples from GeoB 3910-1. Accordingly, we dated mixed benthic assemblages (details in Table S5.1). Miliolid species were excluded, since their low ^{14}C contents may significantly bias ^{14}C ages towards older values [*Magana et al*., 2010]. ^{14}C dating of mixed benthic assemblages may be controversial, since infaunal specimens may also bias ^{14}C ages toward older values and, in turn, toward higher apparent benthic ventilation ages. However, low ventilation ages during peak glacial times that were obtained from mixed benthic assemblages in a sediment core off the Azores [*Balmer and Sarnthein*, resubm. after revision.] clearly argue for an 'unbiased' age signal of mixed benthics. Likewise, the benthic ^{14}C ages of Geo B3910-1 resulted (in a single case) in apparent ventilation ages as low as 184 yr at 13.46–13.82 cal. ka. Also, the three apparent benthic ventilation ages of mixed benthic samples in GeoB 1711-4 at 147.5, 155 and 192.5 cm core depth do not show any offset from the long-term trend of otherwise purely epibenthic ventilation ages. Hence the results may be considered as a robust signal of bottom water age.

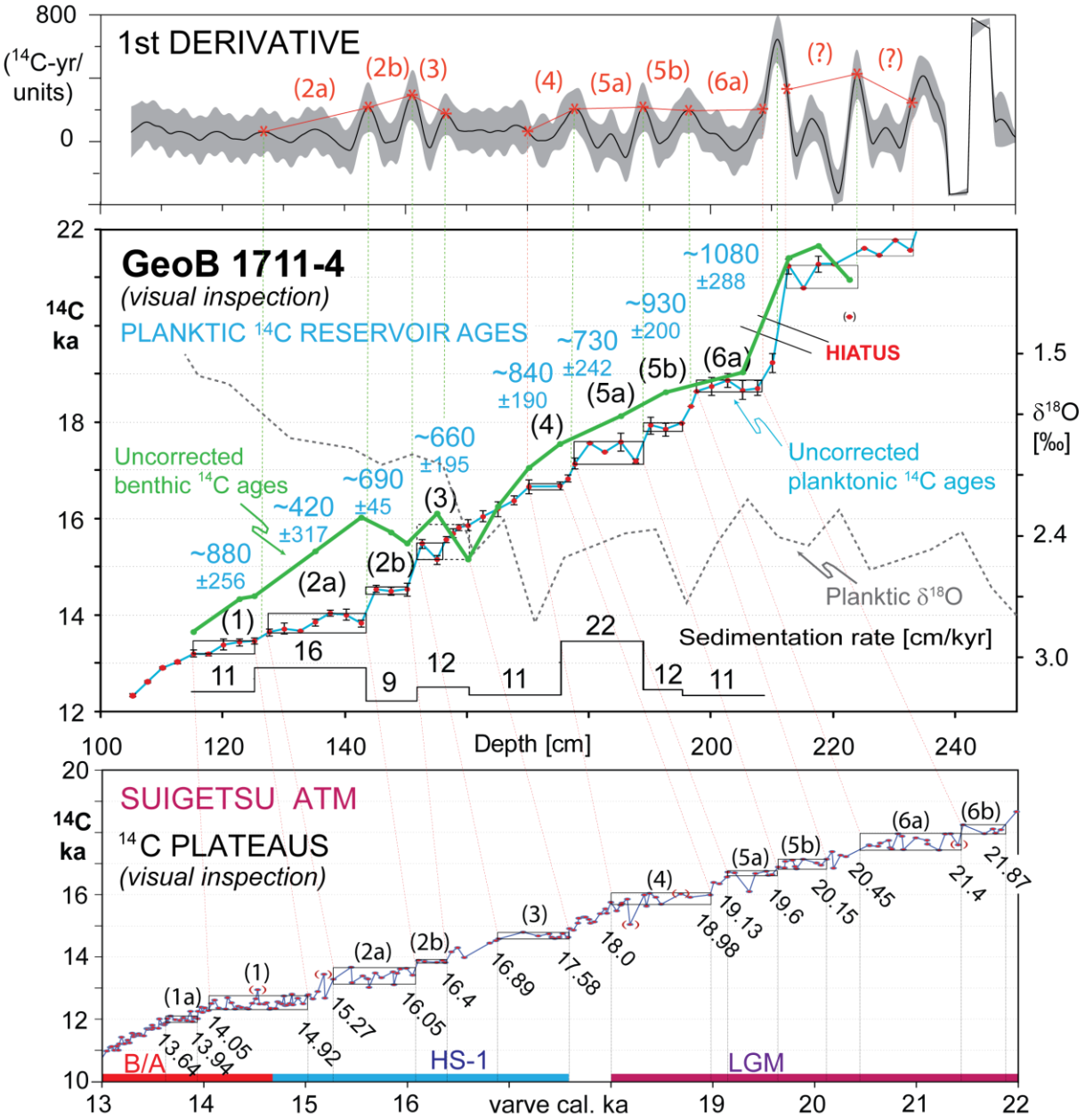

Figure 5.2a: Mid panel: Planktic (blue) and benthic (green) ^{14}C records of Core 1711-4 (Table S.1a) plotted vs. core depth and compared to planktic $\delta^{18}O$ (*G. inflate* in Little et al. [1997], and sedimentation rates (interpolated between plateau boundary ages). Planktic ^{14}C plateaus (horizontal boxes) and ^{14}C jumps are tuned (red dotted lines) to atmospheric (atm) ^{14}C plateau suite of Lake Suigetsu [*Bronk Ramsey et al.*, 2012] (bottom panel). Calendar age scale is based on varve counts. Local planktic reservoir ages (blue numbers in mid panel) result from the difference between the average uncorrected ^{14}C age of planktic ^{14}C plateaus measured in a core and the ^{14}C age of equivalent atmospheric ^{14}C plateaus numbered 1 – 6 (black numbers in brackets). Topmost panel shows 1st derivative units (^{14}C yr per cm core depth; bandwith: 1/3 optimum smoothing at 2.5 cm sample spacing) and 1σ uncertainty range (shaded). Peak values indicate ^{14}C jumps (correlated by dotted green lines). Low values present ^{14}C plateaus constrained at "half-height" of derivative slopes by asterisks (correlation lines and numbers in red). YD = Younger Dryas, B/A = Bølling-Allerød, H1 = Heinrich Stadial 1, LGM = Last Glacial Maximum. Sedimentation rates interpolated between plateau boundary ages. Modified after Balmer et al. [resubm. after rev.].

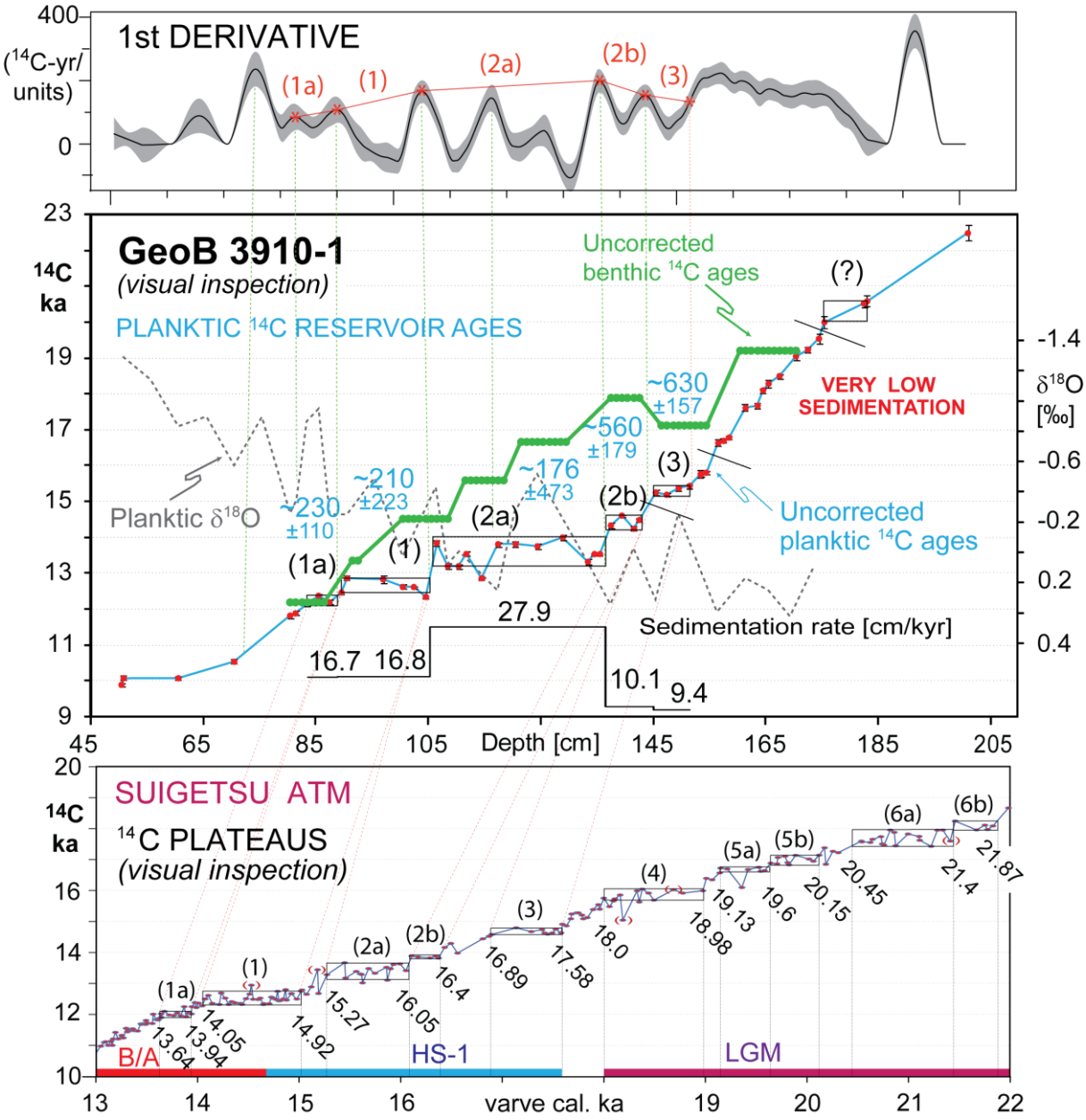

Figure 5.2b: Mid panel: Planktic (blue) and benthic (green) ^{14}C records of Core GeoB 3910-1 (Table S5.1b) plotted vs. core depth compared to planktic $\delta^{18}O$ (*G. ruber* in Balmer et al. [resubm. after rev.]), and sedimentation rates (interpolated between plateau boundary ages). Planktic ^{14}C plateaus (horizontal boxes) and ^{14}C jumps are tuned (red dotted lines) to atmospheric (atm) ^{14}C plateau suite of Lake Suigetsu [*Bronk Ramsey et al.*, 2012] (bottom panel). Calendar age scale is based on varve counts. Local planktic reservoir ages (blue numbers in mid panel) result from the difference between the average uncorrected ^{14}C age of planktic ^{14}C plateaus measured in a core and the ^{14}C age of equivalent atmospheric ^{14}C plateaus numbered 1 – 6 (black numbers in brackets). Topmost panel shows 1st derivative units (^{14}C yr per cm core depth; bandwith: 1/3 optimum smoothing at 2.5 cm sample spacing) and 1σ uncertainty range (shaded). Peak values indicate ^{14}C jumps (correlated by dotted green lines). Low values present ^{14}C plateaus constrained at "half-height" of derivative slopes by asterisks (correlation lines and numbers in red). YD = Younger Dryas, B/A = Bølling-Allerød, H1 = Heinrich Stadial 1, LGM = Last Glacial Maximum. Sedimentation rates interpolated between plateau boundary ages. Modified after Balmer et al. [resubm. after rev.].

AMS ^{14}C ages of benthic samples were measured at the Leibniz Laboratory, University of Kiel (KIA numbers), and the Keck Carbon Cycle AMS facility (UCIAMS numbers), University of California, Irvine. Sample processing in the Leibniz Laboratory included sample cleaning with 15% H_2O_2 in an ultrasonic bath to remove dust and detrital carbonate as well as organic surface coatings. CO_2 was released from the samples with 7% H_3PO_4 at 90°C and graphitized with H_2 using about 2 mg Fe powder as catalyst. The ^{14}C concentration was measured by comparison of simultaneously collected ^{14}C, ^{13}C, and ^{12}C beams of each sample with those of Oxalic Acid standard CO_2 and those of pre-Eemian planktic foraminifera [*Nadeau et al*., 1998]. Samples submitted to the KECK AMS Group were cleaned and leached prior to graphitization and hydrolyzed in H_3PO_4. Before ^{14}C analysis the released CO_2 was graphitized under H_2 on an iron catalyst [*Vogel et al*., 1984]. ^{14}C results were related to spare calcite as ^{14}C-dead blank and converted into conventional ^{14}C ages following Stuiver and Pollach [1977].

5.3.3 Apparent benthic ventilation ages

'Raw' apparent benthic ventilation ages sum up (1) the difference between the benthic ^{14}C age and the ^{14}C average age of a coeval planktic ^{14}C plateau with (2) the contemporaneous reservoir age of local surface waters [*Sarnthein et al*., 2007]. Thus they present the difference in ^{14}C age between the benthic and atmospheric ^{14}C concentrations at any site and time of sediment deposition. As first shown by Adkins and Boyle [1997] and summarized by Cook and Keigwin [2015] the 'raw' values need to be corrected for changes in the atmospheric ^{14}C content between the time of deep-water formation and the time of sediment deposition. To obtain an 'actual' apparent benthic ventilation age we employed the strategy established by Balmer and Sarnthein [resubm. after revision]. It uses a linear approach that disregards any mixing of different water masses. Also, in absence of any other evidence it implicitly assumes that (unknown) surface water reservoir ages at the time and place of deep-water formation

were similar to those found at the time and place of sediment deposition (see Methods in Balmer and Sarnthein, resubm. after revision).

Uncertainty estimates of 'actual' apparent benthic ventilation ages include the propagated errors of (1) benthic ^{14}C analyses, (2) surface water reservoir ages contemporaneous with sediment deposition, and (3) the correction for average changes in atmospheric ^{14}C between deep-water formation and sediment deposition.

5.4 Results and Discussion

5.4.1 Benthic ^{14}C records

Benthic ^{14}C records are depicted in Figs. S5.2a+b and Table S5.1a+b. Most prominent features include several ^{14}C ages that are equally high or younger than paired planktic ^{14}C ages, in particular, between 165 and 135 cm core depth in GeoB1711-4 and at 80.5–86.5 cm core depth in Core GeoB 3910-1.

5.4.2 Apparent benthic ventilation ages

5.4.2.1 GeoB 1711-4

In contrast to modern deep-water ventilation ages at Site GeoB1711-4, that amount to ~1000 yr [*Matsumoto*, 2007], peak LGM values ranged from 1520 to 2020 yr (Fig. 5.3C, Table S5.1a). Right at the onset of HS-1 (17.5 cal ka) ventilation ages dropped to 520 yr suggesting a short pulse of intermediate- or deep-water formation nearby in the Southern Ocean. Possibly, it was the result of major changes in deep-water flow patterns at the onset of HS-1 [*Sarnthein et al.*, 1994]. At 16.0 cal ka ventilation ages reached a maximum of 2900 yr coeval with a short-term drop in Pa/Th (Fig. 5.3D) to values characteristic of the opal belt of the Southern Ocean [*Asmus et al.*, 1999].

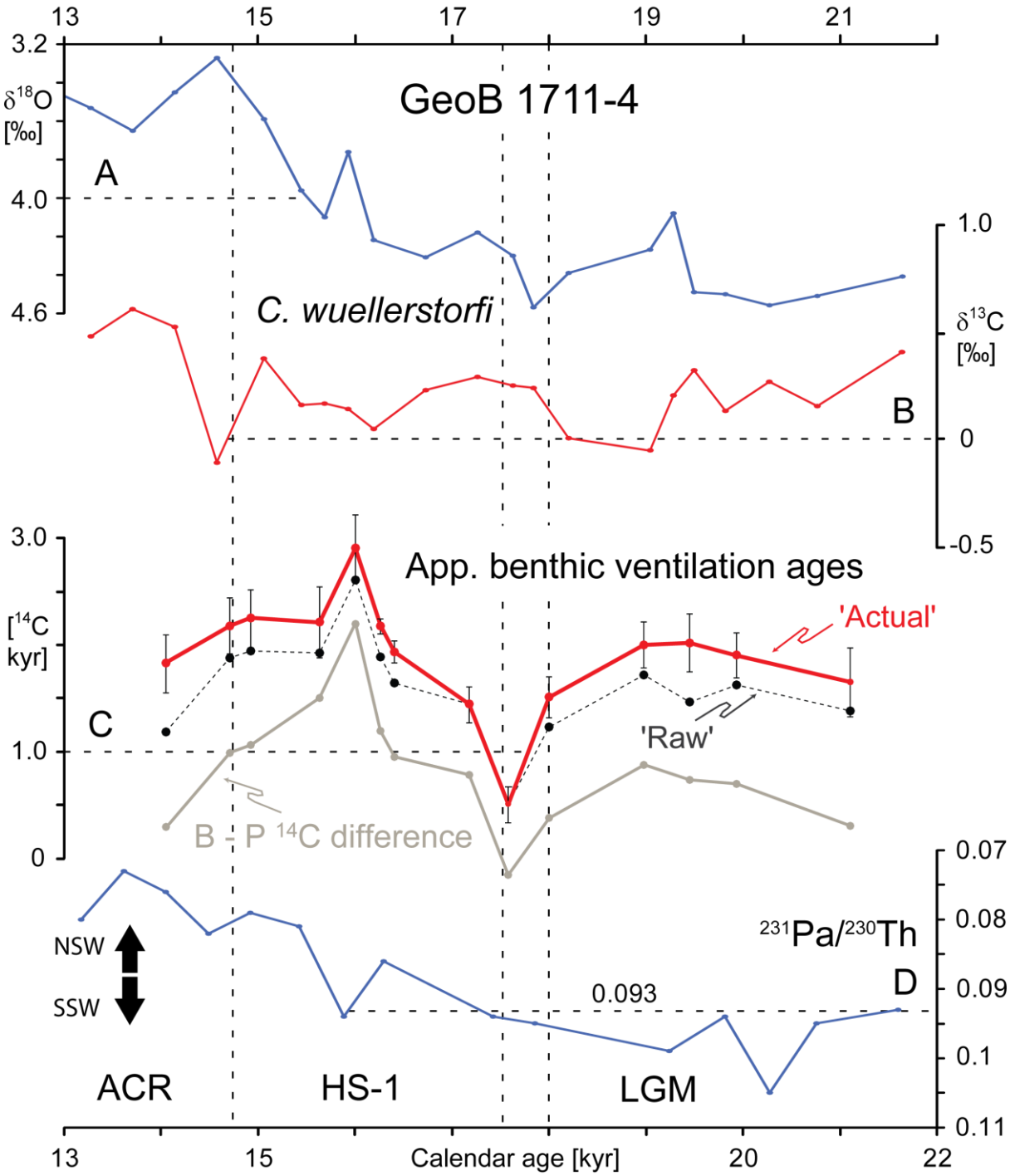

Figure 5.3: (Actual) apparent benthic ventilation ages and further sediment records of Core GeoB 1711-4 vs. calendar age. A: $\delta^{18}O$ record of *C. wuellerstorfi* [*Little et al.*, 1997] B: $\delta^{13}C$ record of *C. wuellerstorfi* [*Waelbreock et al.*, 2006]. C: Apparent benthic ventilation ages corrected for antecedent changes in atmospheric ^{14}C, B – P = benthic-planktic ^{14}C age difference; Raw = Apparent benthic ventilation ages at the time of sediment deposition, not corrected for antecedent changes in atmospheric ^{14}C since the time of deep-water formation. D: $^{231}Pa/^{230}Th$ record [*Lippold et al.*, 2012]; NSW = Northern Sourced Water; SSW = Southern Sourced Water. ACR = Antarctic Cold Reversal, HS-1 = Heinrich Stadial 1, LGM = Last Glacial Maximum.

Both the minimum and maximum may indicate the influence of Southern Source Waters (SSW) at Site GeoB 1711-4 during HS-1. These findings are in line with a HS-1 mode of deep-water circulation [*Sarnthein et al.,* 1994] that led to a reduced influence of NADW in the sub-Antarctic Atlantic Ocean [*Gottschalk et al.,* 2015]. After 16.0 cal. ka, ventilation ages dropped to 2200 yr and were stable until the B/A (14.7 cal. ka), where they further dropped to ~1800 yr (14.05 cal. ka). $\delta^{13}C$ values (Fig. 5.3B) at the core site hardly mirror our changes in ventilation age but reflect a mixture between less well-ventilated SSW and Northern Source Waters NSW [*Waelbroeck et al.,* 2006]. However, we cannot exclude a local overprint of the Benguela Upwelling system. As a result of now increased estimates of the surface water reservoirs age a negative $\delta^{13}C$ excursion of ~-0.2 ‰, a tracer of upwelled deep waters, previously attributed to late HS-1 [*Waelbroeck et al.,* 2006] now shifts from ~15.3 cal. ka to 14.7 cal. ka, that is the onset of B/A.

In summary, the apparent benthic ventilation ages for GeoB 1711-4 in Fig. 5.3C suggest a dominant influence of SSW during HS-1. This conclusion is in harmony with the distribution patterns of glacial-to-deglacial waters in the East Atlantic estimated by epibenthic $\delta^{13}C$ [*Sarnthein et al.,* 1994]. However, we cannot precisely identify the origin of the extreme oscillations, since the core site is located right at the boundary between intermediate and deep waters.

5.4.2.2 GeoB 3910-1

Modern benthic ventilation ages at West Atlantic Site GeoB 3910-1 amount to 800–900 yr [*Matsumoto,* 20007] but strongly varied over glacial-to-deglacial times. During peak LGM (Fig. 5.4, Table S.2b) and the onset of HS-1 (18.35–17.05 cal ka) apparent benthic ventilation ages reached 2700 yr and a maximum of 4600 yr at 16.35–16.1 cal ka. On the one hand this maximum correlates with coeval maxima of apparent benthic ventilation age in the northern

North Atlantic (Fig. 5.5A and 5.5D) [*Thornalley et al.*, 2011] and may suggest that ^{14}C depleted SSW penetrated in the upper deep Atlantic from the Southern Ocean up to 60°N during HS-1, as already inferred by a $\delta^{13}C$ transect [*Sarnthein et al.*, 1994]. After 16.1 cal ka, ventilation ages successively dropped to ~2500 yr at 15.6–14.7 cal. ka. On the other hand, the old waters may present a most distal derivate of AM waters.

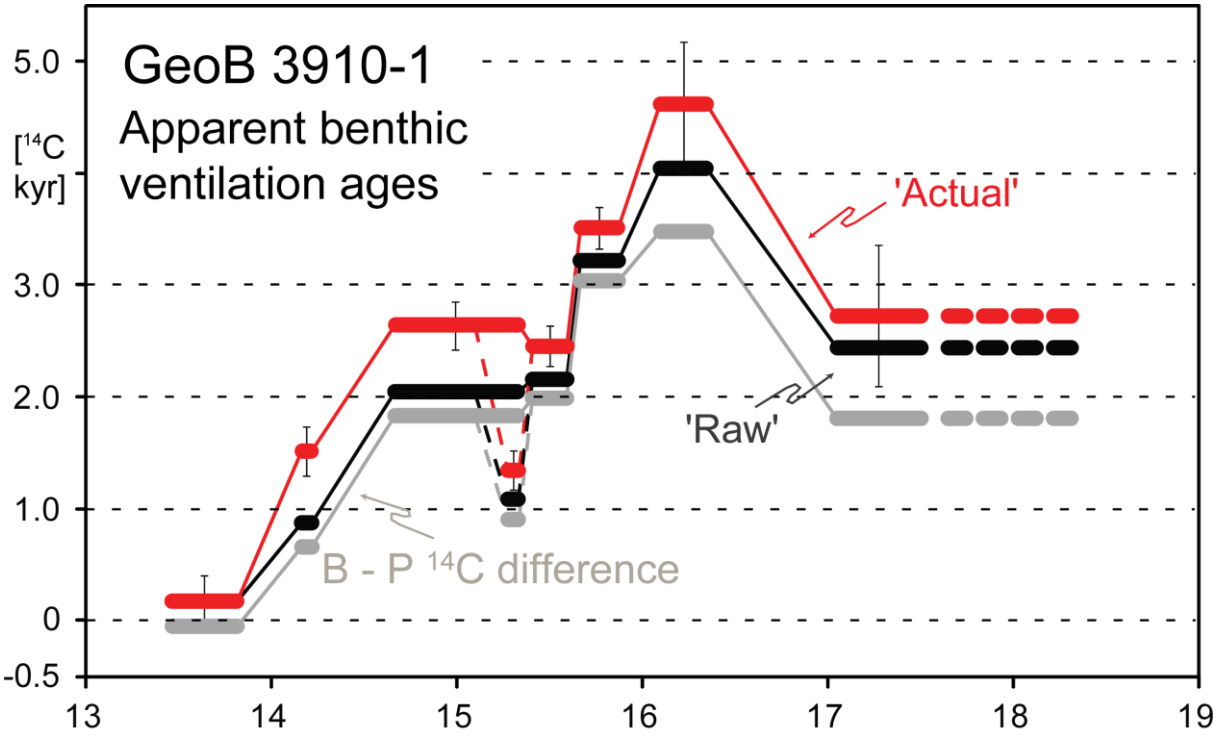

Figure 5.4: Deglacial changes in 'actual' apparent benthic ventilation ages (Actual) of Core GeoB 3910-1. B – P = benthic – planktic ^{14}C age difference, Raw = Apparent benthic ventilation ages at the time of sediment deposition, not corrected for antecedent changes in atmospheric ^{14}C since the time of deep-water formation.

Note the ventilation age spanning 100.5–108.5 cm core depth (14.66–15.33 cal ka) relies on the range of two subsequent planktic ^{14}C plateaus with strongly different average planktic ^{14}C ages (Plateau 2a: 13,600 yr; Plateau 1: 12,680 yr). We decided to attribute the complete uncorrected benthic ^{14}C date to Plateau 1 only, since it matches the main portion of the benthic sample (100.5–105.5 cm), which results in a ventilation age of 2640 yr. On the other hand, the potential ventilation age minimum of 1350 yr at 15.27–15.33 cal. ka (106.5–108.5 cm) during Plateau 2a may possibly reflect a real signal related to an event of Northeast Atlantic deep-water rejuvenation near 15.7 cal. ka [*Thornalley et al.*, 2011] (Fig. 5.5).

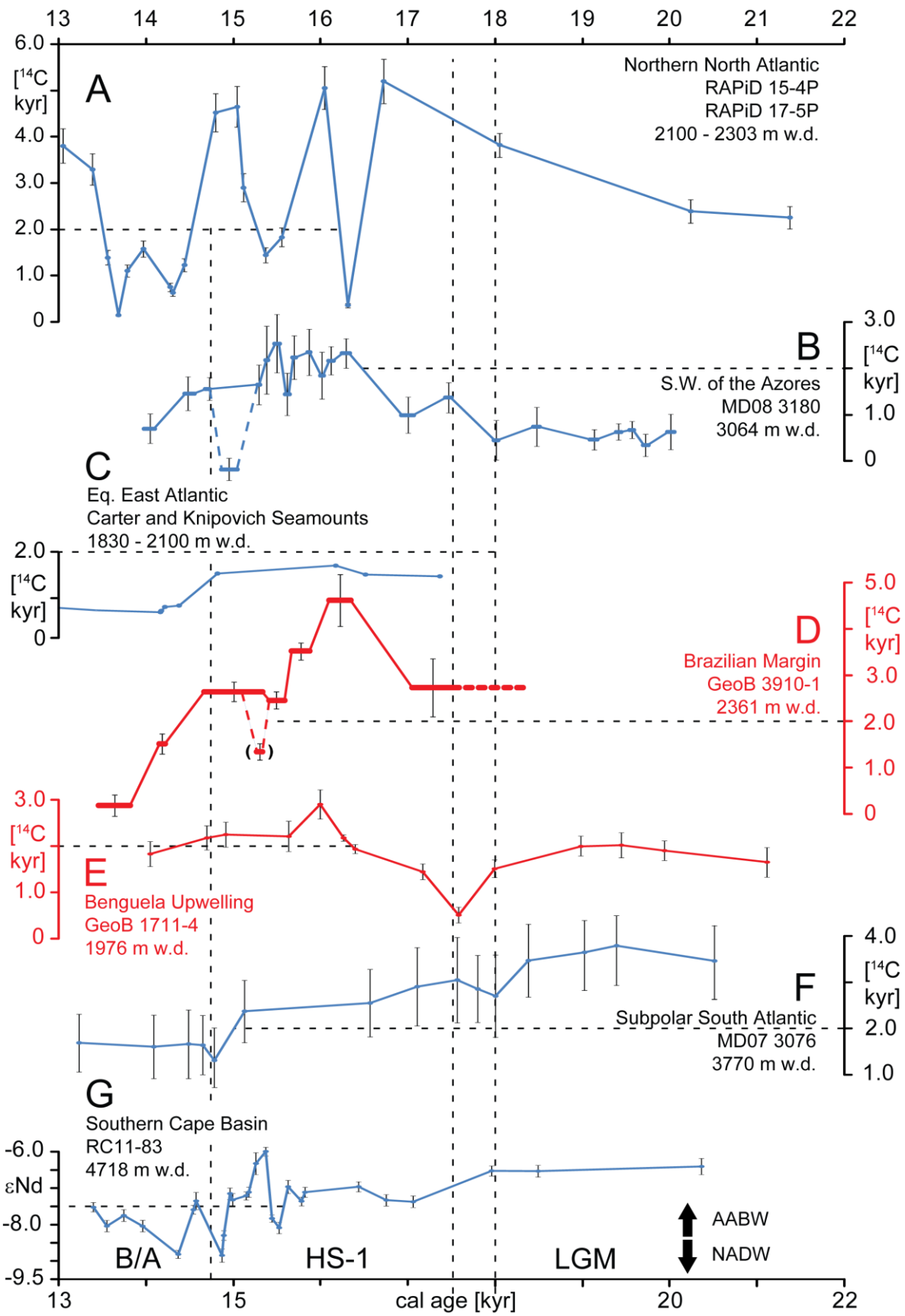

Figure 5.5: Changes in Atlantic deep-water ventilation age at N–S transect of six sites (panel A–F) vs. a benthic εNd record from the southern Cape Basin [*Piotrowski et al.*, 2004] (panel G). Source of ventilation age data: A: [*Thornalley et al.*, 2011]; B: [*Balmer and Sarnthein*, resubm. after revision]; C: [*Chen et al.*, 2015]; D and E: this study; F: [*Skinner et al.*, 2010]. AABW = Antarctic Bottom Water, NADW = North Atlantic Deep Water, B/A = Bølling-Allerød, HS-1 = Heinrich Stadial 1, LGM = Last Glacial Maximum.

After the onset of the B/A benthic ventilation ages dropped to values as low as 180 yr near 13.8–13.5 cal. ka. This drop followed a similar ventilation age drop in the northeastern North Atlantic ([*Thornalley et al*., 2011]; Fig. 5.5A) with a time lag of >400 yr. Accordingly, the major drop along the Brazilian Margin may possibly present the result of North Atlantic deep-water formation near Iceland, in harmony with the flow patterns of modern deep waters [*Matsumoto*, 2007].

5.4.3 Northern versus southern source Atlantic deep-water

The two ventilation-age records from the South Atlantic show incoherent signals as they reflect the circulation at opposed continental margins of the Atlantic (Fig. 5.1). Moreover, the records stem from different water depths (Fig. 5.5), and the ventilation ages of Core GeoB 1711-4 record a changing mixture of deep- and intermediate-water signals. Insufficient sampling resolution (GeoB 1711-4) and ^{14}C dates that average up to 1300 cal. yr each (GeoB 3910-1) prevent an exact timing of millennial-scale changes in deep-water ventilation. In particular, they hinder us to trace centennial-scale changes in deep-water ventilation monitored both in ventilation age records from the North Atlantic [*Thornalley et al*., 2011; *Balmer and Sarnthein*, resubm. after revision] and in an εNd record from the southern Cape Basin [*Piotrowski et al*. 2004]. Therefore these records still are too fragmentary for reconstructing the major features of Atlantic deep-water circulation over HS-1.

Nevertheless, extreme highs in ventilation-age record old, ^{14}C-depleted waters at depths of 2.1–2.4 km off Brazil and south of Iceland during HS-1 (Figs. 5.5A+5.5D). These extremes are also monitored in other records from the Atlantic Ocean, however, to a lower extent (Figs. 5.5A–5.5D). Successively lower ventilation ages towards the eastern part of the Atlantic basin may suggest an increasing local influence of younger deep waters admixed to the old waters. This conceptual model appears in fair agreement with Coriolis forcing and modern deep-

water circulation-patterns, confining a ^{14}C depleted water mass on its northward way from the subpolar Atlantic to the western part of the Atlantic basin.

5.5 Conclusions

The previously accepted dominance of southern-source water (SSW) in the deep Atlantic during Heinrich Stadial 1 (HS-1) was recently challenged. Based on ventilation age records from the Arctic Mediterranean and from the Norwegian Sea Thornalley et al. [2015] suggested that the AM contributed to the $\delta^{13}C$- and ^{14}C-depleted waters in the northern deep Atlantic. To test this hypothesis and to enlarge the set of scarce Atlantic ventilation age records we now generated two ventilation age records from the eastern (GeoB 1711-4) and western (GeoB 3910-1) part of the South Atlantic, that come from 2000 and 2600 m water depth, respectively.

Insufficient sampling density in both cores as well as ^{14}C dates that average up to 1300 cal. yr in GeoB 3910-1, and the position of Core GeoB 1711-4 that records a changing mixture of intermediate- and deep-water signals make it impossible to reconstruct an exact timing of millennial-scale changes in deep water ventilation. In particular, they prevent us from tracing centennial-scale changes in deep-water ventilation monitored in other records of the northern Atlantic. Therefore, we refrain from estimating whether and to which extent the AM contributed to the $\delta^{13}C$- and ^{14}C-depleted waters that dominated the deep North Atlantic during HS-1. However, the two ventilation age records from opposed margins of the South Atlantic monitor an east-west trend that suggest an enhanced intermixing of younger waters with old HS-1 waters in the Eastern Atlantic and confine the major part of the extremely ^{14}C-depleted water mass to the West Atlantic. This pattern is in agreement with Coriolis forcing that influences the flow of a water mass on its way from the South Atlantic towards north.

5.6 Supplementary Information

5.6.1 Supplementary Tables

Table S.5.1a: Benthic ^{14}C dates and species dated in Core GeoB1711-4.

KIA and UCIAMS Sample No.	Centered at core depth [cm]	Benthic ^{14}C age [yr]	Weight [mg]	Number of specimens	Size fraction [µm]	Species
KIA 48386	115	13660±80	11	132	>250	*C. wuellerstorfi, G. soldanii; C. pachyderma*
UCIAMS 140164	122.5	14350±40	9	46	>400	*G. soldanii*
KIA 48387	125	14420±80	12	92	>400	*C. wuellerstorfi, G. soldanii, C. pachyderma*
KIA 49575	135	15350±90	20	80	>400	*C. wuellerstorfi, G. soldanii, C. pachyderma*
UCIAMS 144780	142.5	16040±40	5	32	>400	*C. wuellerstorfi, G. soldanii, C. pachyderma*
UCIAMS 133004	147.5	15740±50	8	273	>315	*Bulimina sp., Globobulimina sp., C. wuellerstorfi*
KIA 49576	150	15500±90	9	57	>400	*C. wuellerstorfi, G. soldanii, C. pachyderma*
UCIAMS 133005	155	16120±50	8	178	>400	*Uvigerina sp., Globobulimina sp., C. wuellerstorfi, Bulimina sp.*
UCIAMS 144781	160	15185±40	6	72	>400	*C. wuellerstorfi, G. soldanii, C. pachyderma*
KIA 48388	165	16270 +100/-90	7	93	>400	*C. wuellerstorfi, G. soldanii, C. pachyderma*
UCIAMS 144782	170	17075±45	5	68	>400	*C. wuellerstorfi, G. soldanii, C. pachyderma*
KIA 49577	175	17570 +110/-100	10	238	>250	*C. wuellerstorfi, G. soldanii, C. pachyderma*
KIA 48389	185	18140±110	8	199	>315	*C. wuellerstorfi, G. soldanii, C. pachyderma*
UCIAMS 133006	192.5	18640±70	10	194	>400	*Uvigerina sp., G. soldanii, Bulimina sp.*
KIA 495778	205	19050±130	8	236	>150	*C. wuellerstorfi, G. soldanii, C. pachyderma*
UCIAMS 140165	212.5	21430±100	4	158	>250	*C. wuellerstorfi, G. soldanii, C. pachyderma*
UCIAMS 140166	217.5	21680±100	6	169	>250	*C. wuellerstorfi, G. soldanii*
KIA 49579	222.5	20970 +160/-150	8	265	>150	*C. wuellerstorfi, G. soldanii, C. pachyderma*

Table S5.1b: Benthic ^{14}C dates and species dated in Core GeoB3910-1.

UCIAMS Sample No.	Centered at core depth [cm]	Benthic ^{14}C age [yr]	Weight [mg]	Number of specimens	Size fraction [µm]	Species
UCIAMS 127529	80.5–86.5	12190±30	5	251	>250	*Globobulimina sp., Bulimina sp., Heoglundina elegans, C. mundulis,*
UCIAMS 144776	91.5–92.5	13350±70	3	74	>150	*Globobulimina sp., Heoglundina elegans, Melonis sp., C. mundulis, C. wuellerstorfi, Uvigerina sp., Laticarinina pauperata,*
UCIAMS 127530	100-5–108.5	14520±35	5	187	>150	*Globobulimin sp., C. wuellerstorfi, Uvigerina sp., Calistomella sp.,*
UCIAMS 127531	111.5–118.5	15595±40	5	240	>150	*Globobulimina sp., Bulimina sp., Calistomella sp., Bolivinata t., C. wuellerstorfi,*
UCIAMS 127532	121.5–129.5	16650±60	5	164	>150	*Globobulimina sp., Bulimina sp., Calistomella sp., Bolivinata t., C. wuellerstorf*
UCIAMS 127533	137.5–142.5	17895±45	6	223	>150	*Globobulimina sp., Oridorsalis umbonatus, Hoeglundina elegans, Bolivinata t., Melonis sp., C. wuellersorfi, Laticarinina pauperata, C. pachyderma*
UCIAMS 127534	146.5–154.5	17120±40	6	337	>150	*Laticarinina pauperata, C. mundulus, Lenticulna sp., Bulimina sp., Globobulimina sp., Melonis sp., Pullenia bulloides, C. wuellerstorfi, Oridorsalis umbonatus, Uvigerina sp. , C. robinsonianus, Bolivinita t, C. bradyi, Calistomella ovoidea, C. pachyderma*
UCIAMS 12753	160.5–170.5	19190±50	6	156	>150	*Melonis sp., C.mundulus, Bulimina sp., Oridorsalis umbonatus, C.wuellerstorfi, Pullenia bulloides, Laticarinina pauperata, Lenticulina* sp.,*Uvigerina sp., Anomalinoides subglobosa*

Table S5.2a: Derivation of 'actual' apparent benthic ventilation ages for GeoB 1711-4. Pla. res. age = planktic reservoir age; B-P = benthic - planktic ^{14}C age difference; benth. vent. age = benthic ventilation age; fMC = average atmospheric ^{14}C concentration during deep-water formation presented as fraction of modern carbon; * Samples do not fall within a planktic ^{14}C plateau.

KIA and UCIAMS No.	Core Depth [cm]	Cal. age [yr]	Benthic ^{14}C [yr]	Planktic res. age [yr]	B-P	'Raw' benthic vent. age	'Actual' benthic vent. age [yr]	'Actual' benthic vent. age [‰]	fMC
KIA 48386	115	14050	13660±80	880±256	300	1180	1830±270	204±43	1.3
UCI 140164	122.5	14703	14350±40	880±256	990	1870	2180±260	238±43	1.35
KIA 48387	125	14921	14420±80	880±256	1060	1940	2250±270	240±43	1.4
KIA 49575	135	15636	15350±90	420±317	1500	1920	2220±330	304±56	1.4
UCIAMS 144780	142.5	16001	16040±40	420±317	2200	2620	2900±320	238±55	1.4
UCIAMS 133004	147.5	16265	15740±50	690±45	1200	1890	2180±70	215±12	1.4
KIA 49576	150	16400	15500±90	690±45	960	1650	1940±100	165±17	1.4
UCIAMS 133005	155	17174	16120±50	660±195	790	1450	1450±170	62±29	1.4
UCIAMS 144781	160	17580	15185±40	660±195	-150	510	520±170	110±29	1.4
UCIAMS 144782	170	18000	17075±45	840±190	390	1230	1520±190	172±34	1.45
KIA 49577	175	18980	17570+110/-100	840±190	880	1720	2000±220	220±39	1.45
KIA 48389	185	19450	18140±110	730±242	740	1470	2020±270	196±48	1.45
UCIAMS 133006	192.5	19938	18640±70	930±200	700	1630	1910±210	211±39	1.5
KIA 49578	205	21111	19050±130	1080±288	300	1380	1660±320	186±59	1.5

Table S5.2b: Derivation of 'actual' apparent benthic ventilation ages for GeoB 3910-1. res. age = reservoir age; B-P = benthic - planktic ^{14}C age difference; vent. age = ventilation age; fMC = average atmospheric ^{14}C concentration during deep-water formation presented as fraction of modern carbon; † Sample falls within range of two planktic ^{14}C plateaus. Apparent deep-water ventilation age due to changing reservoir age of surface waters; * Sample does not fall within a planktic ^{14}C plateau.

Sample No.	Core Depth [cm]	Cal. age [yr]	Benthic ^{14}C [yr]	Planktic res. age [yr]	B-P	'Raw' benthic vent. age	'Actual' benthic vent. age [yr]	'Actual' benthic vent. age [‰]	fMC
UCIAMS 127529	80.5–86.5	13460–13820	12190±30	230±110	-50	180	180±230	271±34	1.2
UCIAMS 144776	91.5–92.5	14162–14218	13350±70	210±223	670	880	1520±220	224±36	1.3
UCIAMS 127530	100.5–108.5	14668–15335	14520±35	210±223	1840	2050	2640±210	392±36	1.4
†UCIAMS 127350	106.5–108.5	15272–15335	14520±35	180±473	920	1100	1350±180	209±30	1.35
UCIAMS 127531	111.5–118.5	15412–15590	15595±40	180±473	1990	2170	2460±180	369±31	1.4
UCIAMS 127532	121.5–129.5	15667–15871	16650±60	180±473	3050	3230	3520±190	496±33	1.4
UCIAMS 127533	137.5–142.5	16100–16350	17895±45	560±179	3480	4040	4620±560	634±98	1.45
UCIAMS 127534	146.5–154.5	17049–18346	17120±40	630±157	1820	2450	2730±630	417±109	1.45

Chapter 6

Conclusions and Outlook

Glacial-to-deglacial planktic ^{14}C records from the low- and mid-latitude Atlantic were analyzed by means of ^{14}C plateau tuning in order to monitor the changes in ^{14}C reservoir age of local surface waters (**Chapter 2** and **3**). The results were combined with paired planktic stable isotope measurements to identify potential meltwater incursions during Heinrich Stadial 1 (HS-1) southwest of the Azores (**Chapter2**). Moreover, plateau-tuning derived ^{14}C reservoir ages were compared to model-based reservoir age estimates for the last glacial and modern times. In particular, the comparison served to test the consistency of data simulated by published General Circulation Models (GCM) and the bearing of changes in ocean circulation the model simulations are based on (**Chapter 3**).

Paired benthic ^{14}C ages were used to obtain apparent benthic ventilation ages that reveal changes in the geometry of the Atlantic Meridional Overturning Circulation (AMOC) over peak glacial to deglacial times. In particular we were interested, whether and to which extent the Arctic Mediterranean (AM) may have contributed to the $\delta^{13}C$- and ^{14}C-depleted waters that dominated the deep North Atlantic during HS-1 (**Chapter 2** and **5**). Finally, we discussed, the possibility that ^{14}C plateau structures in marine sediments are merely a result of short-lasting pulses of sediment deposition instead of intermittent changes in atmospheric ^{14}C concentration (**Chapter 4).** In this context we compared sedimentation rates of five sediment cores, the age models of which are based on plateau tuning, with rates that might have resulted from hypothetical short-lasting events of sediment deposition.

Our results may be summarized as following:

1) Significant spatial and temporal changes in the ^{14}C reservoir age of surface waters imply a major step forward towards a more accurate radiocarbon chronology for the last deglacial. In part, these changes are linked to changes in the habitat depth of planktic tracer species. Thus

different monospecific ^{14}C records had to be taken into account measured in parallel. In part, the changes in ^{14}C reservoir age are linked to seasonal changes of ocean surface waters. Moreover, long-term changes in climate and ocean circulation play a role in affecting the coastal upwelling belts off Southern Africa and Southern Brazil. These changes lead to increased LGM reservoir ages of 750–1000 and 900 yr, respectively, that in turn may serve as tracer of enhanced upwelling intensity as a result of strengthened long-shore winds and the glacial seaward shift of shorelines. On the other hand, ^{14}C reservoir ages of ~1600 and briefly 2170 yr were found near the Azores during HS-1 and by far exceed the local LGM and B/A levels of 320–600 yr, hence suggest that HS-1 meltwaters penetrated as far south as 38°N.

2) Our empiric ^{14}C reservoir ages were found consistent with reservoir age estimates for the LGM simulated by the model of Butzin et al. [2012], but not with estimates derived by the model of Franke et al. [2008] that underestimate our mid-latitude values up to ~2000 ^{14}C yr. Our results suggest that realistic estimates of both freshwater balance and past atmospheric ^{14}C concentrations form important boundary conditions to simulate realistic ^{14}C reservoir ages.

3) To merely explain suites of ^{14}C plateaus by sedimentation rate pulses, hypothetical hemipelagic sedimentation rates of 17–10450 cm/kyr over periods of 300 to 100 yr each are required (if the calculation employs for each ^{14}C plateau the respective base age of the next-possible atmospheric plateau). However, these rates exceed the sedimentation rates reported for contourites, the most likely facies analogue, by a factor of up to 50. Suites of short-term extreme pulses of hemipelagic sedimentation can thus be considered unrealistic as explanatory model. This conclusion also holds true for some sedimentation rate pulses within a plateau suite, that may come close or lie below the maximum rates of contourites, thus might indeed be realistic. Vice versa, the rules for plateau tuning [*Sarnthein et al*., 2007]

clearly suggest us to ascribe complete suites of ^{14}C plateaus to a suite of well-established variable atmospheric ^{14}C concentrations well established in the ^{14}C record of Lake Suigetsu [Bronk Ramsey et al., 2012]. In this way it is also possible to identify possibly sedimentation rate controlled structures such as excessive ^{14}C jumps as tracer of sediment hiatuses. In part, this reasoning might be suspected of circular reasoning, an objection that can be discarded as long as the suite of marine ^{14}C plateaus forms a clear image of a coeval suite of atmospheric ^{14}C plateaus.

4) North Atlantic Deep Water (NADW) was formed near the Azores during peak LGM times, as suggested by apparent benthic ventilation ages as low as 340–740 yr. However, published sea surface temperature and salinity patterns [*Duplessy et al*., 1991; *Pflaumann et al*., 2003] suggest that NADW formation was constrained to a narrow belt of open surface water, a semi-enclosed polynya [*Sarnthein et al*., 2003b] that extended from 50°N/35°W to 60°N/20°W during LGM winter. By contrast, our results show high benthic ventilation ages of 2200–2500 yr near the Azores during HS-1, that reflect an incursion of old, southern-source deep water. The flow was interrupted by brief events of NADW formation near 16.1 and 15.6 cal. ka that alternated with meltwater incursions. Most important, the onset of the Bølling-Allerød is marked by a prominent minimum in ventilation age at 14.9/14.7 cal. ka, that may depict an overshoot of AMOC and probably introduced its long-term renewal.

5) Apparent benthic ventilation age records from two core sites in the South Atlantic show incoherent deep-water signals since each of them represents the circulation regime of opposed continental margins. Off Namibia LGM and B/A ventilation ages amounted to ~2000 yr. Near the onset of HS-1 they dropped to 500 yr. Subsequently, however, they rose to ~3000 yr at 16.0 cal. ka in waters that show geochemical features of Southern Sourced Waters (SSW). At the Brazilian Margin ventilation ages amount to ~2800 yr during early HS-1 and reach a

maximum of 4600 yr at 16.3–16.1 cal. ka. This maximum either suggests a tongue of (Coriolis forced) ^{14}C-depleted SSW advancing north or the terminal advance of AM waters. In contrast, B/A values of ~200 yr record a pulse of northern source deep waters at 13.8–13.4 cal. ka, possibly also one at 15.4 cal. ka. However, sampling density in both cores proves insufficient to constrain more precisely millennial- to centennial-scale changes in deep-water ventilation that already were recorded elsewhere in cores from the North Atlantic. Accordingly the quality of our records is insufficient to precisely constrain the actual timing of contributions of AM waters to predominantly ^{14}C-depleted waters in the deep Atlantic during HS-1.

In summary the spatial and temporal variations in the glacial-to-deglacial reservoir age of (sub-) surface waters from the mid- and low-latitude Atlantic show that it is necessary to add more continuous glacial-to-deglacial reservoir age records to the dataset already existing. They will help to constrain ^{14}C reservoir age characteristics for various ocean regions that are defined by their circulation pattern and paleoceanographic time slots. Also, they will contribute to an increase in the precision of commonly used ^{14}C calibration software and test the consistency of GCM. In each core investigated plateau tuning-derived age models proved superior to the previously established age models for glacial-to-deglacial times. Therefore it was crucial to reassess published paleoceanographic records of these sediment cores under the light of the newly established age models.

Our benthic ventilation age record from near the Azores demonstrates deep-water formation during peak LGM times. To exactly time the onset of deep-water formation it will be necessary to expand the existing dataset farther downcore. In the South Atlantic additional high-resolution ventilation age records are needed from key positions of the conveyor belt to monitor the exact timing of changes in the geometry of water mass distribution. In particular,

it may be important to monitor the short pulses of NADW formation (and their north-south phase shifts) that interfered with the incursion of ^{14}C-depleted southern-source waters in the deep Atlantic during HS-1.

Chapter 7

References

Abrantes, F. (1991), Increased upwelling off Portugal during the last glaciation: diatom evidence, Marine Micropaleontology, 17, 285-310, doi: 10.1016/0377-8398(91)90017-z.

Adkins, J. F., and E. A. Boyle (1997), Changing atmospheric $\Delta^{14}C$ and the record of deep water paleoventilation ages, *Paleoceanography*, 12(3), 337-344, doi: 10.1029/97pa00379.

Adkins, J. F., Cheng, H., Boyle, E.A., Druffel, E.R., and R.L. Edwards (1998), Deep-sea coral evidence for rapid change in ventilation of the deep North Atlantic 15,400 years ago, *Science*, *280*(5364), 725-728, doi: 10.1126/science.280.5364.725.

Andersen, K. K., Azuma, N., Barnola, J.-M., Bigler, M., Biscaye, P., Caillon, N., Chappellaz, J., Clausen, H.B., Dahl-Jensen, D., Fischer, H., Flückiger, J., Fritzsche, D., Fujii, Y., Goto-Azuma, K., Grønvold, K., Gundestrup, N.S., Hansson, M., Huber, C., Hvidberg, C.S., Johnsen, S.J., Jonsell, U., Jouzel, J., Kipftuhl, S., Landais, A., Leuenberger, M., Lorrain, R., Masson-Delmotte, V., Miller, H., Motoyama, H., Narita, H., Popp, T., Rasmussen, S.O., Raynaud, D., Rothilsberger, R., Ruth, U., Samyn, D., Schwander, J., Shoji, H., Siggard-Andersen, M.-L., Steffensen, J.P., Stocker, T., Sveinbjörnsdóttir, A.E., Svensson, A., Takata, M., Tison, J.-L., Thorsteinsson, Th., Watanabe, Q., Wilhelms, F., and J.W.C. White (2004), High-resolution record of Northern Hemisphere climate extending into the last interglacial period, *Nature*, 431(7005), 147-151, doi: 10.1038/nature02805.

Andersen, K. K., Svensson, A., Johnsen, S.J., Rasmussen, S.O., Bigler, M., Röthlisberger, R., Ruth, U., Siggaard-Andersen, M.-L., Steffensen, J.P., Dahl-Jensen, D., Vinther, B.M., and H.B. Clausen (2006), The Greenland ice core chronology 2005, 15 - 42ka. Part 1: Constructing the time scale, *Quaternary Science Reviews*, 25(23), 3246-3257, doi: 10.1016/j.quascirev.2006.08.002.

Asmus, T., Frank, M., Kschmieder, C., Frank, N., Gersonde, R., Kuhn, G., and A. Mangini (1999), Variarions of biogenic particle flux in the southern Atlantic section of the subarctic zone during the late Quarternary: Evidence from sedimentary $^{231}Pa_{ex}$ and $^{230}Th_{ex}$, *Marine Geology*, 159, 63-78, doi: 10.1016/s0025-3227(98)00199-6.

Bacon, M.P. (1984) Glacial to interglacial changes in carbonate and clay sedimentation in the Atlantic Ocean estimated from 230Th measurements, *Chemical Geology* 46(2):97–111, doi: 10.1016/0009-2541(84)90183-9.

Balmer, S, and M. Sarnthein (resubm after rev.), Glacial-to-deglacial changes in North Atlantic meltwater advection and deep-water formation – Millennial-scale ^{14}C records from the Azores Plateau, *Quarternary Science Reviews*.

Balmer, S., Sarnthein, M., Mudelsee, M., and P.M. Grootes (resubm after rev.), Refined modeling and ^{14}C plateau tuning reveal consistent patterns of glacial and deglacial ^{14}C reservoir ages of surface waters in low-latitude Atlantic, *Paleoceanography*.

Bard, E. (1988), Correction of accelerator mass spectrometry ^{14}C ages measured in planktonic foraminifera: Paleoceanographic implications, *Paleocenaography*, 3(6), 635-645, doi: 10.1029/pa003i006p00635.

Bard, E., Arnold, M., Mangerud, J., Paterne, M., Labeyrie, L., Duprat, J., Mélières, M-A., Søstegaard, E. and J-C. Duplessy (1994), The North Atlantic atmosphere-sea surface ^{14}C gradient during the Younger Dryas climatic event, *Earth and Planetary Science Letters*, 126, 275-287, doi: 10.1016/0012-821x(94)90112-0.

Bard, E., Rostek, F., Turon, J.L., and S. Gendreau (2000), Hydrological impact of Heinrich events in the subtropical northeast Atlantic, *Science*, *289*(5483), 1321-1324, doi: 10.1126/science.289.5483.1321.

Bemis, B.E., Spero, H.J., Lea, D.W., and J. Bijma (2000), Temperature influence on the carbon isotopic composition of *Globigerina bulloides* and *Orbulina universa* (planktonic foraminifera), *Marine Micropaleontology*, 38, 213-228, doi: 10.1016/s0377-8398(00)00006-2.

Bitz, C.M., Holland, M.M., Weaver, A.J., and M. Eby (2001), Simulating the ice-thicness distribution in a coupled climate model, Journal of Geophysical Research, 206, 2241-2464, doi: 10.1029/1999jc000113.

Bond, G., and R. Lotti (1995), Iceberg discharges into the North Atlantic on millennial time scales during the last glaciation, *Science*, *267*(5200), 1005-1010, doi: 10.1126/science.267.5200.1005.

Bond, G., Heinrich, H., Broecker, W., Labeyrie, L., McManus, J., Andrews, J., Huon, S., Jantschik, R., Clasen, S., Simet, C., Tedesco, K., Klas, M., Bonani, G., and S. Ivy (1992), Evidence for massive discharges of icebergs into the North Atlantic ocean during the last glacial period, *Nature*, *360*, 245-251, doi: 10.1038/360245a0.

Broecker, W., Barker, S., Clark, E., Hajdas, I., Bonani, G., and L. Stott (2004), Ventilation of the glacial deep Pacific Ocean, Science, 306, 1169-1172, doi: 10.1126/science.1102293.

Bronk Ramsey, C., Staff, R.A., Bryant, C.L., Brock, F., Kitagawa, H., van der Plicht, J., Schlolaut, G., Marshall, M.H., Brauer, A. and H. F. Lamb (2012), A complete terrestrial radiocarbon record for 11.2 to 52.8 kyr BP, *Science*, 338(6105), 370-374, doi: 10.1126/science.1226660.

Bryn, P., Berg, K., Stoker, M.S., Haflidason, H., and A. Solheim (2005) Contourites and their relevance for mass wasting along the Mid-Norwegian Margin, *Marine and Petroleum Geology 22*(1),85–96, doi: 10.1016/j.marpetgeo.2004.10.012.

Butzin, M., Prange, M., and G. Lohmann (2012), Readjustment of glacial radiocarbon chronologies by self-consistent three-dimensional ocean circulation modeling, *Earth and Planetary Science Letters*, 317, 177-184, doi: 10.1016/j.epsl.2011.11.046.

Bühring, C., Sarnthein, M., and H. Erlenkeuser (2004) Toward a high-resolution stable isotope stratigraphy of the last 1.1 my: Site 1144, South China Sea. *In* Prell WL, Wang P, Blum P, Rea DK, Clemens SC. (Eds.), *Proc. ODP, Sci. Results* 184,1-29, doi: 10.2973/odp.proc.sr.184.205.2004.

Came, R.E., Oppo, D.W., and W.B. Curry (2003), Atlantic ocean circulation during the Younger Dryas: Insights from a new Cd/Ca record from the western subtropical South Atlantic, *Paleoceanography*, 18, doi:10.1029/2003PA000888.

Campos, E.J., Velhote, D., and I.C. da Silveira (2000), Shelf break upwelling driven by Brazil Current cyclonic meanders, *Geophysical Research Letters*, 27, 751-754, doi: 10.1029/1999gl010502.

Castelao, R.M., Campos, E.J.D., and J. L. Miller (2004), A modelling study of coastal upwelling driven by wind and meanders of the Brazil Current, *Journal of Coastal Research*, 20(3), 662-671, doi: 10.2112/1551-5036(2004)20[662:amsocu]2.0.co;2.

Chen, T., Robinson, L.F., Burke, A., Southon, J., Spooner, P., Morris, P.J., and C.N. Hong (2015), Synchronous centennial abrupt events in the ocean and atmosphere during the last deglaciation, *Science*, 349, 1537, doi: 10.1126/science.aac6159.

Cook, M.S., and L.D. Keigwin (2015), Radiocarbon profiles of the NW Pacific from the LGM and deglaciation: Evaluating ventilation metrics and the effect of uncertain surface reservoir ages, *Paleoceanography*, 30,174-195, doi: 10.1002/2014pa002649.

Cortijo, E., Duplessy, J.-C., Labeyrie, L., Duprat, J., and D. Paillard (2005), Heinrich events: hydrological impact, *Comptes Rendus Geoscience*, 337(10), 897-907, doi: 10.1016/j.crte.2005.04.011.

Curry, W.B., and D.W. Oppo (2005), Glacial water mass geometry and the distribution of $\delta^{13}C$ of ΣCO_2 in the western Atlantic Ocean, *Paleoceanography*, 20, doi: 10.1029/2004PA001021.

Darling, K.F., and C.M. Wade (2008), The genetic diversity of planktic foraminifera and the global distribution of ribosomal RNA genotypes, Marine Micropaleontology, 67(3), 216-238, doi: 10.1016/j.marmicro.2008.01.009.

Denton, G. H., Broecker, W.S., and R. B. Alley (2006), The mystery interval 17.5 to 14.5 kyrs ago, *PAGES* news, 14(20), 14-16.

Deuser, W., Ross, E., Hemleben, C., and M. Spindler (1981), Seasonal changes in species composition, numbers, mass, size, and isotopic composition of planktonic foraminifera settling into the deep Sargasso Sea, *Palaeogeography, Palaeoclimatology, Palaeoecology*, 33(1), 103-127, doi: 10.1016/0031-0182(81)90034-1.

Dowdeswell, J., Maslin, M., Andrews, J., and I. McCave (1995), Iceberg production, debris rafting, and the extent and thickness of Heinrich layers (H-1, H-2) in North Atlantic sediments, *Geology*, 23(4), 301-304, doi: 10.1130/0091-7613(1995)023<0297:ipdrat>2.3.co;2.

Duplessy, J., Shackleton, N., Fairbanks, R., Labeyrie, L., Oppo, D., and N. Kallel (1988), Deepwater source variations during the last climatic cycle and their impact on the global deepwater circulation, *Paleoceanography*, 3(3), 343-360, doi: 10.1029/pa003i003p00343.

Duplessy, J., Labeyrie, Juillet-Leclerc, A., Maitre, F., Duprat, J., and M. Sarnthein (1991), Surface salinity reconstruction of the North-Atlantic ocean during the last glacial maximum, *Oceanologica Acta*, 14(4), 311-324.

Fairbanks, R. G., Sverdlove, M., Free, R., Wiebe, P.H., and A.W. Bé (1982), Vertical distribution and isotopic fractionation of living planktonic foraminifera from the Panama Basin, *Nature*, 298(5877), 841-844, doi: 10.1038/298841a0.

Fanning , A.F., and A.J. Weaver (1996), An atmospheric energy-moisture balancempdel: climatology, interpentadal climate change, and coupling to an ocean general circulation model, *Journal of Geophys. Research*, 101(D10), 15111-15128, doi: 10.1029/96jd01017.

Ferrari, R., Jansen, M. F., Adkins, J. F., Burke, A., Stewart, A. L. and A. F. Thompson (2014), Antarctic sea ice control on ocean circulation in present and glacial climates, *Proceedings of the National Academy of Sciences*, 111(24), 8753-8758, doi: 10.1073/pnas.1323922111.

Fraile, I., Mulitza, S., and M. Schulz (2009), Modeling planktonic foraminiferal seasonality: Implications for sea-surface temperature reconstructions, *Marine Micropaleontology*, 72 (1), 1-9, doi: 10.1016/j.marmicro.2009.01.003.

Franke, J., Paul, A., and M. Schulz (2008), Modeling variations of marine reservoir ages during the last 45.000 years, *Climate of the Past*, 4, 125-136, doi: 10.5194/cp-4-125-2008.

Freeman, E., Skinner, L., Tisserand, A., Dokken, T., Timmermann, A., Menviel, L., and T. Friedrich (2015), An Atlantic–Pacific ventilation seesaw across the last deglaciation, *Earth and Planetary Science Letters*, 424, 237-244, doi: 10.1016/j.epsl.2015.05.032.

Ganssen, G., and M. Sarnthein (1983), Stable-isotope composition of foraminifers: the surface and bottom water record of coastal upwelling, *in* Coastal Upwelling Its Sediment Record, edited, pp. 99-121, Springer, doi: 10.1007/978-1-4615-6651-9_6.

Gasser, T., and H.-G. Müller (1979), Kernel estimation of regression functions *in* Gasser, T., and Rosenblatt, M., eds., Smoothing Techniques for Curve Estimation, Berlin, Springer, pp. 23–68, doi: 10.1007/bfb0098489.

Gasser, T., and H.-G. Müller (1984), Estimating regression functions and their derivatives by the kernel method, *Scandinavian Journal of Statistics*, 11 (3), 171–185.

Gebbie, G. (2014), How much did glacial North Atlantic Water shoal?, *Paleoceanography*, 29, 190-209, doi: 10.1002/2013pa002557.

Gould, W. J. (1985), Physical oceanography of the Azores Front, *Progress in Oceanography*, 14, 167-190, doi: 10.1016/0079-6611(85)90010-2.

Groeneveld, J., and C.M. Chiessi (2011), Mg/Ca of *Globorotalia inflata* as a recorder of permanent thermocline temperatures in the South Atlantic, *Paleoceanography*, 26(2), doi: 10.1029/2010pa001940.

Grootes, P., and M. Stuiver (1997), Oxygen 18/16 variability in Greenland snow and ice with 1000 to 100000 year time resolution, *Journal of Geophysical Research: Oceans (1978-2012)*, 102(C12), 26455-26470, doi: 10.1029/97jc00880.

Grootes, P.M. (2015), Radiocarbon: Clock and Tracer, *in* Encyclopedia of Marine Geosciences, edited by J. Harff, M. Meschede, S. Petersen, and J. Thiede, pp. 1-7, Springer Netherlands, doi: 10.1007/978-94-007-6644-0_89-2.

Grousset, F., Labeyrie, L., Sinko, J., Cremer, M., Bond, G., Duprat, J., Cortijo, E., and S. Huon (1993), Patterns of ice-rafted detritus in the glacial North Atlantic (40-55 N), *Paleoceanography*, 8(2), 175-192, doi: 10.1029/92pa02923.

Gottschalk, J., Skinner, L.C., Sambuddah, M., Waelbroeck, C., Menviel, L., and A. Timmermann (2015), Abrupt changes in the southern extent of North Atlantic deep water during Dansgaard-Oeschger events. *Nat. Geosci.*, 8, 950-954, doi: 10.1038/NGEO2558.

Harrison, S.P., Kohfeld, K.E., Roelandt, C., ND T. Claquin (2001), The role of dust in climate changes today, at the last glacial maximum and in the future, *Earth-Science Reviews*, 54(1),43–80, doi: 10.1016/s0012-8252(01)00041-1.

Hemleben, C., Spindler, M., and O.R. Anderson (1989), Modern planktonic foraminifera, *Springer, Berlin*, doi: 10.1007/978-1-4612-3544-6.

Hemming, S.R., Broecker, W.S., Sharp, W.D., Bond, G.C., Gwiazda, R.H., McManus, J.F., Klas, M., and I. Hajdas (1998), Provenance of Heinrich layers in core V28-82, northeastern Atlantic: $^{40}Ar/^{39}Ar$ ages of ice-rafted hornblende, Pb isotopes in feldspar grains, and Nd-Sr-Pb isotopes in the fine sediment fraction, *Earth and planetary science letters*, 164(1), 317-333, doi: 10.1016/s0012-821x(98)00224-6.

Hewitt, C.D., Stouffer, R.J., Broccoli, A.J., Mitchell, J.F.B. and P.J. Valdes (2003), The effect of ocean dynamics in a coupled GCM simulation of the Last Glacial Maximum, *Climate Dynamics*, 20, 203-218, doi: 10.1007/s00382-002-0272-6.

Hernández-Molina, F.J., Soto, M., Piola, A.R., Tomasini, J., Preu, B., Thompson, P., Badalini, G., Creaser, A., Violante, R.A., and E. Morales (2015), A contourite depositional system along the Uruguayan continental margin: Sedimentary, oceanographic and paleoceanographic implications. *Marine Geology* http://dx.doi.org/10.1016/j.margeo.2015.10.008.

Hill, J. C., and A. Condron (2014), Subtropical iceberg scours and meltwater routing in the deglacial western North Atlantic, *Nature Geoscience*, 7, 806-810, doi: 10.1038/ngeo2267.

Hua, Q., Yu, K., Zhao, J.-X., Hodge, E., Barbetti, M., Fink, D., and U. Zoppi (2005), Variations in marine reservoir ages for the South China Sea during Holocene, *AMS-10 Conference (Sep. 5.10, 2005), Berkley, CA* (Abstracts), 84.

Huang, E., Skinner, L.C., Mulitza, S., Paul, A., and M. Schulz (2015), Radiocarbon distribution and radiocarbon-based circulation age of the Atlantic Ocean during Last Glacial Maximum, *Nova Acta Leopoldina* NF Nr. 121, Nr. 408, 101-106.

Hughen, K.A., Southon, J.R., Lehman, S.J., and J.T. Overpeck (2000), Synchronous radiocarbon and climate shifts during the last deglaciation. *Science*, 290(5498),1951–1954, doi: 10.1126/science.290.5498.1951.

Hughen, K.A. (2007), Radiocarbon dating of deep-sea sediments, *in* Developments in Marine Geology, Vol. 1, 185-210, Elsevier, doi: 10.1016/s1572-5480(07)01010-x.

Jaeschke, A., Rühlemann, C., Arz, H., Heil, G., and G. Lohmann (2007), Coupling of millennial-scale changes in sea surface temperature and precipitation off northeastern Brazil with high-latitude climate shifts during the last glacial period, *Paleoceanography*, 22, PA4206, doi:10.1029/2006PA001391.

Jansen, J.H.F., van der Gast, S.J., Kostner, B., and A. Vaars (1992), CORETEX, an XRF-scanner for chemical analyses of sediment cores, *GEOMAR Rep.*, 15, GeoMar, Kiel, Germany.

Jouzel, J., Masson-Delmotte, V., Cattani, O., Dreyfus, G., Falourd, S., Hoffmann, G., Minster, B., Nouet, J., Barnola, J.-M., Chappellaz, J., Fischer, H., Gallet, J.C., Johnsen, S., Leuenberger, M., Loulergue, L., Luethi, D., Oerter, H., Parrenin, F., Raisbeck, G., Raynaud, D., Schilt, A., Schwander, J., Selmo, E., Souchez, R., Spahni, R., Stauffer, B., Steffensen, J.P., Stenni, B., Stocker, T.F., Tison, J.L., Werner, M., and E.W. Wolff (2007), Orbital and millennial Antarctic climate variability over the past 800,000 years, *Science*, 317(5839),793–796, doi: 10.1126/science.1141038.

Key, R.M., Kozyr, A., Sabine, C. L., Lee, K., Wanninkhof, R., Bullister, J. L., Feely, R. A., Millero, F. J., Mordy, C., and Peng, T.-H. (2004), A global ocean carbon climatology: Results from Global Data Analysis Project (GLODAP). *Global Biogeochem. Cycles*, 18, doi:10.1029/2004GB002247.

Kissel, C., Kleiven, H., Morin, X., and t. S. S. Party (2008), MD168-AMOCINT/1079/ XVII IMAGES cruise report, *Les rappports de campagne à la mer, IPEV, 1080*(OCE/2008/02).

Kitoh, A., Murakami, S., and H. Koide (2001), A simulation of the Last Glacial Maximum with a coupled atmosphere-ocean GCM, Geophys. Res. Letters, 28(11), 2221-2224, doi: 10.1029/2000gl012271.

Kudrass, H.-R., and E. Seibold (1973), Sedimentation am Kontinentalhang vor Portugal und Marokko im Spätpleistozän und Holozän, *Meteor Forschungsergebnisse*, *C13*, 1-63.

Lambeck, K., Rouby, H., Purcell, A., Sun, Y., and M. Sambridge (2014), Sea level and global ice volumes from the Last Glacial Maximum to the Holocene, *PNAS*, 111(43), 15269-15303, doi: 10.1073/pnas.1411762111.

Little, M., Schneider, R., Kroon, D., Price, B., Bickert, T., and G. Wefer (1997), Rapid palaeoceanographic changes in the Benguela Upwelling System for the last 160,000 years as indicated by abundances of planktonic foraminifera, *Palaeogeography, Palaeoclimatology, Palaeoecology*, 130, 135-161, doi: 10.1016/s0031-0182(96)00136-8.

Liu, Z., Otto-Bliesner, B., He, F., Brady, E., Tomas, R., Clark, P., Carlson, A., Lynch-Stieglitz, J., Curry, W., and E. Brook (2009), Transient simulation of last deglaciation with a new mechanism for Bølling-Allerød warming, *Science*, 325(5938), 310-314, doi: 10.1126/science.1171041.

Magana, A.L., Southon, J.R., Kennett, J.P., Roark, E.B., Sarnthein, M., and L. D. Stott (2010), Resolving the cause of large differences between deglacial benthic foraminifera radiocarbon measurements in Santa Barbara Basin, *Paleoceanography*, *25*(4), doi: 10.1029/2010pa002011.

Marchitto, T.M., and W.S. Broecker (2006), Deep water mass geometry in the glacial Atlantic Ocean: A review of constraints from the paleonutrient proxy Cd/Ca, Geochemistry, Geophysics, Geosystems, 7(12), doi: 10.1029/2006GC001323.

Marcott, S.A., Bauska, T.K., Buizert, C., Steig, E.J., Rosen, J.L., Cuffey, K.M., Fudge, T., Severinghaus, J.P., Ahn, J., Kalk, M.L., McConnel, J.R., Sowers, T., Taylor, K.C., White, J.W.C., and E.J. Brook (2014), Centennial-scale changes in the global carbon cycle during the last deglaciation, *Nature*, 514(7524), 616-619, doi: 10.1038/nature13799.

Matsumoto, K. (2007), Radicocarbon-based circulation age of the world oceans. *Journal of Geophys. Res.*, 112, doi: 10.1029/2007JCD004095.

McManus, J., Francois, R., Gherardi, J.-M., Keigwin, L., and S. Brown-Leger (2004), Collapse and rapid resumption of Atlantic meridional circulation linked to deglacial climate changes, *Nature*, 428(6985), 834-837, doi: 10.1038/nature02494.

Meese, D., Gow, A., Alley, R., Zielinski, G., Grootes, P.M., Ram, M., Taylor, K., Mayewski, P.A., and J. Bolzan (1997), The Greenland Ice Sheet Project 2 depth - age scale: Methods and results, *Journal of Geophysical Research: Oceans (1978 - 2012)*, *102*(C12), 26411-26423, doi: 10.1029/97jc00269.

Mix, A.C., Bard, E., and R. Schneider (2001), Environmental processes of the ice age: land, oceans, glaciers (EPILOG), *Quaternary Science Reviews*, 20(4), 627-657, doi: 10.1016/s0277-3791(00)00145-1.

Monnin, E., Indermühle, A., Dällenbach, A., Flückiger, J., Stauffer, B., Stocker, T.F., Raynaud, D., and J-M. Barnola (2001), Atmospheric CO_2 concentrations over the Last Glacial Termination, *Science*, 291, 112-114, doi: 10.1126/science.291.5501.112.

Mudelsee, M. (2014), Climate Time Series Analysis: Classical Statistical and Bootstrap Methods, 2nd ed. Cham, Springer, 454 pp.

Mulitza, S., Wolff, T., Pätzold, J. R., Hale, W., and G. Wefer (1998), Temperature sensitivity of planktic foraminifera and its influence on the oxygen isotope record, *Marine Micropaleontology*, 33(3), 223-240, doi: 10.1016/s0377-8398(97)00040-6.

Nadeau, M.-J., Grootes, P.M., Schleicher, M., Hasselberg, P., Rieck, A., and M. Bitterling (1998), Sample throughput and data quality at the Leibniz-Labor AMS facility, *Radiocarbon*, 40(1), 239-245.

Nydal, R., Lovseth, K., and F.H. Skogseth (1980), Transfer of bomb ^{14}C to the ocean surface, *Radiocarbon*, 22(3), 626-635.

Pflaumann, U., Sarnthein, M., Chapman, M., d'Abreu, L., Funnell, B., Huels, M., Kiefer, T., Maslin, M., Schulz, H., Swallow, J., van Kreveld, S., Vautravers, M., Vogelsang, E., and M. Weinelt (2003), Glacial North Atlantic: Sea - surface conditions reconstructed by GLAMAP 2000, *Paleoceanography*, 18(3), 1065, doi: 10.1029/2002pa000774.

Prell, W.L., Imbire, J., Martinson, D.G., Morley, J.J., Pistas, N.G., Shackleton, N.J., and H. F. Streeter (1986), Graphic correlation of oxygen isotope stratigraphy application to the Late Quarternary, *Paleoceanography*, 1(2), 137-162, doi: 10.1029/pa001i002p00137.

Piotrowski, A.M., Goldstein, S.L., Hemming, S.R., and R.G. Fairbanks (2004), Intensification and variability of ocean thermohaline circulation through the last deglaciation, *Earth and Planetary Science Letters*, 225, 205-220, doi: 10.1016/j.epsl.2004.06.002.

Rasmussen, S.O., Bigler, M., Blockley, S.P., Blunier, T., Buchardt, S.L., Clausen, H.B., Cvijanovic, I., Dahl-Jensen, D., Johnsen, S.J., Fischer, H., Gkinis, V., Guillevic, M., Hoek, W.Z., Lowe, J.J., Pedro, J.B., Popp, T., Seierstad, I.K., Steffensen, J.P., Svensson, A.M., Vallelonga, P., Vinther, B.M., Walker, M.J.C., Wheatley, J.J., and M. Winstrup (2014), A stratigraphic framework for abrupt climatic changes during the Last Glacial period based on three synchronized Greenland ice-core records: refining and extending the INTIMATE event stratigraphy, *Quaternary Science Reviews*, 106,14–28, doi: 10.1016/j.quascirev.2014.09.007.

Ravelo, A.C. and C. Hillaire-Marcel (2007), The use of oxygen and carbon isotopes of foraminifera in paleoceanography, *in* Developmentsin Marine Geology, Vol. 1, 735-764, Elsevier, doi: 10.1016/s1572-5480(07)01023-8.

Reimer, P.J., Bard, E., Bayliss, A., Beck, J.W., Blackwell, P.G., Bronk Ramsey, C., Buck, C.E., Cheng, H., Edwards, R.L., Friedrich, M., Grootes, P.M., Guilderson, T.P., Haflidason, H., Hajdas, I., Hatté, C., Heaton, T.J., Hoffmann, D.L., Hogg, A.G., Hughen, K.A., Kaiser, K.F., Kromer, B., Manning, S.W., Niu, M., Reimer, R.W., Richards, D.A., Scott, E.M., Southon, J.R., Staff, R.A., Turney, C.S.M., and J. van der Pflicht (2013), INTCAL13 and MARINE13 radiocarbon age calibrationcurves 0-50,000 years cal BP, *Radiocarbon*, 55(4), 1869-1887, doi: 10.2458/azu_js_rc.55.16947.

Repschläger, J., Weinelt, M., Kinkel, H., Andersen, N., Garbe-Schönberg, D., and C. Schwab (2015), Response of the subtropical North Atlantic surface hydrography on deglacial and Holocene AMOC changes, *Paleoceanography*, 30(5), 456-476 doi:10.1002/2014PA002637.

Richter, T. (1998), Sedimentary fluxes at the mid-atlantic ridge-sediment sources, accumulation rates, and geochemical characterisation, *GEOMAR Report, GEOMAR Research Center for Marine Geosciences, Christian Albrechts University in Kiel, 73*, 173.

Robinson, L.F., Adkins, J.F., Keigwin, L.D., Southon, J., Fernandez,, D.P. Wang, S., and D.S. Scheirer (2005), Radiocarbon variability in the western North Atlantic during the last deglaciation, *Science*, 310(5753), 1469-1473, doi: 10.1126/science.1114832.

Rogerson, M., Rohling, E.J., Weaver, P.P.E., and J.W. Murray (2004), The azores front since the last glacial maximum, *Earth and planetary science letters*, 222(3), 779-789, doi: 10.1016/s0012-821x(04)00223-7.

Sadler, P. (1999), The influence of hiatuses on sediment accumulation rates, paper presented at *GeoResearch Forum* 5,15–40.

Sarnthein, M., Winn, K., Duplessy, J.-C., and M.R. Fontugne, (1988), Global variations of surface ocean productivity in low and mid latitudes: influence on CO_2 reservoirs of the deep ocean and atmosphere during the last 21,000 years, *Paleoceanography*, 3(3), 361–399, doi: 10.1029/pa003i003p00361.

Sarnthein, M., Winn, K., Jung, S.J.A., Duplessy, J-C., Labeyrie, L., Erlenkeuser, H., and G. Ganssen (1994), Changes in east Atlantic deep water circulation over the last 30,000 years: Eight time slice reconstructions, *Paleoceanography*, 9(2), 209-267, doi: 10.1029/93pa03301.

Sarnthein, M., Stattegger, K., Dreger, D., Erlenkeuser, H., Grootes, P.M., Haupt, B.J., Jung, S., Kiefer, T., Kuhnt, W., Pflaumann, U., Schäfer-Neth, C., Schulz, H., Schulz, M., Seidov, D., Simstich, J., van Kreveld, S., Vogelsang, E., Völker, A., and M. Weinelt (2001), Fundamental modes and abrupt changes in North Atlantic

circulation and climate over the last 60 ky – Concepts, reconstruction and numerical modeling, *in* The North Atlantic: A Changing Environment, edited, 365-410, Springer, doi: 10.1007/978-3-642-56876-3_21.

Sarnthein, M., Gersonde, R., Niebler, S., Pflaumann, U., Spielhagen, R., Thiede, J., Wefer, G., and M. Weinelt (2003a): Overview of Glacial Atlantic Ocean Mapping (GLAMAP-2000), *Paleoceanography* 18(2), 1-6, doi: 10.1029/2002pa000769.

Sarnthein, M., Pflaumann, U., and M. Weinelt (2003b), Past extent of sea ice in the northern North Atlantic inferred from foraminiferal paleotemperature estimates, *Paleoceanography*, 18(2), doi: 10.1029/2002pa000771.

Sarnthein, M., Grootes, P.M., Kennett, J.P., and M. Nadeau (2007), ^{14}C Reservoir Ages Show Deglacial Changes in Ocean Currents and Carbon Cycle, *Geophysical Monogaph-American Geophysical Union*, 173, 175-196, doi: 10.1029/173gm13.

Sarnthein, M., Grootes, P.M., Holbourn, A., Kuhnt, W., and H. Kuhn (2011), Tropical warming in the timor sea led deglacial antarctic warming and atmospheric CO_2 rise by more than 500 yr, *Earth and planetary science letters*, 302, 337-348, doi: 10.1016/j.epsl.2010.12.021.

Sarnthein, M., Schneider, B., and P.M. Grootes (2013), Peak glacial ^{14}C ventilation ages suggest major draw-down of carbon into the abyssal ocean, *Climate of the Past*, 9(1), 925-965, doi: 10.5194/cpd-9-925-2013.

Sarnthein, M., Balmer, S., Grootes, P.M., and M. Mudelsee (2015), Planktic and benthic14C reservoir ages for three ocean basins, calibrated by a suite of ^{14}C plateaus in the glacial-to-deglacial Suigetsu atmospheric ^{14}C record, *RADICARBON*, 57(1), 129-151, doi: 10.2458/azu_rc.57.17916.

Sautter, L. R., and C. Sancetta (1992), Seasonal associations of phytoplankton and planktic foraminifera in an upwelling region and their contribution to the seafloor, *Marine Micropaleontology*, 18, 263-278, doi: 10.1016/0377-8398(92)90043-j.

Schiebel, R., Schmuker, B., Alves,, M. and C. Hemleben (2002), Tracking the Recent and late Pleistocene Azores front by the distribution of planktic foraminifers, *Journal of marine systems*, *37*(1), 213-227, doi: 10.1016/s0924-7963(02)00203-8.

Schlitzer, R. (2015), Ocean Data View, http://odv.awi.de

Schmuker, B., and R. Schiebel (2002), Planktic foraminifers and hydrography of the eastern and northern Caribbean Sea, *Marine Micropaleontology*, 46(3), 387-403, doi: 10.1016/s0377-8398(02)00082-8.

Schneider von Deimling, T., Ganopolski, A., Held, H., and S. Rahmstorf (2006), How cold was the Last Glacial Maximum, *Geophys. Res. Letters*, 33, doi: 10.1029/2006GL026484.

Schott, F.A., Zantopp, R., Stramma, L., Dengler, M., Fischer, J.R., and M. Wibaux (2004), Circulation and deep-water export at the western exit of the subpolar North Atlantic, *Journal of Physical Oceanography*, *34*(4), 817-843, doi: 10.1175/1520-0485(2004)034<0817:cadeat>2.0.co;2.

Schwab, C., Kinkel, H., Weinelt, M., and J. Repschläger (2012), Coccolithophore paleoproductivity and ecology response to deglacial and Holocene changes in the Azores Current System, *Paleoceanography*, *27*(3), doi: 10.1029/2012pa002281.

Seibold, E., and W.H. Berger (1996), The sea floor: an introduction to marine geology, *Springer Science & Business Media*.

Shakun, J.D., Clark, P.U., He, F., Marcott, S.A., Mix, A.C., Liu, Z., Otto-Bliesner, B., Schmittner, A., and E. Bard (2012), Global warming preceded by increasing carbon dioxide concentrations during the last deglaciation, *Nature*, 484(7392), 49–54, doi: 10.1038/nature10915.

Shao, L., Li, X.J., Geng, J.H., Pang, X., Lei, Y.C., Qiao, P.J., Wang, L.L., and H.B. Wang (2007), Deep water bottom current deposition in the northern South China Sea, *Science in China Series D-Earth Sciences*, 50(7), 1060–1066, doi: 10.1007/s11430-007-0015-y.

Simstich, J., Sarnthein, M., and H. Erlenkeuser (2003), Paired $\delta^{18}O$ signals of *Neogloboquadrina pachyderma* (s) and *Turborotalita quinqueloba* show thermal stratification structure in Nordic Seas, *Marine Micropaleontology*, 48(1), 107-125, doi: 10.1016/s0377-8398(02)00165-2.

Skinner L.C., Fallon, S., Waelbroeck, C., Michel, E., and S. Barker (2010), Ventilation of the deep Southern Ocean and deglacial CO_2 rise. *Science*, 328, doi: 10.1126/science.1183627.

Skinner, L.C., Waelbroeck, C., Scrivner, A.E., and S.J. Fallon (2014), Radiocarbon evidence for alternating northern and southern sources of ventilation of the deep Atlantic carbon pool during the last deglaciation, *Proceedings of the National Academy of Sciences*, 111(15), 5480-5484, doi: 10.1073/pnas.1400668111.

Smith, C.R., and C. Rabouille (2002), What controls the mixed-layer depth in deep-sea sediments? The importance of POC flux, *Limnology and Oceanography*, 47(2), 418–426, doi: 10.4319/lo.2002.47.2.0418.

Sortor, R.N. and D.C. Lund (2011), No evidence for a deglacial intermediate water $\Delta^{14}C$ anomaly in the SW Atlantic, *Earth and Planetary Science Letters*, 310, 65-72, doi: 10.1016/j.epsl.2011.07.017.

Steffensen, J.P., Andersen, K.K., Bigler, M., Clausen, H.B., Dahl-Jensen, D., Fischer, H., Goto-Azuma, K., Hansson, M., Johnsen, S.J.J., Jouzel, J., Masson-Delmotte, V., Popp, T., Rasmussen, S.O., Röthlisberger, R., Ruth, U., Stauffer, B., Siggard-Andersen, M.-L., Sveinsbjörnsdóttir, Á.E., Svensson, A., and J. W. C. White (2008), High-resolution Greenland ice core data show abrupt climate change happens in few years, *Science*, 321(5889), 680-684, doi: 10.1126/science.1157707.

Stern, J.V. and L.E. Lisiecki (2013), North Atlantic circulation and reservoir age changes over the past 41,000 years, *Geophysical Research Letters*, 40, 3693-3697, doi: 10.1002/grl.50679.

Stuiver, M., and H. A. Polach (1977), Discussion; reporting of C-14 data, *Radiocarbon*, *19*(3), 355-363.

Stuiver, M., and T.F. Braziunas (1993), Modelling atmospheric ^{14}C influences and ^{14}C ages of marine samples to 10,000 BC, *RADICARBON*, 35(1), 137-189.

Stuiver, M. and P.J. Reimer (1993), Extended ^{14}C database and revised CALIB radiocarbon calibration program, Radiocarbon, 35, 215-230.

Stocker, T.F. (1998), The seesaw effect, *Science*, 282, 61-62, doi: 10.1126/science.282.5386.61.

Svensson, A., Andersen, K.K., Bigler, M., Clausen, H.B., Dahl-Jensen, D., Davies, S., Johnsen, S.J., Muscheler, R., Parrenin, F., Rasmussen, S.O., Röthlisberger, R., Seierstad, I., Steffensen, J.P., and B.M. Vinther (2008), A 60 000 year Greenland stratigraphic ice core chronology, *Climate of the Past*, 4(1), 47-57, doi: 10.5194/cp-4-47-2008.

Sweeney, C., Gloor, E., Jacobsen, A. R., Key, R. M., McKinley, G., Sarmiento, J. l., and R. Wanninkof (2007), Constraining global air-sea gas exchange for CO_2 with recent bomb ^{14}C measurments, *Global Biochem. Cycles*, 21, doi: 10.1029/2006GB002784.

Thiagarajan, N., Subhas, A.V., Southon, J.R., Eiler, J.M., and J.F. Adkins (2014), Abrupt pre-Bølling-Allerød warming and circulation changes in the deep ocean, *Nature*, 511, 75-78, doi: 10.1038/nature13472.

Thornalley D.J.R., Barker, S., Broecker, W.S., Elderfield, H., and N.I. McCave (2011), The degalcial evolution of North Atlantic deep convection, *Science*, 331, doi: 10.1126/science.1196812.

Thornalley, D.J.R., Bauch, H.A., Gebbie, G., Guo, W., Ziegler, M., Bernasconi, S.M., Barker, S., Skinner, L.C., and J. Yu (2015), A warm and poorly ventilated deep Arctic Mediterranean during the last glacial period, *Science*, 349, doi: 10.1126/science.aaa9554.

Thurman, H.V., and E.A. Burton (2001) *Introductory Oceanography*, ninth ed. Prentice Hall, Englewood Cliffs.

Toucanne, S., Mulder, T., Schönfeld, J., Hanquiez, V., Gonthier, E., Duprat, J., Cremer, M., and S. Zaragosi (2007), Contourites of the Gulf of Cadiz: a high-resolution record of the paleocirculation of the Mediterranean outflow water during the last 50,000 years, *Palaeogeography, Palaeoclimatology, Palaeoecology*, 246(2), 354–366, doi: 10.1016/j.palaeo.2006.10.007.

Trauth, M.H., Sarnthein, M., and M. Arnold (1997), Bioturbational mixing depth and carbon flux at the seafloor, *Paleoceanography*, 12(3), 517–526, doi: 10.1029/97pa01764.

van Kreveld, S., Sarnthein, M., Erlenkeuser, H., Grootes, P.M., Jung, S., Nadeau, M., Pflaumann, U., and A. Voelker (2000), Potential links between surging ice sheets, circulation changes, and the Dansgaard - Oeschger Cycles in the Irminger Sea, 60 - 18 Kyr, *Paleoceanography*, 15(4), 425-442, doi: 10.1029/1999pa000464.

Vidal, L., Labeyrie, L., Cortijo, E., Arnold, M., Duplessy, J., Michel, E., Becqué, S., and T.C.E. van Weering (1997), Evidence for changes in the North Atlantic Deep Water linked to meltwater surges during the Heinrich events, *Earth and planetary science letters*, *146*(1), 13-27, doi: 10.1016/s0012-821x(96)00192-6.

Vidal, L., Schneider R.R., Marchal, O., Bickert, T., Stocker, T., and G. Wefer (1999), Link between the North and South Atlantic during the Heinrich events of the last glacial period, *Climate Dynamics*, 15, 909-919, doi: 10.1007/s003820050321.

Vogel, J.S., Southon, J.R., Nelson, D., and T. A. Brown (1984), Performance of catalytically condensed carbon for use in accelerator mass spectrometry, *Nuclear Instruments and Methods in Physics Research Section B: Beam Interactions with Materials and Atoms*, 5(2), 289-293, doi: 10.1016/0168-583x(84)90529-9.

Volkov, D.L., and L.-L. Fu (2011), Interannual variability of the Azores Current strength and eddy energy in relation to atmospheric forcing, *Journal of Geophysical Research: Oceans (1978-2012)*, 116(C11), doi: 10.1029/2011jc007271.

Waelbroeck, C., Labeyrie, L., Duplessy, J.-C., Guiot, J., Labracherie, M., Leclaire, H., and J. Duprat (1998), Improving past sea surface temperature estimates based on planktonic fossil faunas, *Paleoceanography*, 13(3), 272-283, doi: 10.1029/98pa00071.

Waelbroeck, C., Duplessy, J.C., Michel, E., Labeyrie, L., Paillard, D., and J. Duprat (2001), The timing of the last deglaciation in North Atlantic climate records, *Nature*, 412(6848), 724-727, doi: 10.1038/35106623.

Waelbroeck, C., Levi, C., Duplessy, J.-C., Labeyrie, L., Michel, E., Cortijo, E., Bassinot, F., and F. Guichard (2006), Distant origin of circulation changes in the Indian Ocean during the last deglaciation. *Earth and Planetary Science Letters*, 243, 244-251, doi: 10.1016/j.epsl.2005.12.031.

Wallmann, K., Schneider, B., and M. Sarnthein (2016), Effects of eustatic sea-level change, ocean dynamics, and nutrient utilization on atmospheric pCO_2 and seawater composition over the last 130,000 years: a model study. *Clim. Past*, 12, 339–375, doi: 10.5194/cp-12-339-2016.

Wang, X., Auler, A.S., Edwards, R.L., Cheng, H., Cristalli, P.S., Smart, P.L., Richards, D.A., and C.-C. Shen (2004), Wet periods in northeastern Brazil over the past 210 kyr linked to distant climate anomalies, *Nature*, 432, 740-743, doi: 10.1038/nature03067.

Wetzel, A. (1981), Ökologische und stratigraphische Bedeutung biogener Gefüge in quartären Sedimenten am NW-afrikanischen Kontinentalrand, *"Meteor"-Forschungs-Ergebnisse* ,34, 1-47.

Warren, B.A., and K.G. Speer (1991), Deep circulation in the eastern South Atlantic Ocean, *Deep-Sea Research*, 38, 281-322, doi: 10.1016/s0198-0149(12)80014-8.